

FTAS/TR - 67 - 17

LAMINAR FLOWS IN POROUS
ELASTIC CHANNELS

by

Eric F. Grabowski and Simon Ostrach

June
1967

ABSTRACT

This thesis examines the nature of laminar flows of viscous fluids in porous, elastic channels. It is shown that for a wide range of such flows the importance of inertia effects is governed by the modified inlet axial Reynolds number. In particular, when this Reynolds number is small compared to unity, inertia effects can be neglected.

The significance of two other parameters important to these flows is also discussed. One, the ratio of a Reynolds number for the flow through the porous walls to the modified inlet axial Reynolds number, describes the degree to which wall porosity affects the axial flow. The other, a combination of this Reynolds number ratio, the ratio of the characteristic normal (vertical) wall displacement to the unstressed channel half-thickness, and the Strouhal number, governs the relative importance, in unsteady flows, of normal wall unsteadiness and wall porosity.

The mathematical model chosen for this study is based on the thin-film blood flow observed in parallel plate artificial kidneys. The channel walls, however, are taken to be much more rigid than those found at present. Solutions are obtained for the axial and normal velocity components, the fluid pressure, and the normal wall displacement. The effects on these solutions of varying the significant dimensionless parameters governing the flow field and the normal wall displacement are discussed.

ACKNOWLEDGMENTS

The authors wish to thank the National Aeronautics and Space Administration for providing financial support under Grant number NGR - 36 - 003 - 088.

TABLE OF CONTENTS

ABSTRACT	ii
ACKNOWLEDGMENTS	iii
LIST OF SYMBOLS	vi
LIST OF FIGURES	ix
CHAPTER I. INTRODUCTION	1
1.1 PRESENT ARTIFICIAL KIDNEYS AND RECENT RESEARCH TRENDS	1
1.2 THE CHALLENGE TO THE ENGINEERING SCIENCES OF FLUID AND SOLID MECHANICS	4
CHAPTER II. CHARACTERISTICS OF THE PHYSICAL SYSTEM TO BE STUDIED	9
2.1 THE TYPE OF ARTIFICIAL KIDNEY ASSUMED	9
2.2 THE RHEOLOGY OF BLOOD	10
2.3 THE DRIVING FORCE FOR THE FLOW	12
CHAPTER III. ASSUMPTIONS	14
CHAPTER IV. BASIC EQUATIONS AND BOUNDARY CONDITIONS FOR THE SYSTEM	19
4.1 THE FLOW EQUATIONS	19
4.2 THE CHANNEL WALL EQUATIONS	21
4.3 THE BOUNDARY CONDITIONS	24
4.4 SUMMARY	29
CHAPTER V. DERIVATION OF SIMPLIFIED GOVERNING EQUATIONS	31
5.1 INTRODUCTION	31
5.2 NONDIMENSIONALIZATION OF THE EQUATIONS AND BOUNDARY CONDITIONS FOR THE SYSTEM	33

5.3	DERIVATION OF SIMPLIFIED EQUATIONS AND BOUNDARY CONDITIONS	43
5.4	COMPARISON OF THE NONDIMENSIONAL FLOW EQUATIONS AND SOLUTION SCHEME WITH THE EQUATIONS AND SCHEME OF BERMAN	51
5.5	SUMMARY	56
CHAPTER VI	STEADY FLOW IN A POROUS ELASTIC CHANNEL FOR MODIFIED INLET AXIAL REYNOLDS NUMBERS SMALL COMPARED TO UNITY	59
6.1	GENERAL SOLUTION FOR THE FLOW	59
6.2	GENERAL SOLUTION FOR THE NORMAL WALL DISPLACEMENT	62
6.3	LIMITING CASES OF THE GENERAL SOLUTIONS	65
CHAPTER VII	DISCUSSION OF RESULTS	69
CHAPTER VIII	CONCLUSIONS AND SUMMARY	74
REFERENCES		79
APPENDIX A:	DETERMINATION OF CHARACTERISTIC DATA FOR THE FLOW VARIABLES AND CHANNEL HALF- THICKNESS NOT GIVEN EXPLICITLY IN THE LITERATURE	83
APPENDIX B:	DETERMINATION OF CHARACTERISTIC VALUES FOR THE NORMAL WALL DISPLACEMENT AND THE WALL THICKNESS	88
APPENDIX C:	A FURTHER NOTE ON THE RANGE OF VALIDITY OF OF THE SIMPLIFIED EQUATIONS OF THIS STUDY	90
APPENDIX D:	FIGURES	92

LIST OF SYMBOLS

x	Axial space coordinate
y	Spanwise space coordinate
z	Normal space coordinate
t	Time
u	Axial fluid velocity component
v	Spanwise fluid velocity component
w	Normal fluid velocity component
P	Fluid (blood) pressure
r	Axial component of wall displacement
s	Spanwise component of wall displacement
η	Normal component of wall displacement
μ	Dynamic viscosity of the fluid
ν	Kinematic viscosity of the fluid
ρ_f	Fluid Density
ρ	Density of wall material
σ	Poisson's ratio for a purely elastic material
E	Young's modulus
m	Wall thickness
m'	Membrane thickness
ϕ	Membrane permeability
D	Flexural rigidity
P_D	Dialysate pressure

ΔP_D	Dialysate pressure drop along the channel
P_{Di}	Dialysate pressure at dialysate flow inlet
ΔP_{os}	Osmotic pressure difference across the membranes
ΔP_m	Characteristic pressure difference across the membranes
P_o	Inlet fluid (blood) pressure
β	Inlet fluid axial pressure gradient
Q_o	Inlet flow rate
$N_x, N_y, N_x y$	Magnitudes per unit length of forces acting in the middle plane of a thinplate
q_x, q_y	Components of plate tangential loading per unit area
q_z	Normal loading per unit area
q_{xD}, q_{yD}	Components of the contribution to the plate tangential loading per unit area due to the dialysate flow
Ω	Angular frequency
a_n, b_n, c_n, d_n	Constants
j, k, m, n, i	Integers
w_p	Local velocity of flow through the porous walls
e	"At the edges"
N	Direction normal to the wall edges
h	Unstressed channel half-thickness
ℓ	Channel half-width
L	Channel length
T	Period of a heart pulse
U, V, W	Characteristic values for the fluid velocity components
W_p	Characteristic velocity of flow through the porous walls
r_o, n_o	Characteristic values for the wall displacement components

- R The modified inlet axial Reynolds number, $\left(\frac{UL}{\nu}\right) \left(\frac{h}{L}\right)^2$
- R_B Berman's Reynolds number based on the flow through the porous walls, $\left(\frac{W_p h}{\nu}\right)$
- α Ratio of R_B to R , $\left(\frac{W L}{U h}\right)$
- γ The modified ratio of R_B to R ,

$$\frac{3}{R} \left(\frac{\rho_f U^2}{P_o} \right) \left(\frac{P_o}{\Delta P_m} \right) \propto$$

$\bar{A}, \bar{B}, \bar{C}, \bar{D}, \bar{E}, \bar{F}$ Constants

u_o Inlet axial velocity at middle plane

f_n, G_n Functions of the dimensionless normal coordinate

g_n Functions of α and the dimensionless normal coordinate

K Constant

q_o Uniform loading on a thin plate

A bar (-) over a quantity indicates that the quantity is dimensionless and of unit order.

An asterick (*) next to a quantity denotes evaluation at the porous walls.

LIST OF FIGURES

FIGURE	PAGE
1. THE BLOOD AND DIALYSATE CHANNELS IN AN ARTIFICIAL KIDNEY	93
2. KOLFF KIDNEY (KULF)	94
3. KIIL KIDNEY (KEEL)	95
4. CROSS-SECTION OF BLOOD CHANNEL IN THE KIIL KIDNEY (FLOW IS INTO THE PAPER)	96
5. CONE SUPPORTS OF LEONARD AND BLUEMLE	97
6. POROUS MATERIAL SUPPORTS OF BABB AND GRIMSRUD	98
7. CHANNEL GEOMETRY	99
8. COMPONENTS OF DISPLACEMENT OF AN ELEMENT OF THE CHANNEL WALLS	100
9. AXIAL FLUID VELOCITY PROFILES FOR VARIOUS VALUES OF $\frac{x}{L}$	101
10. AXIAL FLUID VELOCITY COMPONENT AT MID-PLANE FOR VARIOUS VALUES OF γ	102
11. AXIAL FLUID VELOCITY COMPONENT AT MID-PLANE FOR VARIOUS VALUES OF $\left(\frac{-\beta L}{P_o}\right)$	103
12. AXIAL FLUID VELOCITY COMPONENT AT MID-PLANE FOR VARIOUS VALUES OF $\left(\frac{\Delta P_m}{P_o}\right)$	104
13. AXIAL FLUID VELOCITY COMPONENT AT MID-PLANE FOR VARIOUS VALUES OF $\left(\frac{\Delta P_D}{P_o}\right)$	105
14. NORMAL FLUID VELOCITY PROFILES FOR VARIOUS VALUES OF $\frac{x}{L}$	106
15. NORMAL FLUID VELOCITY COMPONENT AT WALL FOR VARIOUS VALUES OF γ	107
16. NORMAL FLUID VELOCITY COMPONENT AT WALL FOR VARIOUS VALUES OF $\left(\frac{-\beta L}{P_o}\right)$	108

FIGURE	PAGE
17. NORMAL FLUID VELOCITY COMPONENT AT WALL FOR VARIOUS VALUES OF $\left(\frac{\Delta P_m}{P_o}\right)$	109
18. NORMAL FLUID VELOCITY COMPONENT AT WALL FOR VARIOUS VALUES OF $\left(\frac{\Delta P_D}{P_o}\right)$	110
19. PRESSURE DISTRIBUTION FOR VARIOUS VALUES OF γ	111
20. PRESSURE DISTRIBUTION FOR VARIOUS VALUES OF $\left(\frac{-\beta L}{P_o}\right)$	112
21. PRESSURE DISTRIBUTION FOR VARIOUS VALUES OF $\left(\frac{\Delta P_m}{P_o}\right)$	113
22. PRESSURE DISTRIBUTION FOR VARIOUS VALUES OF $\left(\frac{\Delta P_D}{P_o}\right)$	114
23. NORMAL WALL DISPLACEMENT MIDWAY BETWEEN SIDE WALLS FOR VARIOUS VALUES OF γ	115
24. NORMAL WALL DISPLACEMENT MIDWAY BETWEEN SIDE WALLS FOR VARIOUS VALUES OF $\left(\frac{-\beta L}{P_o}\right)$	116

ERRATA

<u>PAGE</u>	<u>LINE</u>	<u>CORRECTION</u>
9	2	paralled change to parallel
17	25	dialsate change to dialysate
27	18	"to the product of membrane thickness" change to " to the membrane thickness"
60	1	replace $\frac{\partial^2 u}{\partial \bar{z}^2}$ by $\frac{d^2 u}{d\bar{z}^2}$
	5	replace $\frac{d\bar{P}}{dx}$ by $\frac{d\bar{P}}{d\bar{x}}$
63	15	place () about $\frac{\sqrt{Y}}{\pi \Pi}$
64	1	place () about $\frac{\sqrt{Y}}{m \Pi}$
85	20	replace $0(-L)$ by $0(-\beta L)$
87	12	maxiamum change to maximum
	12	$20 \text{ cm}^3/\text{min.}$ change to $20 \text{ cm}^3/\text{min}$
	13	$20,000 \text{ cm}$ change to $20,000 \text{ cm}^2$
	14	$\left(\frac{20 \text{ cm}^3/\text{min}}{20,000} \times \frac{1 \text{ min}}{60 \text{ sec.}} \right)$ change to $\left(\frac{20 \text{ cm}^3/\text{min}}{20,000 \text{ cm}^2} \times \frac{1 \text{ min}}{60 \text{ sec.}} \right)$
91	9	replace $(1-z)^2$ by $(1-z^2)$

CHAPTER I

INTRODUCTION

One of the most exciting challenges to engineering and medicine today is the development of highly efficient, low-cost artificial kidneys. Present artificial kidneys are themselves a remarkable achievement. However, further improvements in these complex devices are mandatory if artificial kidney treatment is ever to become inexpensive enough as to be widely available. Current costs, for example, are such that only a relatively few from the thousands in this country each year who need such treatment can be helped. These further improvements can best come about through the combined efforts of specialists in physical and biological science fields.

1.1 Present Artificial Kidneys and Recent Research Trends.

Artificial kidney techniques have made astounding progress over the last decade. Sufferers from chronic renal(kidney) failure, for instance, have now been kept alive for periods exceeding five years⁽¹⁷⁾. Artificial kidneys have also been used in the treatment of certain types of poisoning^(29,9). The way for much of the research responsible for this progress has been led by research teams under the direction of Kolff at the Cleveland Clinic and Scribner at the University of Washington School of Medicine. Many of the estimated 100,000 people each year who succumb to illnesses related to renal failure⁽²⁹⁾ now have a new chance for life.

An artificial kidney duplicates two functions of a natural

kidney: it maintains the body's water and electrolytic balances; it also removes from the bloodstream the nitrogenous end-products of protein metabolism, among which are urea and creatinine^(29,9).

Unlike the natural kidney, however, the artificial device removes molecules of these blood impurities by means of dialysis, the membrane separative process based on diffusional transport of molecules through polymeric membranes which separate two fluids. (The mechanism of the natural kidney is much more complicated). In an artificial kidney the impurities diffuse from the blood as it flows through channels bounded by cellophane membranes. In passing through the cellophane these impurities then enter other channels filled with a fluid known as "dialysate". (See Figure 1.) Inasmuch as the dialysate itself is flowing, it serves to remove continuously the impurities from the neighborhood of the membranes. The driving force for the diffusional transport, of course, is then a perpetuated concentration gradient of the impurities across the cellophane^(29,13). In order to avoid the undesirable transport of such larger molecules in the blood as proteins, however, the actual cellophane membranes used are "selectively permeable"; they effectively transport molecules only of a certain maximum size.

Excess water is removed from the blood, on the other hand, by means of ultrafiltration, the process by which pure liquid is extracted from a solution or suspension using, again, a semi-permeable membrane. The driving force for the extraction, however, is a fluid pressure gradient across the membrane. In an artificial kidney such a pressure gradient is caused by the excess of blood over dialysate

pressure. This pressure gradient, also, is sometimes augmented by the imposition of an osmotic pressure gradient. Such a pressure gradient can be established simply by adding glucose to the dialysate.

Interconnecting tubes join the blood flow channel with the bloodstream. One tube passes from an artery in an arm or leg to the channel; another, from the channel to a vein in the same arm or leg (29). A pump may or may not be required to drive the blood.

Two artificial kidney designs are in widespread use today: the Kolff, or "twin-coil", and the Kiil, or "parallel plate" (29,15). These are pictured in Figures 2 and 3. In the first design, blood flows through two ten-meter lengths of cellophane tubing wrapped together in several layers about a ten-inch diameter plastic spool. Fiberglass screening, coiled with the tubing, provides spacing between the tubing layers for the flow of dialysate. A blood pump is used. One chief advantage of the design is that it is commercially available in assembled, sterilized form.

In the second kidney type, however, blood passes through two one-meter lengths of cellophane tubing held nearly flat between closely-spaced, parallel ribbed plates. Dialysate flows between the tubing and the ribbed plates in the spaces provided by the ribs. (See Figure 4.) One key advantage of this design is that it requires no blood pump; the arterial-venous pressure gradient is sufficient to drive the flow. Because of this advantage and because of the superior theoretical efficiency of the parallel plate geometry (15), the Kiil-type kidney will be emphasized in the study herein.

In recent years a number of new or modified artificial kidney designs have been proposed and tested. However, all aim towards increased efficiency at lowest possible cost^(29,9). This is because present kidney machines, cumbersome and expensive to operate and maintain, are not available to many who need them. For example, the cost of kidney treatment today ranges from \$5000 to \$7500⁽⁹⁾! The expenses of semi-weekly hospital visits, kidney machine maintenance, and regular care by medical personnel contribute to this high figure. It has been obvious to researchers for some time that the solution to this state of affairs is the development of an artificial kidney so efficient, reliable, easy to assemble and operate, and yet inexpensive, as to require a minimum of medical attention^(29,9). Ultimately such a device might be portable - perhaps even able to be worn on the person - and able to be operated safely in the home.⁽²⁹⁾

1.2 The Challenge to the Engineering Sciences of Fluid and Solid Mechanics.

It is also clear that the evolution of such an artificial kidney can be most swiftly brought about by bringing to bear on the problems involved the talents of engineers as well as medical people. Moreover, there is a particular challenge to workers in the engineering areas of fluid and solid mechanics. Much of the operation of an artificial kidney, after all, involves a rather complex flow of fluids. For instance, in such a device blood issues as a thin film between parallel, flexible and somewhat porous membranes. Also, the interconnecting tubes which lead into and out of the blood flow channel cause flow divergence effects at the channel inlet and con-

vergence effects at the outlet. And, in the case of Kiil-type kidneys, the blood flow, driven as it is by the arterial-venous pressure gradient, is in general pulsatile. An understanding of this complex flow is important to optimal artificial kidney design.

Indeed, a number of artificial kidney phenomena are connected with the flow. Red cell sedimentation in the blood channel is one. (Blood is a suspension of several types of particles, including red cells, in a watery plasma.) However, while this sedimentation can pose a very real problem in practice, it can be controlled by keeping local flow velocities everywhere above some arbitrary minimum (29,6).

Secondly, membrane relaxation and sagging (see Figure 4) causes irregularities in the flow pattern⁽⁵⁾. This relaxation and sagging, brought about by the action of the blood-dialysate pressure difference, is characteristic of polymeric membrane materials like cellophane when wet. Moreover, it diminishes the transfer of undesirable excesses of blood solutes and increases the blood flow channel volume. This volume should be minimized in order to make blood priming unnecessary⁽²⁶⁾.

Cole, Pollard and Murray⁽⁷⁾ have measured the effects of such membrane distentions on the blood volume. In studies on a modified Kiil kidney they report that there exists no linear relationship between this volume and the nominal membrane separation distance. Instead, the channel volume was found to be much more dependent on the fluid pressure difference across the membranes. Because small membrane distentions can significantly affect the channel volume if

the membrane separation distance is itself small, this conclusion should not be surprising.

Moreover, membrane distentions detract from the efficiency of parallel plate kidneys. According to Leonard⁽¹⁵⁾, for example, "the flat plate geometry rapidly degenerates in performance as very small dimensional variations are introduced"

At least three research efforts have been directed towards improving parallel plate kidney performance and reducing blood flow channel volume by minimizing membrane distentions. First, Bluemler and Leonard⁽¹⁶⁾ have tested a kidney having "cones" molded onto its exterior plates. (See Figure 5). The cones serve in part to support the kidney membranes at a number of points on the dialysate side. They also increase membrane transfer by inducing some mixing of the dialysate.

Secondly, Sachs and Funck-Bretano⁽²⁶⁾ have tested a kidney model having membranes to which lateral tension is applied. The application of such tension seems to be intended to offset the effects of membrane sag. Decreased blood volume and increased dialysance (a measure of favorable kidney performance) are observed.

More recently, Babb and Grimsrud⁽¹⁾ have sought to make the blood film thickness more nearly uniform by using nickel foam to support the membrane at all points on the dialysate side. The nickel foam, which can be machined to an extremely level surface, completely fills the dialysate flow space. Since the foam is porous, it allows the dialysate as well as the excesses of water and blood solutes to pass freely. It even causes some mixing of the dialysate, as do the

cones of Leonard and Bluemle. Babb and Grimsrud believe the use of this foam is superior to the application of tension to the kidney membranes in that such tension cannot be maintained indefinitely in view of membrane relaxation. Again, decreased blood volume (and film thickness) and improved dialysance is reported.

Some special consideration is due the removal of excess water in an artificial kidney. This process, known as ultrafiltration depends on both membrane porosity and the local fluid pressure gradient across the membranes. At present, it appears that ultrafiltration affects the blood flow only slightly. However, the converse need not be true. For instance, the local fluid pressure gradient across the membranes - the driving force for ultrafiltration - can depend on position along the flow channel. Furthermore, it may be true in some future artificial kidneys that membrane porosity does significantly affect the blood flow. After all, as Sparks⁽²⁹⁾ has stated, membranes much more permeable than the cellophane ones currently used are required if kidneys are ever to be developed having larger fluxes for blood solutes and water. Hence, the removal of water from the blood flow can be of consequence.

Outside the realm of research motivated by artificial kidney development, work has been conducted on porous, rigid channel and non-porous, elastic tube flows. Properly interpreted, this work should have bearing on kidney design. In the case of porous, rigid channel flow, Berman⁽²⁾ has obtained a perturbation solution for the flow for small, constant suction or blowing at the channel walls.

Sellars⁽²⁸⁾, Yuan⁽³⁹⁾, Terrill^(31,32), and Terrill and Shrestha⁽³³⁾ have extended this work to encompass the cases of large suction and blowing at the walls and mixed suction and blowing. In addition, equations similar to Berman's have been used by Eckert, Donoughe, and Moore⁽⁴³⁾ in correlating flows in porous channels with flows in porous tubes and in boundary layers over porous surfaces, and by Wageman and Guevara⁽⁴⁴⁾ in investigating experimentally flows in porous tubes. Knight and McInteer⁽⁴⁵⁾ have examined the analytical behavior of Berman's equations.

As for flows in non-porous elastic tubes (thin-walled), Morgan⁽¹⁹⁾ has studied the steady, fully-developed case. The transmission of small amplitude, large wavelength pressure waves in these tubes has been examined by Morgan and Kiely⁽²¹⁾ and Morgan and Ferrante⁽²⁰⁾. Kuchar and Ostrach⁽¹⁴⁾ have investigated axial flow development. Still further work has been carried out by Womersley⁽³⁸⁾, Karreman⁽¹²⁾, and Sacks and Abbott^(24,25).

It is the purpose of this analysis to investigate the nature of the blood flow in an artificial kidney. However, only two characteristics of the flow - those judged to be of the greatest immediate importance - will be taken into account herein: wall porosity and wall elasticity. Further, the latter characteristic will be accounted for in a restricted sense in that the kidney membranes will be assumed to be supported by relatively rigid porous material. The particular physical situations for which the analysis applies and the limitations of this study will be discussed in the following two chapters.

CHAPTER II

Characteristics of the Physical System to be Studied

2.1 The Type of Artificial Kidney Assumed.

This analysis will be applicable to artificial kidneys of the parallel plate type whose membranes are supported at all points on the dialysate side by relatively rigid porous material. The porous material, moreover, will be such that it presents a level surface to the membranes and completely fills the dialysate flow space. (See Figure 6.) The extent of porosity will be such that resistance to water and blood solute transfer is essentially membrane resistance.

It is immediately apparent that such kidneys are very similar to the one proposed by Babb and Grimsrud⁽¹⁾, employing membrane supports made from nickel foam. While relatively rigid porous material is certainly not used to back membranes in present kidneys, there are, nevertheless, valid reasons for studying kidneys which make use of such material. First, it is much easier to examine a kidney blood flow bounded by membranes having relatively rigid backing material than one bounded by membranes subject to relaxation and sagging. To do otherwise would overly complicate the analysis herein by the introduction of a complex flow geometry. At the same time, results concerning the flow should still hold at least qualitatively for present kidneys.

Secondly, it appears likely that future kidney designs will incorporate some of the membrane-support ideas being worked on today. If indeed this is the case, the flow results of this analysis will

become quantitatively correct. Further, the analysis should predict accurately the blood channel wall motions when relatively rigid, porous backing is used.

Some changes in the terminology of this study are now in order. Henceforth, the membranes, porous backing material, and the non-porous external kidney plates will collectively be referred to as the channel "walls." "Deflections" of these walls will be spoken of instead of membrane sag or relaxation.

In most other respects, the kidney of this analysis will be like the Kiil in widespread use. It will have similar flow channel dimensions (20 cm.x111 cm.), two pairs of flow channels with such dimensions in parallel, and a comparable total membrane area (1.8m^2). These and further details of the Kiil are given by Sparks⁽²⁹⁾ and Sachs and Funck-Bretano⁽²⁶⁾.

2.2 The Rheology of Blood.

Blood, the fluid of this flow analysis, is neither homogeneous nor Newtonian. Instead, it is a suspension of three kinds of particles in a watery plasma: red cells (erythrocytes), white cells (leukocytes), and platelets (thrombocytes). However, the red cells, present in the concentration of 5×10^6 particles per cubic centimeter, comprise the great bulk of the suspended particles. Shaped like biconcave disks, somewhat deformable and approximately eight microns in diameter and two microns thick, these particles constitute 40 to 48 percent by volume of normal whole blood.

Accordingly, the apparent viscosity of blood, a key fluid property, can depend on several factors. These include the hematocrit, or red cell concentration in percent by volume, the shear rate, and the size of the vessel or channel in which flow takes place. Of these factors, the first, the hematocrit, can be affected in the flow of this study by red cell sedimentation in the flow channel. However, Charm⁽⁶⁾ has observed that such sedimentation is important only for relatively low shear rates - shear rates on the order of 0.1 to 1.0 second⁻¹. In addition, the red cell concentration can be increased by the outflow of watery plasma through the porous channel walls; red cells do not take part in this outflow.

With regard to the dependence of blood viscosity on the shear rate, the viscosity of blood decreases as the shear rate is increased at low shear rates, but becomes virtually constant at shear rates above approximately 100 seconds⁻¹. Thus, for practical purposes blood is Newtonian above this value of shear rate.

The third factor - vessel or channel size - assumes importance when the smallest characteristic length in the flow, such as channel height, is no longer large compared to the diameter of a red cell. Fahraeus and Lindquist⁽¹⁰⁾, for example, have shown that in tubes having diameters smaller than twenty to thirty red cell diameters (about 0.016 to 0.024 centimeters), the apparent viscosity of blood is less than that in larger tubes. And since the nominal blood film thickness in Kill-type artificial kidneys ranges from one to a few hundredths of a centimeter, it would seem that channel size

could be important.

A more complete discussion of the rheology of blood is given by Merrill and Wells⁽¹⁸⁾ and by Rudinger⁽²³⁾.

2.3 The Driving Force for the Flow.

Since artificial kidneys of the parallel plate type require no blood pump, the blood flow in these kidneys is driven entirely by the arterial-venous pressure gradient. In general, this pressure gradient can be considered to be the superposition of a steady (through-flow) part and a time-dependent part⁽³⁵⁾. This latter contribution is periodic and represents the pulsatile portion of blood flow. A similar two-part pressure gradient will be assumed to drive the flow of this study.

It should be noted, however, that inasmuch as the arterial-venous pressure gradient must drive the flow through interconnecting tubes as well as the blood flow channel, only a portion of this pressure gradient actually drives the flow in the channel. Some pressure losses must occur in the interconnecting tubes⁽¹¹⁾.

The driving forces for the channel wall motions, on the other hand, are the blood and dialysate viscous and normal stresses at the walls. In particular, the net normal stress on the walls is largely the blood-dialysate pressure difference. (Velocity gradients at the walls can afford a small contribution.) Like the pressure gradient, this pressure difference consists of steady and pulsatile

parts. On the other hand, the pressure difference can change independently of the pressure gradient; that is, the mean pressure levels at the blood flow channel inlet and outlet can rise simultaneously as the body's blood pressure rises, thereby increasing the pressure difference across the porous channel walls while not affecting the axial pressure gradient.

The dialysate flow may be driven by a pump or by gravity⁽²⁹⁾. It will be considered steady.

CHAPTER III

ASSUMPTIONS

The thin-film blood flow bounded by porous elastic walls encountered in artificial kidney design is of great complexity and not well understood. Consequently, in this flow analysis a number of assumptions and simplifications must be made. These assumptions and simplifications, however, should be such as to retain the salient features of the physical system. With this in mind, the mathematical model for the flow will be as follows:

1. Blood will be assumed to be a homogeneous, incompressible fluid having a constant viscosity.

This assumption implies that the effects of red cell sedimentation and the outflow of watery plasma on the red cell concentration and hence the blood viscosity will be neglected. Furthermore, these effects will not be appreciable provided the shear rate is everywhere above about 1.0 second^{-1} (6) and provided the total outflow through the porous walls is small compared to the blood channel inflow.

The assumption also implies that the effects of channel size on the viscosity of blood will not be considered. Although these effects are possibly significant, a proper accounting of them would add an undue complication to the present analysis.

2. Blood will be taken to be Newtonian.

This assumption is a good one if the shear rate is everywhere above about 100 seconds^{-1} . (See section 2.2.)

(Hence, the minimum shear rate for which blood can be considered Newtonian is much higher than the minimum shear rate for which red cell sedimentation is negligible.)

3. The effects of flow divergence and convergence from and to interconnecting tubes will be neglected.
4. The flow will be laminar.
5. Effects of the gravitational body force will be neglected.
6. The flow at the channel inlet will be taken to be fully-developed.

This assumption is justified on the grounds that the fluid at the channel inlet has already passed through several meters of slender interconnecting tubing.

On the other hand, by no means does the assumption imply that the flow in the channel itself is necessarily fully-developed. Flow through the porous wall can still be of such extent that axial inertia effects become important. For example, large suction at the walls can lead to a large decrease in the axial mass flow and hence significant flow deceleration.

7. Mass transfer will have a negligible effect on the blood and dialysate volumes.
8. In the unstressed situation (no flow; no blood-dialysate pressure difference) the spacing between the porous channel walls will be uniform and small compared to channel length and width.
9. The porous material backing the membranes and the non-porous

exterior plates with which this material is in contact are together of such high flexural rigidity as to keep channel wall deflections small compared to the unstressed channel half-thickness and to nullify the effects of membrane relaxation and sagging.

One consequence of this assumption is that the rigidity of the walls will be essentially that of the porous backing and non-porous exterior plates, the rigidities of the membranes themselves being negligible in comparison.

In addition, the smallness of channel wall deflections compared to the unstressed channel half-thickness implies the smallness of channel wall deflections compared to wall (porous backing and exterior plate) thickness. This is because the wall thickness can reasonably be expected to be at least as large as the unstressed channel half-thickness (a few hundredths of a centimeter.) More important, for deflections small compared to wall thickness a linear theory of elasticity will be applicable.

A means for estimating the wall flexural rigidity required to ensure sufficiently small deflections is given in Appendix B.

10. Although the wall thickness is at least as large as the unstressed channel half-thickness, it will still be small compared to the wall length and width. Moreover, the wall thickness will be uniform and constant.

Accordingly, thin-plate theory can be used to describe the

wall motions.

11. The channel walls will be considered purely elastic and isotropic. Young's modulus and Poisson's ratio will be constants.

12. The membranes will be of uniform permeability.

This assumption does not imply that the velocity of flow through the porous walls need as a result be constant. In general, this velocity can vary with position along the channel since it depends on the difference in the normal fluid stresses acting on the membranes on the blood and dialysate sides. (The difference in the normal fluid stresses can be a function of position along the channel.)

13. The channel walls will be simply-supported at the edges.

At the edges the wall displacement, therefore, is fixed and the bending moment is zero.

14. The side walls, the walls which span the membrane separation distance will be perfectly rigid and non-porous.

15. The dialysate flow will be in a direction opposite to that of the blood flow; that is, a countercurrent flow situation exists.

This is in agreement with what is found in actual kidneys.

16. The volume of the dialysate flow region will be large enough in comparison with that of the blood that the dialysate flow is little affected by membrane porosity.

17. The dialysate flow will be fully-developed at the dialysate

flow inlet.

Together with the preceeding one, this assumption indicates that the dialysate flow will be everywhere fully-developed.

- 18, Viscous shear forces acting on the porous walls caused by the dialysate flow will be of the same order of magnitude as, or smaller than, viscous shear forces acting on these walls caused by the blood flow.

In brief, it is felt that the mathematical model set forth by these assumptions will adequately represent the essential aspects of the flow in a parallel plate artificial kidney blood channel away from the inlet and outlet. (Near the inlet and outlet the effects of channel divergence and convergence become important.) The model should be particularly good, moreover, for the physical situation in which the kidney membranes are supported by relatively rigid porous material at all points on the dialysate side. In this instance the model will accurately describe the motions of the channel walls-motions coupled to the flow. Particular care must be taken, however, that the assumptions concerning the constant viscosity and the Newtonian nature of blood be valid: the ratio of the total outflow through the porous walls to the channel inflow should be small and the shear rate should everywhere be above 100 seconds^{-1} .

CHAPTER IV

Basic Equations and Boundary Conditions for the System

Because of the parallel plate geometry of the artificial kidney blood flow channel being studied, use will be made of a rectangular Cartesian coordinate system. The origin of the coordinate system will be located midway between the parallel membrane surfaces and midway between the side walls at the inlet cross-section. The x - coordinate denotes the longitudinal, or axial direction; the y - coordinate, the spanwise direction; the z - coordinate, the direction normal to the membrane surfaces, or normal direction. Figure 7 illustrates the coordinate system.

4.1 The Flow Equations.

The equations describing the flow are expressions of two physical laws: the local conservation of fluid mass and the local balance between forces applied to the fluid and the resultant change in its momentum. The first of these laws is stated by the continuity equation. In Cartesian coordinates and for an incompressible fluid this equation can be written

$$\frac{\partial u}{\partial x} + \frac{\partial v}{\partial y} + \frac{\partial w}{\partial z} = 0 \quad , \quad 4.1$$

where u, v and w are the components of the fluid velocity vector in the x, y and z - directions, respectively.

For a Newtonian fluid the second of these laws is stated by the Navier-Stokes, or fluid momentum, equations. These equations can be given as follows for a fluid of constant density and viscosity subject to no applied body forces:

$$\begin{aligned} \frac{\partial u}{\partial t} + u \frac{\partial u}{\partial x} + v \frac{\partial u}{\partial y} + w \frac{\partial u}{\partial z} = \\ - \frac{1}{\rho_f} \frac{\partial P}{\partial x} + \nu \left(\frac{\partial^2 u}{\partial x^2} + \frac{\partial^2 u}{\partial y^2} + \frac{\partial^2 u}{\partial z^2} \right) \\ \frac{\partial v}{\partial t} + u \frac{\partial v}{\partial x} + v \frac{\partial v}{\partial y} + w \frac{\partial v}{\partial z} = \\ - \frac{1}{\rho_f} \frac{\partial P}{\partial y} + \nu \left(\frac{\partial^2 v}{\partial x^2} + \frac{\partial^2 v}{\partial y^2} + \frac{\partial^2 v}{\partial z^2} \right) \\ \frac{\partial w}{\partial t} + u \frac{\partial w}{\partial x} + v \frac{\partial w}{\partial y} + w \frac{\partial w}{\partial z} = \\ - \frac{1}{\rho_f} \frac{\partial P}{\partial z} + \nu \left(\frac{\partial^2 w}{\partial x^2} + \frac{\partial^2 w}{\partial y^2} + \frac{\partial^2 w}{\partial z^2} \right), \end{aligned}$$

4.2

where P is the static pressure measured from some reference level, ρ_f is the fluid density, and ν denotes the fluid kinematic viscosity. Equations 4.2 are the local scalar equations of motion for the fluid.

Detailed derivations and discussions of the continuity and Navier-Stokes equations are given by Schlichting⁽²⁷⁾ and Bird,

Stewart and Lightfoot⁽⁴⁾.

4.2 The Channel Wall Equations.

The equations describing the wall motions express Newton's law in the three coordinate directions and can be obtained from the following thin-plate equations written in terms of the coordinate system of Figure 7:

$$\begin{aligned} \frac{\partial N_x}{\partial x} + \frac{\partial N_{xy}}{\partial y} + q_x &= 0 \\ \frac{\partial N_{xy}}{\partial x} + \frac{\partial N_y}{\partial y} + q_y &= 0 \\ D \nabla^4 \eta &= q_z + N_x \frac{\partial^2 \eta}{\partial x^2} + N_y \frac{\partial^2 \eta}{\partial y^2} + 2N_{xy} \frac{\partial^2 \eta}{\partial x \partial y} \\ &\quad - q_x \frac{\partial \eta}{\partial x} - q_y \frac{\partial \eta}{\partial y}, \end{aligned} \quad 4.3$$

where η is the component of plate (or wall) displacement in the normal direction (see Figure 8) and where N_x , N_y and N_{xy} , the magnitudes per unit length of the forces acting in the middle plane of the plate, are functions of r and s , the axial and spanwise components of plate (or wall) displacement, respectively. q_x and q_y denote the two components of the tangential loading per unit area (dimensions of pressure) of the middle plane of the plate, while q_z denotes the normal loading per unit area. D is the plate

flexural rigidity, defined as

$$D = \frac{E m^3}{12 (1 - \sigma^2)} , \quad 4.4$$

where E is Young's modulus; σ , Poisson's ratio; and m, wall thickness.

In particular, for the physical system under study the quantities N_x , N_y , N_{xy} , q_x , and q_y are as follows

$$\begin{aligned} N_x &= \frac{E m}{1 - \sigma^2} \left(\frac{\partial r}{\partial x} + \sigma \frac{\partial s}{\partial y} \right) \\ N_y &= \frac{E m}{1 - \sigma^2} \left(\frac{\partial s}{\partial y} + \sigma \frac{\partial r}{\partial x} \right) \\ N_{xy} &= \frac{E m}{2(1+\sigma)} \left(\frac{\partial r}{\partial y} + \frac{\partial s}{\partial x} \right) \\ q_x &= -\mu \left(\frac{\partial u}{\partial z} + \frac{\partial w}{\partial x} \right)_* - \rho m \frac{\partial^2 r}{\partial t^2} + q_{xD} \\ q_y &= -\mu \left(\frac{\partial v}{\partial z} + \frac{\partial w}{\partial y} \right)_* - \rho m \frac{\partial^2 s}{\partial t^2} + q_{yD} \\ q_z &= \left(P - 2\mu \frac{\partial w}{\partial z} \right)_* + \rho m \frac{\partial^2 \eta}{\partial t^2} , \end{aligned} \quad 4.5$$

where μ is the dynamic viscosity of blood; ρ , the wall density; and q_{xD} and q_{yD} , the components of the contribution to the tangential loading due to the dialysate flow. The quantities marked with an asterisk are to be evaluated at the channel walls; that is,

they are to be evaluated at

$$z = \pm h + \eta$$

But because plate (or wall) displacements are assumed small compared to the unstressed channel half-thickness, they can with the introduction of little error be evaluated instead at

$$z = \pm h$$

Substitution of equations 4.5 and 4.6 into equations 4.3, then, gives the equations for the wall motions:

$$\begin{aligned} & \frac{E m}{1 - \sigma^2} \left(\frac{\partial^2 r}{\partial x^2} + \sigma \frac{\partial^2 s}{\partial x \partial y} \right) + \frac{E m}{2(1+\sigma)} \left(\frac{\partial^2 r}{\partial y^2} + \frac{\partial^2 s}{\partial x \partial y} \right) \\ & - \mu \left(\frac{\partial u}{\partial z} + \frac{\partial w}{\partial x} \right)_* - \rho m \frac{\partial^2 r}{\partial t^2} + q_{xD} = 0 \\ & \frac{E m}{1 - \sigma^2} \left(\frac{\partial^2 s}{\partial y^2} + \sigma \frac{\partial^2 r}{\partial x \partial y} \right) + \frac{E m}{2(1+\sigma)} \left(\frac{\partial^2 r}{\partial x \partial y} + \frac{\partial^2 s}{\partial x^2} \right) \\ & - \mu \left(\frac{\partial v}{\partial z} + \frac{\partial w}{\partial y} \right)_* - \rho m \frac{\partial^2 s}{\partial t^2} + q_{yD} = 0 \\ & D \nabla^4 \eta = \left(P - 2\mu \frac{\partial w}{\partial z} \right)_* + \rho m \frac{\partial^2 \eta}{\partial t^2} \\ & + \frac{E m}{1 - \sigma^2} \left(\frac{\partial r}{\partial x} + \sigma \frac{\partial s}{\partial y} \right) \frac{\partial^2 \eta}{\partial x^2} + \frac{E m}{1 - \sigma^2} \left(\frac{\partial s}{\partial y} + \sigma \frac{\partial r}{\partial x} \right) \frac{\partial^2 \eta}{\partial y^2} \\ & + \frac{E m}{1 + \sigma} \left(\frac{\partial r}{\partial y} + \frac{\partial s}{\partial x} \right) \frac{\partial^2 \eta}{\partial x \partial y} \end{aligned}$$

$$\begin{aligned}
 & + \left\{ \mu \left(\frac{\partial u}{\partial z} + \frac{\partial w}{\partial x} \right)_* + \rho m \frac{\partial^2 r}{\partial t^2} - q_{xD} \right\} \frac{\partial \eta}{\partial x} \\
 & + \left\{ \mu \left(\frac{\partial v}{\partial z} + \frac{\partial w}{\partial y} \right)_* + \rho m \frac{\partial^2 s}{\partial t^2} - q_{yD} \right\} \frac{\partial \eta}{\partial y} .
 \end{aligned} \tag{4.7}$$

A more detailed derivation and discussion of equations 4.3 and 4.5 is given by Timoshenko and Woinowsky - Krieger⁽³⁴⁾, Wang⁽³⁷⁾ and Reissner⁽²²⁾. Equations 4.6 follow from the definition of the fluid stress tensor^(27,4) and the use of d'Alembert's principle⁽³⁰⁾.

4.3 The Boundary Conditions.

A complete statement of the mathematical problem yet requires the specification of a number of boundary conditions. In the first place, because fluid is lost through the porous walls, the energy needed at successive channel positions to drive the flow decreases. The axial pressure gradient must then diminish with position along the channel, implying that the flow is not independent of the axial coordinate and hence not fully-developed in the channel. Hence, either the inlet velocity profile or the inlet axial pressure gradient must be specified. If the latter is considered to be the "driving force" for the flow, one flow boundary condition will be

$$\left. \frac{\partial P}{\partial x} \right|_{x=0} = \beta \left\{ 1 + \sum_{n=1}^J \left[a_n \cos(n \Omega t) + b_n \sin(n \Omega t) \right] \right\}, \quad 4.8$$

where β is a negative constant representing that portion of the entrance axial pressure gradient associated with the steady part of the flow. The pulsatile, time-dependent portion is in the form of the "Fourier polynomial," where the a_n and b_n are constants assumed known and Ω is the angular frequency of the basic periodic oscillation. It can be shown that any continuous periodic function can be approximated by such a finite Fourier polynomial. In fact, the approximation will be the "best" one in the mean square sense. (See, for instance, Courant and Hilbert,⁽⁸⁾ pp. 68 - 69.)

The constant β in equation 4.8, further, can be expressed in terms of measurable quantities. To begin with, the flow at the inlet cross-section has been assumed to be fully-developed. The steady portion of this flow, moreover, because of the smallness of the unstressed channel half-thickness compared to channel width, is approximately a two-dimensional Poiseuille flow. (All flow properties and characteristics are essentially independent of the spanwise coordinate over the bulk of the inlet.) And for such an inlet flow the following relation is valid

$$\beta = - \frac{3}{4} \left(\frac{Q_o \mu}{l h^3} \right), \quad 4.9$$

where Q_0 is the steady part of the axial flow rate at the inlet and where l is the channel half-width.

Next, the inlet pressure must be stated. As Kuchar and Ostrach (14) point out, the flow situation in an elastic channel is quite different from that in a rigid one. In the rigid channel case, pressure gradients, as the driving forces for the flow, are of direct interest. However, in elastic channel flow, pressure levels, upon which the channel wall motions depend, are of importance as well. Thus, while the inlet pressure is not of immediate concern in rigid channel flow and need not be stated so long as the axial pressure drop is known, this pressure must be given in the problem under consideration. This pressure, taken to be uniform over the inlet cross-section, will be as follows:

$$P|_{x=0} = P_0 \left\{ 1 + \sum_{n=1}^k \left[c_n \cos (n \Omega t) + d_n \sin (n \Omega t) \right] \right\}, \quad 4.10$$

where P_0 is that portion of the inlet pressure level due to the steady part of the flow. The c_n and d_n are constants assumed known.

Other conditions which must be specified are the no-slip condition at the walls and the porous channel condition. The first of these is that the components of fluid velocity in the axial and spanwise directions, evaluated at the channel walls, must be equal to the axial and spanwise components, respectively, of the wall

velocity. The second of these is that the normal component of fluid velocity, evaluated at the channel walls, must be equal to the sum of the velocity of flow through the porous walls and the normal component of wall velocity. The conditions are as follows:

$$u|_* = \frac{\partial r}{\partial t} \quad 4.11$$

$$v|_* = \frac{\partial s}{\partial t} \quad 4.12$$

$$w|_* = w_p + \frac{\partial n}{\partial t}, \quad 4.13$$

where w_p is the local velocity of flow through the porous walls and where the asterisks denote evaluation at the channel walls in the manner described in Section 4.2.

In general, the local velocity of flow through the porous walls, w_p , can be considered to be proportional to the difference between the blood and dialysate normal fluid stresses acting on the membranes (29,13). It can also, however, have a contribution due to an osmotic pressure difference across the membranes (29,13). Consequently,

$$w_p = \frac{\phi}{m} \left[\left\{ \left(P - 2\mu \frac{\partial w}{\partial z} \right) - P_D \right\}_* + \Delta P_{os} \right] \quad 4.14$$

The constant of proportionality $\frac{\phi}{m}$, is the ratio of membrane permeability ϕ to the product of membrane thickness m , ΔP_{os} is the osmotic pressure difference,

considered in this study a constant. P_D denotes the dialysate pressure. Because the dialysate flow is assumed to be fully-developed and countercurrent, this pressure can be taken to be

$$P_D = P_{Di} - (L - x) \left(\frac{\Delta P_D}{L} \right), \quad 4.15$$

where P_{Di} is the pressure level at the dialysate inlet; P_D , the dialysate pressure drop along the channel length; and L , the channel length itself.

As for the boundary conditions on the wall motions, the channel walls have been assumed to be simply supported (no bending moment) at the edges. This assumption gives the conditions

$$\eta|_e = 0 \quad 4.16$$

$$\frac{\partial^2 \eta}{\partial N^2} \Big|_e = 0, \quad 4.17$$

where N is the direction normal to the wall edges and where the subscript "e" denotes "at the edges." Also, if the walls are under no tension when not deformed in the normal direction and if the edges are not deformed when the walls are deformed, the conditions on the axial and spanwise components of wall displacement can be given as

$$r|_e = 0 \quad 4.18$$

$$s|_e = 0 \quad 4.19$$

Although an unsteady problem is being considered, initial conditions are not required. This is because the unsteadiness is in the form of a periodic oscillation and thus involves no transients.

In the special case of steady flow, the boundary conditions on the fluid pressure and velocity components become

$$\left. \frac{\partial P}{\partial x} \right|_{x=0} = \beta \quad 4.20$$

$$\left. P \right|_{x=0} = P_o \quad 4.21$$

$$\left. u \right|_* = 0 \quad 4.22$$

$$\left. v \right|_* = 0 \quad 4.23$$

$$\left. w \right|_* = \pm w_p \quad 4.24$$

This flow case prevails when the elastic bloodstream-to-blood channel interconnecting tubes are of such length as to damp out most of the pulsatile portion of the blood flow before it reaches the channel inlet.

4.4 Summary.

The continuity equation 4.1, the Navier-Stokes equations 4.2, and the channel wall equations 4.3, subject to the specified boundary conditions, describe completely the assumed porous, elastic channel flow. The equations, moreover are a system of seven partial differential equations in seven unknowns. The unknowns include the three

fluid velocity components, $u(x,y,z,t)$, $v(x,y,z,t)$ and $w(x,y,z,t)$, the fluid pressure, $P(x,y,z,t)$, and the three components of wall displacement, $r(x,y,t)$, $s(x,y,t)$, and $n(x,y,t)$. These equations are consistent with the mathematical model set forth in Chapter III.

It can be seen that in general coupling exists between the blood flow described and the dialysate flow and between the blood flow and the channel wall motions. The latter coupling is such, however, that the blood flow is dependent on the wall motions only through the boundary conditions on the three fluid velocity components. In contrast, the wall motions depend directly on the flow through terms in the wall equations of motion.

In addition, the flow has been taken to be three-dimensional. This may appear surprising since it has been assumed that the unstressed channel half-thickness is small compared to channel width and that normal wall displacements are small compared to the unstressed channel half-thickness. On the other hand, the spanwise component of wall velocity can drive flow in the spanwise direction in accordance with the no slip condition at the walls. Also, it has not yet been shown that the velocity of flow through the porous walls is independent of the spanwise coordinate. Thus, in general the flow depends on all three coordinate directions.

In the steady flow case, the case for which solutions will be sought in this analysis, the flow will later be indeed shown to be two-dimensional.

CHAPTER V

DERIVATION OF SIMPLIFIED GOVERNING EQUATIONS

5.1 Introduction

In Chapter IV a system of seven partial differential equations in seven unknowns was shown to describe the flow and associated wall motions. The unknowns are the three fluid velocity components, $u(x,y,z,t)$, $v(x,t,z,t)$ and $w(x,y,z,t)$; the fluid pressure, $P(x,y,z,t)$; and the three components of wall displacement, $r(x,y,t)$, $s(x,y,t)$ and $\eta(x,y,t)$. It is immediately clear, however, that the system of equations and boundary conditions is extremely difficult to solve exactly. The Navier-Stokes equations, for instance, have nonlinear inertia terms, while the wall equations include products of the derivatives of unknowns. Then, too, the wall equations are coupled to the flow equations both directly and through boundary conditions. It is thus desirable to make simplifications where justifiable and to seek some approximate solution of the system of equations.

To this end, a formal simplification technique - the nondimensionalization and ordering of the system of equations and boundary conditions - will be used. This will be employed in conjunction with a formal perturbation solution of the system of equations. The equations and boundary conditions will be rewritten in dimensionless form, each of the unknowns and independent variables being replaced by the product of a dimensionless quantity and a characteristic value for the unknown or independent variable.

The dimensional characteristic values appearing in the equations and boundary conditions will then be grouped in such a way as to produce dimensionless parameters. Each of these parameters, which will possess definite values from the physics of the problem, will express the importance of one type of force or effect in the flow or wall motions relative to another. Since these parameters will appear multiplying nondimensional terms or groups of terms of unit order, ordering the parameters with respect to powers of the perturbation parameter (yet to be chosen) will indicate the importance of certain terms in the equations and boundary conditions over others. The less important terms can then be neglected, at least in the equations of zeroth order in the perturbation parameter. Hopefully these latter equations, while retaining the physical essence of the problem, will lend themselves much more easily to solution.

One advantage of this procedure is that it will show under what physical conditions certain of the terms really can be neglected. Another is that, unlike reasoning from a strictly physical viewpoint, the scheme gives, through the ordering of the parameters, an estimate of the error incurred by the neglect of higher-order (those other than the zeroth) solutions.

On the other hand, care must be taken that terms involving the highest derivatives of one of the unknowns are not neglected. Otherwise, all boundary conditions on that unknown can no longer be satisfied and error may be introduced in the solutions near boundaries.

5.2 Nondimensionalization of the Equations and Boundary Conditions for the System

Because the flow and wall equations and the boundary conditions are in general interdependent, they will be nondimensionalized simultaneously. Dimensionless variables will be introduced by the following transformations:

$$\begin{array}{lll}
 x = L \bar{x} & u = U \bar{u} & P = P_0 \bar{P} \\
 y = \ell \bar{y} & v = V \bar{v} & r = r_0 \bar{r} \\
 z = h \bar{z} & w = W \bar{w} & s = r_0 \bar{s} \\
 t = T \bar{t} & w_p = W_p \bar{w}_p & \eta = \eta_0 \bar{\eta} \\
 & P_D = P_{Di} \bar{P}_D &
 \end{array} \quad 5.1$$

where L , ℓ , and h are characteristic values for the flow channel length, half-width and unstressed half-thickness, respectively. T is the period of one heart pulse. Characteristic values for the axial, spanwise and normal velocity components are denoted by U, V and W , respectively. W_p , on the other hand, is an estimate for the velocity of flow through the porous walls and because of wall unsteadiness in the normal direction is, in general, different from the characteristic quantity W . P_{Di} and P_0 are characteristic values for the dialysate and blood pressures. Finally, r_0 and η_0 are characteristic values for the axial (or spanwise) and normal components of wall displacement. Numerical values for these characteristic quantities are given in Section 5.3.

The characteristic axial wall displacement r_0 has been used as the characteristic spanwise wall displacement also. This can

readily be explained. To begin with, because the channel walls in the unstressed (no flow) state are subject to no stretching, any stretching that does occur in the stressed state must be such that the axial and spanwise components of wall tension are of the same order of magnitude. Hence, it can be expected that the axial and spanwise components of wall displacement are of the same order of magnitude.

Now, substitution of the transformations 5.1 into boundary conditions 4.11 and 4.12 and wall equation 4.7a and grouping dimensional quantities to form dimensionless parameters gives

$$\bar{v}|_* = \left(\frac{r_o}{VT} \right) \frac{\partial \bar{s}}{\partial \bar{t}} \quad 5.2$$

$$\bar{w}|_* = \left(\frac{W_p}{W} \right) \bar{w}_o + \left(\frac{\eta_o}{WT} \right) \frac{\partial \bar{\eta}}{\partial \bar{t}} \quad 5.3$$

$$\begin{aligned} & \left(\frac{\ell}{L} \right)^2 \frac{\partial^2 \bar{r}}{\partial \bar{x}^2} + \sigma \left(\frac{\ell}{L} \right) \frac{\partial^2 \bar{s}}{\partial \bar{x} \partial \bar{y}} + \frac{1-\sigma}{2} \left[\frac{\partial^2 \bar{r}}{\partial \bar{y}^2} + \left(\frac{\ell}{L} \right) \frac{\partial^2 \bar{s}}{\partial \bar{x} \partial \bar{y}} \right] \\ & - (1-\sigma^2) \left(\frac{\ell}{m} \right) \left(\frac{\ell}{r_o} \right) \left(\frac{\mu U}{Eh} \right) \left[\frac{\partial \bar{u}}{\partial \bar{z}} + \left(\frac{W_p L}{U h} \right) \left(\frac{h}{L} \right)^2 \frac{\partial \bar{w}}{\partial \bar{x}} - 1 \right] \\ & = (1-\sigma^2) \left(\frac{\rho \ell^2}{ET} \right) \frac{\partial^2 \bar{r}}{\partial \bar{t}^2} \end{aligned} \quad 5.4$$

where use has been made in equation 5.4 of the assumption that the dialysate viscous stresses on the walls are of the same order of magnitude as, or less than, the blood viscous stresses. Equations 5.2, 5.3 and 5.4 can now serve to give relations among certain of

the characteristic values. These relations will aid in simplifying the nondimensionalization procedure.

First, because flow in the spanwise direction is driven by wall motion in that direction, the two terms in equation 5.2 must be of the same order. Thus, the parameter $\left(\frac{r_o}{VT}\right)$ can be set equal to unity. This gives a relationship between the characteristic fluid velocity in the spanwise direction V , on the one hand, and the characteristic axial wall displacement r_o and the period of one heart pulse T , on the other:

$$V = \left(\frac{r_o}{T}\right) \quad 5.5$$

As for the two terms on the right hand side of equation 5.3 nothing can immediately be said about their relative importance. However, the sum of these two terms - and hence the sum of the parameters appearing in them - must be of unit order. Setting the sum of the parameters $\left(\frac{W_p}{W}\right)$ and $\left(\frac{\eta_o}{WT}\right)$ equal to unity, then, leads to the following relation between the characteristic normal fluid velocity W , on the one hand, and the characteristic velocity of flow through the porous walls W_p , the characteristic normal wall displacement η_o , and the period of one blood pulse T , on the other:

$$W = W_p + \frac{\eta_o}{T} \quad 5.6$$

The physical significance of equation 5.6 is that the characteristic normal fluid velocity consists of a part due to wall porosity and a part due to wall unsteadiness. Depending on the particular situation encountered, one or the other of these contributions may predominate. Thirdly, in equation 5.4 the magnitude of the fourth term is

determined by the dimensionless group

$$(1 - \sigma^2) \left(\frac{\ell}{m} \right) \left(\frac{\ell}{r_o} \right) \left(\frac{\mu U}{Eh} \right).$$

Now, since viscous stresses drive the wall motions in the axial and spanwise directions and since inertia effects can be expected to be small compared to viscous effects, the leading wall displacement and viscous stress terms of this equation should be of the same order, namely unity. As a result, the dimensionless group $(1 - \sigma^2) \left(\frac{\ell}{m} \right) \times \left(\frac{\ell}{r_o} \right) \left(\frac{\mu U}{Eh} \right)$ can be set equal to one. This gives a relationship between the characteristic axial wall displacement r_o and other, more easily measured quantities :

$$r_o = (1 - \sigma^2) \left(\frac{\ell}{m} \right) \left(\frac{\mu U}{Eh} \right) \ell \quad 5.7$$

Further, combining relation 5.7 with 5.5 yields

$$V = (1 - \sigma^2) \left(\frac{\ell}{m} \right) \left(\frac{\mu U}{Eh} \right) \left(\frac{\ell}{T} \right), \quad 5.8$$

If equations 5.6, 5.7 and 5.8 are now used together with the transformations 5.1 and if, in addition, the symbols α and R are employed to denote the dimensionless groups $\left(\frac{W_p L}{U h} \right)$ and $\left(\frac{U L}{v} \right) \left(\frac{h}{L} \right)^2$, respectively, the continuity, Navier-Stokes, and wall equations can be written in dimensionless form as follows :

$$\begin{aligned} \frac{\partial \bar{u}}{\partial \bar{x}} + (1 - \sigma^2) \left(\frac{\ell}{m} \right) \left(\frac{\mu U}{Eh} \right) \left(\frac{L}{UT} \right) \left(\frac{\ell}{L} \right) \frac{\partial \bar{v}}{\partial \bar{y}} \\ + \left\{ \alpha + \left(\frac{\eta_o}{h} \right) \left(\frac{L}{UT} \right) \right\} \frac{\partial \bar{w}}{\partial \bar{z}} = 0 \end{aligned} \quad 5.9$$

$$\begin{aligned}
 & \left(\frac{L}{UT} \right) \frac{\partial \bar{u}}{\partial \bar{t}} + \bar{u} \frac{\partial \bar{u}}{\partial \bar{x}} + (1 - \sigma^2) \left(\frac{\ell}{m} \right) \left(\frac{\mu U}{Eh} \right) \left(\frac{L}{UT} \right) \left(\frac{\ell}{L} \right) \bar{v} \frac{\partial \bar{u}}{\partial \bar{y}} \\
 & + \left\{ \alpha + \left(\frac{\eta_o}{h} \right) \left(\frac{L}{UT} \right) \right\} \bar{w} \frac{\partial \bar{u}}{\partial \bar{z}} = \\
 & - \left(\frac{P_o}{\rho_f U^2} \right) \frac{\partial \bar{P}}{\partial \bar{x}} + \frac{1}{R} \left[\left(\frac{h}{L} \right)^2 \frac{\partial^2 \bar{u}}{\partial \bar{x}^2} + \left(\frac{h}{\ell} \right)^2 \frac{\partial^2 \bar{u}}{\partial \bar{y}^2} + \frac{\partial^2 \bar{u}}{\partial \bar{z}^2} \right] \\
 & (1 - \sigma^2) \left(\frac{\ell}{m} \right) \left(\frac{\mu U}{Eh} \right) \left(\frac{L}{UT} \right) \left(\frac{\ell}{L} \right) \left[\left(\frac{L}{UT} \right) \frac{\partial \bar{v}}{\partial \bar{t}} + \bar{u} \frac{\partial \bar{v}}{\partial \bar{x}} \right. \\
 & + (1 - \sigma^2) \left(\frac{\ell}{m} \right) \left(\frac{\mu U}{Eh} \right) \left(\frac{L}{UT} \right) \left(\frac{\ell}{L} \right) \bar{v} \frac{\partial \bar{v}}{\partial \bar{y}} + \left. \left\{ \alpha + \left(\frac{\eta_o}{h} \right) \left(\frac{L}{UT} \right) \right\} \bar{w} \frac{\partial \bar{v}}{\partial \bar{z}} \right] \\
 & = - \left(\frac{L}{\ell} \right)^2 \left(\frac{P_o}{\rho_f U^2} \right) \frac{\partial \bar{P}}{\partial \bar{y}} + (1 - \sigma^2) \left(\frac{\ell}{m} \right) \left(\frac{\mu U}{Eh} \right) \left(\frac{L}{UT} \right) \left(\frac{\ell}{L} \right) \frac{1}{R} \left[\left(\frac{h}{L} \right)^2 \frac{\partial^2 \bar{v}}{\partial \bar{x}^2} \right. \\
 & \quad \left. + \left(\frac{h}{\ell} \right)^2 \frac{\partial^2 \bar{v}}{\partial \bar{y}^2} + \frac{\partial^2 \bar{v}}{\partial \bar{z}^2} \right] \\
 & \left\{ \alpha + \left(\frac{\eta_o}{h} \right) \left(\frac{L}{UT} \right) \right\} \left[\left(\frac{L}{UT} \right) \frac{\partial \bar{w}}{\partial \bar{t}} + \bar{u} \frac{\partial \bar{w}}{\partial \bar{x}} \right. \\
 & + (1 - \sigma^2) \left(\frac{\ell}{m} \right) \left(\frac{\mu U}{Eh} \right) \left(\frac{L}{UT} \right) \left(\frac{\ell}{L} \right) \bar{v} \frac{\partial \bar{w}}{\partial \bar{y}} + \left. \left\{ \alpha + \left(\frac{\eta_o}{h} \right) \left(\frac{L}{UT} \right) \right\} \bar{w} \frac{\partial \bar{w}}{\partial \bar{z}} \right] \\
 & - \left(\frac{L}{h} \right)^2 \left(\frac{P_o}{\rho_f U^2} \right) \frac{\partial \bar{P}}{\partial \bar{z}} + \left\{ \alpha + \left(\frac{\eta_o}{h} \right) \left(\frac{L}{UT} \right) \right\} \frac{1}{R} \left[\left(\frac{h}{L} \right)^2 \frac{\partial^2 \bar{w}}{\partial \bar{x}^2} \right. \\
 & \quad \left. + \left(\frac{h}{\ell} \right)^2 \frac{\partial^2 \bar{w}}{\partial \bar{y}^2} + \frac{\partial^2 \bar{w}}{\partial \bar{z}^2} \right]
 \end{aligned}$$

$$\left(\frac{\ell}{L}\right)^2 \frac{\partial^2 \bar{r}}{\partial \bar{x}^2} + \sigma \left(\frac{\ell}{L}\right) \frac{\partial^2 \bar{s}}{\partial \bar{x} \partial \bar{y}} + \frac{1-\sigma}{2} \left[\frac{\partial^2 \bar{r}}{\partial \bar{y}^2} + \left(\frac{\ell}{L}\right) \frac{\partial^2 \bar{s}}{\partial \bar{x} \partial \bar{y}} \right] \\ - \left[\frac{\partial \bar{u}}{\partial \bar{y}} + \alpha \left(\frac{h}{L}\right)^2 \frac{\partial \bar{w}}{\partial \bar{x}} - 1 \right] * = (1-\sigma^2) \left(\frac{\rho \ell^2}{ET}\right) \frac{\partial^2 \bar{r}}{\partial \bar{t}^2}$$

$$\frac{\partial^2 \bar{s}}{\partial \bar{y}^2} + \left(\frac{\ell}{L}\right) \frac{\partial^2 \bar{r}}{\partial \bar{x} \partial \bar{y}} + \frac{1-\sigma}{2} \left(\frac{\ell}{L}\right) \frac{\partial^2 \bar{r}}{\partial \bar{x} \partial \bar{y}} + \left(\frac{\ell}{L}\right)^2 \frac{\partial^2 \bar{s}}{\partial \bar{x}^2} \\ - \left[(1-\sigma^2) \left(\frac{\ell}{m}\right) \left(\frac{\mu U}{Eh}\right) \left(\frac{L}{UT}\right) \left(\frac{\ell}{L}\right) \frac{\partial \bar{v}}{\partial \bar{z}} + \alpha \left(\frac{h}{\ell}\right)^2 \frac{\partial \bar{w}}{\partial \bar{y}} \right] * \\ = (1-\sigma^2) \frac{\rho \ell^2}{ET} \frac{\partial^2 \bar{s}}{\partial \bar{t}^2}$$

$$\left(\frac{\ell}{L}\right)^4 \frac{\partial^4 \bar{\eta}}{\partial \bar{x}^2} + 2 \left(\frac{\ell}{L}\right)^2 \frac{\partial^4 \bar{\eta}}{\partial \bar{x}^2 \partial \bar{y}^2} + \frac{\partial^4 \bar{\eta}}{\partial \bar{y}^4} \\ + 12 (1-\sigma^2) \left(\frac{\ell}{m}\right)^2 \left(\frac{\rho \ell^2}{ET}\right) \frac{\partial^2 \bar{\eta}}{\partial \bar{t}^2} = \\ 12 (1-\sigma^2) \left(\frac{\ell}{m}\right)^3 \left(\frac{\ell}{h}\right) \left(\frac{h}{\gamma_o}\right) \left\{ \left(\frac{P_o}{E}\right) \bar{P} - 2\alpha \left(\frac{\mu U}{Eh}\right) \left(\frac{h}{L}\right) \frac{\partial \bar{w}}{\partial \bar{z}} \right\} * \\ + 12 (1-\sigma^2) \left(\frac{\ell}{m}\right)^3 \left(\frac{\mu U}{Eh}\right) \left(\left(\frac{\ell}{L}\right)^2 \left[\left(\frac{\ell}{L}\right) \frac{\partial \bar{r}}{\partial \bar{x}} + \sigma \frac{\partial \bar{s}}{\partial \bar{y}} \right] \frac{\partial^2 \bar{\eta}}{\partial \bar{x}^2} \right. \\ \left. + \left[\frac{\partial \bar{s}}{\partial \bar{y}} + \sigma \left(\frac{\ell}{L}\right) \frac{\partial \bar{r}}{\partial \bar{x}} \right] \frac{\partial^2 \bar{\eta}}{\partial \bar{y}^2} + (1-\sigma) \left(\frac{\ell}{L}\right) \left[\frac{\partial \bar{r}}{\partial \bar{y}} + \left(\frac{\ell}{L}\right) \frac{\partial \bar{s}}{\partial \bar{x}} \right] \frac{\partial^2 \bar{\eta}}{\partial \bar{x} \partial \bar{y}} \right)$$

$$\begin{aligned}
 & + 12(1 - \sigma^2) \left(\frac{\ell}{m}\right)^3 \left(\frac{\mu U}{Eh}\right) \left(\frac{\ell}{L}\right) \left[(1 - \sigma^2) \left(\frac{\rho \ell^2}{ET^2}\right) \frac{\partial^2 \bar{r}}{\partial \bar{t}^2} \right. \\
 & \quad \left. + \frac{\partial \bar{u}}{\partial \bar{z}} \Big|_* + \alpha \left(\frac{h}{L}\right)^2 \frac{\partial \bar{w}}{\partial \bar{x}} \Big|_* - 1 \right] \frac{\partial \bar{\eta}}{\partial \bar{x}} \\
 & \quad + \left[(1 - \sigma^2) \left(\frac{\rho \ell^2}{ET^2}\right) \frac{\partial^2 \bar{s}}{\partial \bar{t}^2} \right. \\
 & \quad \left. + (1 - \sigma^2) \left(\frac{\ell}{m}\right) \left(\frac{\mu U}{Eh}\right) \left(\frac{L}{UT}\right) \left(\frac{\ell}{L}\right) \frac{\partial \bar{v}}{\partial \bar{z}} \Big|_* + \alpha \left(\frac{h}{\ell}\right)^2 \frac{\partial \bar{w}}{\partial \bar{y}} \Big|_* \right] \frac{\partial \bar{\eta}}{\partial \bar{y}} \Bigg)
 \end{aligned}
 \tag{5.11}$$

Similarly, the boundary conditions can be written

$$\begin{aligned}
 \frac{\partial \bar{p}}{\partial \bar{x}} \Big|_{\bar{x}=0} &= - \left(\frac{-\beta L}{P_o}\right) \left\{ 1 + \sum_{n=1}^j \left[a_n \cos (2n\pi \bar{t}) \right. \right. \\
 & \quad \left. \left. + b_n \sin (2n\pi \bar{t}) \right] \right\}
 \end{aligned}
 \tag{5.12}$$

$$\begin{aligned}
 \bar{p} \Big|_{\bar{x}=0} &= 1 + \sum_{n=1}^k \left[c_n \cos (2n\pi \bar{t}) \right. \\
 & \quad \left. + d_n \sin (2n\pi \bar{t}) \right]
 \end{aligned}
 \tag{5.13}$$

$$\bar{u} \Big|_* = (1 - \sigma^2) \left(\frac{\ell}{m}\right) \left(\frac{\mu U}{Eh}\right) \left(\frac{L}{UT}\right) \left(\frac{\ell}{L}\right) \frac{\partial \bar{r}}{\partial \bar{t}}
 \tag{5.14}$$

$$\bar{v}|_* = \frac{\partial \bar{s}}{\partial \bar{t}} \quad 5.15$$

$$\begin{aligned} \bar{w}|_* &= \frac{1}{1 + \left\{ \left(\frac{\eta_o}{\alpha h} \right) \left(\frac{L}{UT} \right) \right\}} = \bar{w}_p \\ &+ \frac{\left\{ \left(\frac{\eta_o}{\alpha h} \right) \left(\frac{L}{UT} \right) \right\}}{1 + \left\{ \left(\frac{\eta_o}{\alpha h} \right) \left(\frac{L}{UT} \right) \right\}} \frac{\partial \bar{\eta}}{\partial \bar{t}} \end{aligned} \quad 5.16$$

$$\begin{aligned} \bar{w}_p &= \left(\frac{P_o}{\Delta P_m} \right) \left[\left\{ \bar{P} - 2\alpha \left(\frac{\mu U}{Eh} \right) \left(\frac{E}{P_o} \right) \left(\frac{h}{L} \right) \frac{\partial \bar{w}}{\partial \bar{z}} \right. \right. \\ &\quad \left. \left. - \left(\frac{P_{Di}}{P_o} \right) \bar{P}_D \right\} + \left(\frac{\Delta P_{os}}{P_o} \right) \right] \end{aligned} \quad 5.17$$

where

$$\bar{P}_D = 1 - (1 - \bar{x}) \left(\frac{\Delta P_D}{P_o} \right) \left(\frac{P_o}{P_{Di}} \right) \quad 5.18$$

and

$$\begin{aligned} \Delta P_m &= \frac{m'}{\phi} W_p \\ &= P_o \left\{ 1 - 2\alpha \left(\frac{\mu U}{Eh} \right) \left(\frac{E}{P_o} \right) \left(\frac{h}{L} \right) \right. \\ &\quad \left. - \left(\frac{P_{Di}}{P_o} \right) + \left(\frac{\Delta P_D}{P_o} \right) + \left(\frac{\Delta P_{os}}{P_o} \right) \right\} \end{aligned} \quad 5.19$$

$$\bar{\eta}|_e = 0 \quad 5.20$$

$$\left. \frac{\partial^2 \bar{\eta}}{\partial \bar{N}^2} \right|_e = 0 \quad 5.21$$

$$\bar{r}|_e = 0 \quad 5.22$$

$$\bar{s}|_e = 0 \quad 5.23$$

These equations and boundary conditions indicate that the significant nondimensional parameters for the system are

$$\begin{aligned} & \sigma, \left(\frac{\ell}{m} \right), \left(\frac{\mu U}{Eh} \right), \left(\frac{L}{UT} \right), \left(\frac{\ell}{L} \right), \alpha, \left(\frac{\eta_o}{h} \right), \\ & \left(\frac{P_o}{\rho_f U^2} \right), R, \left(\frac{h}{L} \right), \left(\frac{h}{\ell} \right), \left(\frac{\rho \ell^2}{ET^2} \right), \left(\frac{P_o}{E} \right), \left(\frac{-BL}{P_o} \right), \\ & \left(\frac{\Delta P_m}{P_o} \right), \left(\frac{P_{Di}}{P_o} \right), \left(\frac{\Delta P_{os}}{P_o} \right) \text{ and } \left(\frac{\Delta P_D}{P_o} \right). \end{aligned}$$

All of these have physical meaning. The parameter σ is Poisson's ratio; $\left(\frac{\ell}{m} \right)$, the ratio of channel half-width to wall thickness; $\left(\frac{\mu U}{Eh} \right)$, a measure of the importance of viscous shear forces compared to elastic forces; $\left(\frac{L}{UT} \right)$, the Strouhal number, a measure of the importance of fluid unsteady effects compared to fluid inertia effects; $\left(\frac{\ell}{L} \right)$, the ratio of channel half-width to length; α , a

measure of the importance of the flow through the porous walls compared with the axial flow; $\left(\frac{\eta_o}{h}\right)$, the ratio of the characteristic normal component of wall displacement to the unstressed channel half-thickness; $\left(\frac{P_o}{\rho_f U^2}\right)$, the Euler number, the ratio of pressure to fluid inertia forces; R , the modified inlet axial flow Reynolds number, a measure of the importance of fluid inertia forces compared with viscous forces; $\left(\frac{h}{L}\right)$, the ratio of unstressed channel half-thickness to channel length; $\left(\frac{h}{\ell}\right)$, the ratio of the unstressed channel half-thickness to the half-width; $\left(\frac{\rho \ell^2}{ET^2}\right)$, a measure of the importance of wall inertia to wall elastic forces; $\left(\frac{P_o}{E}\right)$, a measure of the importance of pressure to wall elastic forces; $\left(\frac{-BL}{P_o}\right)$, the ratio of the absolute value of the inlet axial pressure gradient to the inlet pressure divided by the channel length; $\left(\frac{\Delta P_m}{P_o}\right)$, the ratio of the maximum total across-membrane pressure difference to the inlet blood pressure; $\left(\frac{P_{Di}}{P_o}\right)$, the ratio of the dialysate pressure at the dialysate inlet to the inlet blood pressure; $\left(\frac{\Delta P_{os}}{P_o}\right)$, the ratio of the osmotic pressure difference to the inlet blood pressure; and $\left(\frac{\Delta P_D}{P_o}\right)$, the ratio of the dialysate pressure drop to the inlet blood pressure.

In particular, the parameter α can be interpreted as the ratio of a Reynolds number for the flow through the porous walls, $\left(\frac{W_p h}{v}\right)$, to the modified inlet axial Reynolds number, R ; that is

$$\frac{\left(\frac{W_p h}{v}\right)}{\left(\frac{UL}{v}\right) \left(\frac{h}{L}\right)^2} = \left(\frac{W_p L}{Uh}\right) = \alpha \quad 5.24$$

As such, this parameter is a measure of the relative importance of the porous wall and axial mass flows.

Also, the dimensionless group $\left\{ \frac{1}{\alpha} \left(\frac{\eta_o}{h} \right) \left(\frac{L}{UT} \right) \right\}$ has special significance as a measure of the relative importance of wall unsteadiness in the normal direction to the flow through the porous walls. Hence, the group describes the relative importance of the terms on the right-hand-side of boundary condition 5.16. (Note that this group depends on the parameter α .)

5.3 Derivation of Simplified Governing Equations and Boundary Conditions.

The values of the various nondimensional parameters for a modified Kii1 kidney can be deduced from characteristic data taken from Billmeyer⁽³⁾, Cole, Pollard and Murray⁽⁷⁾, Merrill and Wells⁽¹⁸⁾, McDonald⁽⁴²⁾, Sachs and Funck-Bretano⁽¹⁰⁾, Sparks⁽²⁹⁾ and Wilcox, Freeman, Maher and Schreiner⁽⁴⁰⁾. The data is as follows:

L = channel length = 111 cm.

l = channel half-width = 10 cm.

h = unstressed channel half-thickness
= 2.0×10^{-2} cm.

T = period of one blood pulse = 0.8 sec.

U = characteristic axial blood velocity
= 1.56 cm/sec.

W_p = maximum velocity of flow through the porous
walls = $1.7 \times 10^{-5} \text{ cm/sec.}$

- P_o = inlet blood pressure
= 12.5×10^4 dynes/cm²
- η_o = characteristic normal wall displacement
= 2×10^{-3} cm.
- P_{Di} = dialysate pressure at dialysate inlet
= 6.4×10^4 dynes/cm²
- ΔP_D = dialysate pressure drop
= 5×10^4 dynes/cm²
- ΔP_{os} = maximum osmotic pressure difference
= 1.0×10^6 dynes/cm²
- $-\beta$ = absolute value of the inlet blood axial pressure gradient
= 3.28×10^3 dynes/cm³
- ΔP_m = maximum total pressure difference across the membranes
= 1.0×10^6 dynes/cm²
- μ = dynamic viscosity of blood
= 4.2×10^{-2} gm/cm-sec.
- ρ_f = density of whole blood
= 1.06 gm/cm³
- E = Young's modulus for polypropylene walls
= 1.4×10^{10} dynes/cm²
- σ = Poisson's ratio = 0.3
- ρ = wall density = 0.905 gm/cm³
- m = wall thickness = 4.63 cm.

Certain of the above values, however, do not appear explicitly in the literature cited. Instead, they are estimated from other flow and wall information. (See Appendices A and B.)

This data yields the following values for the significant non-dimensional parameters:

$$\begin{array}{ll}
 \sigma = 0.3 & \left(\frac{\rho \ell^2}{ET} \right) = 1.01 \times 10^{-8} \\
 \left(\frac{\ell}{m} \right) = 2.16 & \left(\frac{P_o}{E} \right) = 8.93 \times 10^{-6} \\
 \left(\frac{\mu U}{Eh} \right) = 2.34 \times 10^{-10} & \\
 \left(\frac{L}{UT} \right) = 80 & \left(\frac{-\beta L}{P_o} \right) = 0.262 \\
 \left(\frac{\ell}{L} \right) = 9.07 \times 10^{-2} & \left(\frac{\Delta P_m}{P_o} \right) = 8.0 \\
 \alpha = 5.5 \times 10^{-2} & \\
 \left(\frac{\eta_o}{h} \right) = 0.1 & \left(\frac{P_{Di}}{P_o} \right) = 0.512 \\
 \left(\frac{P_o}{\rho_f U^2} \right) = 4.85 \times 10^4 & \left(\frac{\Delta P_{os}}{P_o} \right) = 8.0 \\
 R = 1.58 \times 10^{-4} & \\
 \left(\frac{h}{L} \right) = 2.0 \times 10^{-4} & \left(\frac{\Delta P_D}{P_{Di}} \right) = 0.78 \\
 \left(\frac{h}{\ell} \right) = 2.0 \times 10^{-3} &
 \end{array}$$

Since the modified inlet Reynolds number R governs the importance of axial fluid inertia effects and also is small compared to unity, a perturbation solution of the nondimensional equations and boundary conditions will be sought using this Reynolds number as the perturbation parameter. The other parameters appearing in the

equations and boundary conditions, then, will be ordered, for the case under study, with respect to powers of the parameter R . The ordering, moreover, will be such that a parameter will be considered to be of order i in R if its value lies between $R^{i-\frac{1}{2}}$ and $R^{i+\frac{1}{2}}$.

For instance, a parameter of order zero in R will be one whose value lies between $R^{-\frac{1}{2}}$ and $R^{\frac{1}{2}}$. (See, for instance, Van Dyke⁽³⁶⁾).

The ordering of parameters other than R in powers of R is as follows:

$$\begin{aligned} \left(\frac{\mu U}{Eh} \right) &= \bar{A} R^2 & \left(\frac{h}{\ell} \right) &= \bar{D} R \\ \left(\frac{P_o}{\rho_f U^2} \right) &= \bar{B} R^{-1} & \left(\frac{\rho \ell^2}{ET} \right) &= \bar{E} R^2 \\ \left(\frac{h}{L} \right) &= \bar{C} R & \left(\frac{P_o}{E} \right) &= \bar{F} R \end{aligned} \quad 5.25$$

where the constants $\bar{A}, \bar{B}, \bar{C}, \bar{D}, \bar{E}$, and \bar{F} all are of order zero in R . Parameters other than R not appearing above are also all of order zero in R . (The ordering given by equations 5.25, of course, is valid only for the value of R associated with the problem under study. Thus this ordering need not be the same in other problems and for other values of R .)

Next, solutions of the seven unknowns will be sought in the form

$$\bar{u} = \bar{u}_0 + \bar{u}_1 R + \bar{u}_2 R^2 + \dots$$

$$\bar{v} = \bar{v}_0 + \bar{v}_1 R + \dots$$

$$\bar{w} = \bar{w}_0 + \bar{w}_1 R + \dots$$

$$\bar{p} = \bar{p}_0 + \bar{p}_1 R + \dots$$

$$\bar{r} = \bar{r}_0 + \bar{r}_1 R + \dots$$

$$\bar{s} = \bar{s}_0 + \bar{s}_1 R + \dots$$

$$\bar{\eta} = \bar{\eta}_0 + \bar{\eta}_1 R + \dots$$

5.26

The barred quantities on the right-hand sides of the above relations are all independent of the parameter R but still dependent on the other parameters of the problem.

Now, substitution of transformations 5.25 and 5.26 into the nondimensional flow equations for the system (equations 5.9 and 5.10) and collecting terms of like powers in the parameter R gives

$$\begin{aligned} & \left[\frac{\partial \bar{u}_0}{\partial \bar{x}} + \left\{ \alpha + \left(\frac{\eta_b}{h} \right) \left(\frac{L}{UT} \right) \right\} \frac{\partial \bar{w}_0}{\partial \bar{z}} \right] \\ & + \left[\frac{\partial \bar{u}_1}{\partial \bar{x}} + \left\{ \alpha + \left(\frac{\eta_0}{h} \right) \left(\frac{L}{UT} \right) \right\} \frac{\partial \bar{w}_1}{\partial \bar{z}} \right] R + \dots = 0 \end{aligned}$$

5.27

$$\left[\bar{B} \frac{\partial \bar{p}_0}{\partial \bar{x}} - \frac{\partial^2 \bar{u}_0}{\partial \bar{z}^2} \right]$$

$$\begin{aligned}
 & + \left[\left(\frac{L}{UT} \right) \frac{\partial \bar{u}_o}{\partial \bar{t}} + \bar{u}_o \frac{\partial \bar{u}_o}{\partial \bar{x}} + \left\{ \alpha + \left(\frac{n_o}{h} \right) \left(\frac{L}{UT} \right) \right\} \bar{w}_o \frac{\partial \bar{u}}{\partial \bar{z}} \right. \\
 & \left. + \bar{B} \frac{\partial \bar{P}_1}{\partial \bar{x}} - \frac{\partial^2 \bar{u}_1}{\partial \bar{z}^2} \right] R + \dots = 0 \\
 & \left[\bar{B} \frac{\partial \bar{P}_o}{\partial \bar{y}} \right] + \left[\bar{B} \frac{\partial \bar{P}_1}{\partial \bar{y}} \right] R + \dots = 0 \\
 & \left[\bar{B} \frac{\partial \bar{P}_o}{\partial \bar{z}} \right] + \left[\bar{B} \frac{\partial \bar{P}_1}{\partial \bar{z}} \right] R + \dots = 0
 \end{aligned}$$

5.28

Since the unknowns in each bracket of terms above are independent of the parameter R, each bracket must be separately equal to zero in order for the equations to be valid for all values of the parameter R less than unity. Hence, the zeroth-order in R flow equations are the following:

$$\frac{\partial \bar{u}_o}{\partial \bar{x}} + \left\{ \alpha + \left(\frac{n_o}{h} \right) \left(\frac{L}{UT} \right) \right\} \frac{\partial \bar{w}_o}{\partial \bar{z}} = 0 \quad 5.29$$

$$\bar{B} \frac{\partial \bar{P}_o}{\partial \bar{x}} - \frac{\partial^2 \bar{u}_o}{\partial \bar{z}^2} = 0$$

$$\frac{\partial \bar{P}_o}{\partial \bar{x}} = 0$$

$$\frac{\partial \bar{P}_o}{\partial \bar{z}} = 0 \quad 5.30$$

In a similar manner the zeroth-order in R wall equations and boundary conditions can be shown to be

$$\begin{aligned}
 & \left(\frac{\ell}{L}\right)^2 \frac{\partial^2 \bar{r}_o}{\partial \bar{x}^2} + \sigma \left(\frac{\ell}{L}\right) \frac{\partial^2 \bar{s}_o}{\partial \bar{x} \partial \bar{y}} + \frac{1-\sigma}{2} \left[\frac{\partial^2 \bar{r}_o}{\partial \bar{y}^2} + \left(\frac{\ell}{L}\right) \frac{\partial^2 \bar{s}_o}{\partial \bar{x} \partial \bar{y}} \right] \\
 & - \left[\frac{\partial \bar{u}_o}{\partial \bar{z}} - 1 \right]_* = 0 \\
 & \frac{\partial^2 \bar{s}_o}{\partial \bar{y}^2} + \sigma \left(\frac{\ell}{L}\right) \frac{\partial^2 \bar{r}_o}{\partial \bar{x} \partial \bar{y}} + \frac{1-\sigma}{2} \left[\left(\frac{\ell}{L}\right) \frac{\partial^2 \bar{r}_o}{\partial \bar{x} \partial \bar{y}} + \left(\frac{\ell}{L}\right)^2 \frac{\partial^2 \bar{s}_o}{\partial \bar{x}^2} \right] = 0 \\
 & \left(\frac{\ell}{L}\right)^4 \frac{\partial^4 \bar{\eta}_o}{\partial \bar{x}^4} + 2 \left(\frac{\ell}{L}\right)^2 \frac{\partial^4 \bar{\eta}_o}{\partial \bar{x}^2 \partial \bar{y}^2} + \frac{\partial^4 \bar{\eta}_o}{\partial \bar{y}^4} = \\
 & 12(1-\sigma^2) \left(\frac{\ell}{m}\right) \left(\frac{h}{\eta_o}\right) \left(\frac{\ell}{h}\right) \left(\frac{P_o}{E}\right) \bar{P}_o
 \end{aligned} \tag{5.31}$$

$$\begin{aligned}
 \left. \frac{\partial \bar{P}_o}{\partial \bar{x}} \right|_{\bar{x}=0} = - \left(\frac{-\beta L}{P_o} \right) \left\{ 1 + \sum_{n=1}^j \left[a_n \cos(2n\bar{\eta}\bar{t}) \right. \right. \\
 \left. \left. + b_n \sin(2n\bar{\eta}\bar{t}) \right] \right\}
 \end{aligned} \tag{5.32}$$

$$\begin{aligned}
 \bar{P} \big|_{\bar{x}=0} = 1 + \sum_{n=1}^k \left[c_n \cos(2n\bar{\eta}\bar{t}) \right. \\
 \left. + d_n \sin(2n\bar{\eta}\bar{t}) \right]
 \end{aligned} \tag{5.33}$$

$$\left. \bar{u}_o \right|_* = 0 \tag{5.34}$$

$$\left. \bar{v}_o \right|_* = \frac{\partial \bar{s}_o}{\partial \bar{t}} \quad 5.35$$

$$\left. \bar{w}_o \right|_* = \frac{1}{1 + \left\{ \frac{1}{\alpha} \left(\frac{\eta_o}{h} \right) \left(\frac{L}{UT} \right) \right\}} \bar{w}_p + \frac{\left\{ \frac{1}{\alpha} \left(\frac{\eta_o}{h} \right) \left(\frac{L}{UT} \right) \right\}}{1 + \left\{ \frac{1}{\alpha} \left(\frac{\eta_o}{h} \right) \left(\frac{L}{UT} \right) \right\}} \frac{\partial \eta}{\partial \bar{t}} \quad 5.36$$

$$\bar{w}_p = \left(\frac{P_o}{\Delta P_m} \right) \left[\left\{ \bar{P}_o - \left(\frac{P_{Di}}{P_o} \right) \bar{P}_D \right\}_* + \left(\frac{\Delta P_{os}}{P_o} \right) \right] \quad 5.37$$

$$\left. \bar{\eta}_o \right|_e = 0 \quad 5.38$$

$$\left. \frac{\partial^2 \bar{\eta}_o}{\partial \bar{N}^2} \right|_e = 0 \quad 5.39$$

$$\left. \bar{r}_o \right|_e = 0 \quad 5.40$$

$$\left. \bar{s}_o \right|_e = 0 \quad 5.41$$

Equations 5.29 through 5.41, then, are the simplified governing equations and boundary conditions for the problem under consideration. Their structure is such that the wall motion is always coupled to the flow. However, in the steady (pulse period $T = \infty$), non-porous (flow velocity through the porous walls $w_p = 0$), rigid wall (flexural rigidity $E = \infty$) case, the equations reduce to those for fully-developed channel flow. Their relation, to the porous channel equations of Berman⁽²⁾ will be discussed in the next section.

The solution of these equations provides a solution to the problem under study accurate to the order of the perturbation parameter R .

5.4 Comparison of the Nondimensional Flow Equations and Solution Scheme with the Equations and Scheme of Berman.

As pointed out in Chapter I, Berman ⁽²⁾ and a number of other investigators (28, 39, 31, 32, 33, 43, 44, 45) have previously studied flows in porous, rigid channels. It would be particularly interesting to compare their basic equations and solution methods with the equations and scheme of this study. However, because the work of these investigators is based on the approach taken by Berman ⁽²⁾, such a comparison need only be made with Berman's studies.

In the first place, the flow equations and boundary conditions of this analysis reduce to Berman's for steady (pulse period $T = \infty$), rigid channel (flexural rigidity $D = \infty$), two-dimensional (channel half-width $l = \infty$), flow in which the velocity of flow through the porous walls, w_p , is independent of the axial and spanwise coordinates ($w_p = \text{constant}$). Hence, while the flows described in the two studies are somewhat similar, they do have important physical differences.

A more fundamental difference lies in the choice of perturbation parameter. (Both analyses seek perturbation solutions of relevant equations.) Berman, on the one hand, uses a Reynolds number based on the flow through the porous walls, R_B , and solves the

case for which this Reynolds number is small compared to unity. In the present study, however, the modified axial flow Reynolds number R , is used. This is advantageous in that it shows clearly that for a wide class of flows in porous channels the importance of axial inertia effects depends on the latter Reynolds number, not one based on the porous flow. (See equations 5.10). For example, for values of the modified axial flow Reynolds number small compared to unity, axial inertia effects in these flows can be neglected. To the contrary, in Berman's scheme, in which the smallness of the modified axial flow Reynolds number compared to unity is a tacit assumption, axial inertia forces can be neglected only in the absence of flow through the porous walls.

Berman's porous wall solutions, which include inertia effects, are, of course, valid even when the Reynolds number R is small compared to unity. But, at least to zeroth order in the modified axial Reynolds number, the use of the full Navier-Stokes equations (including nonlinear inertia terms) is in this case unnecessary. In fact, in Section 6.3 it will be shown that the general steady flow solutions of the simplified equations obtained in the last section reduce to Berman's for the case of constant velocity of flow through the porous walls.

In addition, one important consequence of the fact that nonlinear inertia terms can be neglected in this situation is that major mathematical difficulties are removed in the solution of slow, viscous flows in porous channels for which the velocity of flow

through the walls is not a constant. Solutions of these flows are now possible when this velocity is, for example, a function of the pressure field. Such is the case in the problem under study.

Another fundamental difference between the two analyses is that the importance of wall porosity effects is shown here to be governed by a second parameter, α , the ratio of Berman's Reynolds number to the modified axial flow Reynolds number. (See equation 5.24). This second parameter is implicit in Berman's solutions, but it is given no special significance.

As a Reynolds number ratio, this parameter is, moreover, a measure of the importance of the flow through the porous walls compared to the axial flow. And since in the present study the parameter α is assumed to be of order unity or less, the simplified equations derived are not limited only to situations in which the mass flow through the porous walls is small compared to the axial mass flow. In fact, for a velocity of flow through the porous walls independent of the axial and spanwise coordinates and for a value of this parameter equal to unity, the inlet flow will just balance the flow through the porous walls. For values of this parameter greater than unity the channel will empty.

A special situation arises, however, when the absolute value of the parameter α is larger than unity. (This is possible for either large injection or large suction of fluid at the porous walls). In this case the importance of axial inertia forces is governed not by the modified axial flow Reynolds number, but rather by the product

of that Reynolds number and the Reynolds number ratio. Consider, for instance, equation 5.10a rewritten for steady flow:

$$R \left(\bar{u} \frac{\partial \bar{u}}{\partial x} + \alpha \bar{w} \frac{\partial \bar{u}}{\partial z} \right) = - R \left(\frac{P_o}{\rho_f U^2} \right) \frac{\partial \bar{P}}{\partial x} + \left(\frac{h}{L} \right)^2 \frac{\partial^2 \bar{u}}{\partial x^2} + \left(\frac{h}{\ell} \right) \frac{\partial^2 \bar{u}}{\partial y^2} + \frac{\partial^2 \bar{u}}{\partial z^2} \quad 5.42$$

It is clear from this equation that at least one of the axial inertia terms is now of order $R |\alpha|$, not of order R . (The other axial inertia term may also be of order $R |\alpha|$. However, this cannot be shown from the ordering used in the present problem.)

Moreover, the product of parameters $R \alpha$, as it turns out, is exactly Berman's Reynolds number for the flow through the porous walls. The obvious implication is that in this flow situation the flow through the porous walls is of greater importance than the axial flow. Axial inertia effects are then sensibly important regardless of how small the modified axial Reynolds number may be. Furthermore, in this case the extent of importance of these effects is governed by the parameter R_B . A set of equations like Berman's, which retains inertia terms, must be solved. Hence, while Berman's equations unnecessarily keep inertia terms for small values of the parameter R_B other investigators are correct in using these equations to obtain solutions for large (in absolute value) values of the parameter R_B . (In the latter situation the reciprocal of R_B is used as the perturbation parameter.)

Phenomena associated with flow unsteadiness and channel wall elasticity are also introduced here. Although the mathematical model is such that the flow is largely independent of the wall motions, but the wall motions are dependent on the flow, the simplified equations and boundary conditions permit an investigation of the effects of wall porosity on the normal wall displacement.

In the unsteady situation, moreover, the flow is shown to be coupled to the wall motions through the wall boundary condition on the normal fluid velocity component. The importance of this coupling - in the form of wall unsteadiness in the normal direction - relative to wall porosity effects is governed by the parameter

$\left\{ \frac{1}{\alpha} \left(\frac{\eta_0}{h} \right) \left(\frac{L}{UT} \right) \right\}$, a combination of the porosity parameter α , the ratio of the characteristic normal wall displacement η_0 to the unstressed channel half-thickness h , and the Strouhal number. (See boundary condition 5.36).

In short, it is felt that the parameters of this analysis give greater physical insight to porous channel flows than those used by Berman. First it is made clear that axial inertia forces need not always be important. In particular, in flows with finite wall porosity for values of the porosity parameter less than or equal to order unity, these forces are shown to be negligible for values of the parameter R small compared to unity. The simplified equations and boundary conditions obtained are valid for this case. (See Appendix C for further comments on the above).

Secondly, it is pointed out that other investigators have been correct in using Berman's equations to obtain solutions for large

(in absolute value) values of the Reynolds number R_B .

5.5 Summary.

The simplifications arrived at in determining the final equations of the last section have physical significance. In the first place, the flow has been shown to be two-dimensional to first order in the parameter R ; the spanwise fluid velocity component is zero to this order, while the pressure field and axial and normal fluid velocity components are independent of the spanwise coordinate. This is a consequence both of the smallness of the unstressed channel half-thickness compared to channel width and of the smallness spanwise wall unsteadiness.

Secondly, the pressure field has also been shown to be independent of the normal coordinate, to first order in the parameter R . This results from the smallness of the unstressed channel half-thickness compared to channel length. Hence, the pressure field is a function of the axial coordinate alone.

As for the wall motion, it is apparent that, to first order in the parameter R , the normal component of wall displacement can be solved for independently of the axial and spanwise components of wall displacement. No coupling exists to this order between the normal and the other components. This is largely a consequence of the dominance of wall bending forces over forces arising from pure extensions or wall stretching due to fluid viscous shear at the walls.

A determination of the axial and spanwise components of wall displacement, on the other hand, involves the solution of two simultaneous linear partial differential equations.

Next, fluid inertia forces have been shown to be unimportant to first order in the Reynolds number R . (This has been discussed in the last section).

The neglect of viscous terms in the zeroth-order in the parameter R normal fluid momentum equation, on the other hand, indicates that the normal component of fluid velocity at the channel inlet cannot be specified. Ideally, because the flow at the inlet is assumed to be fully-developed, one would like to specify this velocity component to be zero at the inlet. But this cannot be done unless the full Navier-Stokes equations are used. Therefore, the normal component of fluid velocity will take on some non-zero distribution at the inlet and the zeroth-order equations will be somewhat in error very near this location. This error, however, is standard in many analyses of fluid flow in channels with low aspect ratios.

Then, too, since the unknowns of the flow are independent of the spanwise coordinate to first order in the parameter R , boundary conditions cannot be satisfied for the axial and normal fluid velocity components at the non-porous side walls; that is, these velocity components cannot be made to vanish at the side walls. However, the solutions for the flow are valid away from these walls.

Finally, the zeroth-order flow equations and boundary conditions can be seen to become uncoupled from the wall motion for steady flow.

In fact, were it not for the coupling with wall unsteadiness in the normal direction provided by the boundary condition at the porous walls on the normal fluid velocity component, this would be true for unsteady flow as well. The importance of such coupling relative to wall porosity effects is governed by the dimensionless group

$$\left\{ \frac{1}{\alpha} \left(\frac{\eta_o}{h} \right) \left(\frac{L}{UT} \right) \right\} .$$

CHAPTER VI

Steady Flow in a Porous Elastic Channel for Modified Inlet Axial Reynolds Numbers Small Compared to Unity.

The simplified governing equations derived in the previous chapter (equations 5.29 through 5.41) will now be solved for the steady flow case (blood pulse period $T = \infty$). This flow case physically corresponds to the situation in which several feet of body-to-kidney interconnecting tubing is used. Because of tube elasticity, such lengths of tubing tend to "damp out" the pulsatile portion of the blood flow.

The axial and spanwise wall displacement components, however, will not be solved for. In the first place, the normal wall displacement component is of much greater interest. Secondly, the information known concerning the axial and spanwise wall displacement components is incomplete. Apart from an order of magnitude, nothing is known about the dialysate flow contribution to the viscous shear stresses acting on the walls

6.1 General Solution for the Flow.

The velocity components and pressure will now be solved for exactly. First, equations 5.29, 5.30, 5.36 and 5.37 combine in the steady case to give (zeroth-order subscripts omitted)

$$\frac{\partial \bar{u}}{\partial \bar{x}} + \alpha \frac{\partial \bar{w}}{\partial \bar{z}} = 0 \quad 6.1$$

$$\bar{B} \frac{d\bar{P}}{dx} - \frac{\partial^2 \bar{u}}{\partial \bar{z}^2} = 0 \quad 6.2$$

$$\bar{w} \Big|_* = \left(\frac{P_o}{\Delta P_m} \right) \bar{P} - \left(\frac{P_{Di}}{P_o} \right) \bar{P}_D + \left(\frac{\Delta P_{os}}{P_o} \right) \quad 6.3$$

Integrating equation 6.2 and making use of boundary conditions 5.34 for steady flow results in

$$\bar{u} = \frac{1}{2} \bar{B} \left(- \frac{d\bar{P}}{dx} \right) (1 - \bar{z}^2) \quad 6.4$$

Equations 6.1 and 6.3 then become

$$\bar{w} = - \frac{1}{2\alpha} \bar{B} \left(\frac{d^2 \bar{P}}{dx^2} \right) \left(\bar{z} - \frac{1}{3} \bar{z}^3 \right) \quad 6.5$$

$$\left(\frac{1}{3\alpha} \bar{B} \right) \frac{d^2 \bar{P}}{dx^2} = \left(\frac{P_o}{\Delta P_m} \right) \bar{P} - \left(\frac{P_{Di}}{P_o} \right) \bar{P}_D + \left(\frac{\Delta P_{os}}{P_o} \right) \quad 6.6$$

Equation 6.6 is an ordinary differential equation for the dimensionless pressure \bar{P} . Once it is solved, the axial and normal velocity components can be obtained from relations 6.4 and 6.5.

The solution of equation 6.6 is

$$\begin{aligned} \bar{P} = & C_1 \sinh \sqrt{\gamma} \bar{x} + C_2 \cosh \sqrt{\gamma} \bar{x} \\ & + \left(\frac{P_{Di}}{P_o} \right) \bar{P}_D - \left(\frac{\Delta P_{os}}{P_o} \right) \end{aligned} \quad 6.7$$

where \bar{P}_D is a linear function of the dimensionless axial coordinate (See equation 5.18) and where C_1 and C_2 are constants to be deter-

mined from the inlet conditions on the pressure and pressure gradient.

The parameter γ is defined as

$$\gamma = \frac{3\alpha}{\bar{B}} \left(\frac{P_o}{\Delta P_m} \right) . \quad 6.8$$

Making use of the transformation 5.25 b, however, the constant \bar{B} can be eliminated from the above expression. This gives

$$\gamma = \frac{3\alpha}{R} \left(\frac{\rho_f U^2}{P_o} \right) \left(\frac{P_o}{\Delta P_m} \right) . \quad 6.9$$

The parameter γ can be seen to be simply a modified version of the Reynolds number ratio α .

Further, from boundary conditions 5.32 and 5.33 for steady flow, it can be shown that

$$C_1 = - \frac{1}{\sqrt{\gamma}} \left(\frac{-\beta L}{P_o} \right) - \frac{1}{\sqrt{\gamma}} \left(\frac{\Delta P_D}{P_o} \right) \quad 6.10$$

$$C_2 = 1 - \left(\frac{P_{Di}}{P_o} \right) + \left(\frac{\Delta P_D}{P_o} \right) \left(\frac{\Delta P_{os}}{P_o} \right) = \left(\frac{\Delta P_m}{P_o} \right) \quad 6.11$$

Substituting relations 6.10 and 6.11 into equation 6.7 now gives the dimensionless pressure drop:

$$\begin{aligned} \frac{P-P_o}{P_o} = & - \left(\frac{-\beta L}{P_o} \right) \frac{\sinh \sqrt{\gamma} \bar{x}}{\sqrt{\gamma}} \\ & + \left(\frac{\Delta P_m}{P_o} \right) \left\{ \cosh \sqrt{\gamma} \bar{x} - 1 \right\} \\ & + \left(\frac{\Delta P_D}{P_o} \right) \left\{ \bar{x} - \frac{\sinh \sqrt{\gamma} \bar{x}}{\sqrt{\gamma}} \right\} \end{aligned} \quad 6.12$$

Finally, with the aid of equation 6.12, the dimensionless axial and normal velocity components can be written

$$\begin{aligned} \frac{u}{U} = & \frac{1}{2}R \left(\frac{P_o}{\rho_f U^2} \right) \left[\left(\frac{-\beta L}{P_o} \right) \cosh \sqrt{\gamma} \bar{x} \right. \\ & - \left(\frac{\Delta P_m}{P_o} \right) \sqrt{\gamma} \sinh \sqrt{\gamma} \bar{x} \\ & \left. + \left(\frac{\Gamma P_D}{P_o} \right) \left\{ \cosh \sqrt{\gamma} \bar{x} - 1 \right\} \right] (1 - \bar{z}^2) \end{aligned} \quad 6.13$$

$$\begin{aligned} \frac{w}{W_p} = & \frac{3}{2} \left[\cosh \sqrt{\gamma} \bar{x} \right. \\ & - \left. \frac{\left(\frac{-\beta L}{P_o} \right) + \left(\frac{\Delta P_D}{P_o} \right)}{\left(\frac{\Delta P_m}{P_o} \right)} \sinh \sqrt{\gamma} \bar{x} \right] \bar{x} \left(\bar{z} - \frac{1}{3} \bar{z}^3 \right) \end{aligned} \quad 6.14$$

The spanwise component of velocity has not been solved for since it is smaller than order one in the perturbation parameter R.

6.2 General Solution for the Normal Wall Displacement.

The solution of the normal wall displacement equation (equation 5.31) subject to appropriate boundary conditions yields the dimensionless wall displacement, $\frac{\eta}{\eta_o}$, as a function of the axial and spanwise coordinates.

To begin with, the wall boundary conditions (equations 5.38 and 5.39) are satisfied if the dimensionless wall displacement is taken to be the Fourier series

$$\frac{\eta}{\eta_0} = \sum_{m=1}^{\infty} \sum_{n=1}^{\infty} \bar{A}_{mn} \sin m \Pi \bar{x} \sin n \Pi (\bar{y} + 0.5) \quad 6.15$$

The coefficients \bar{A}_{mn} , yet to be determined, are such that equation 5.31 is satisfied.

Wang (37) has evaluated these coefficients for the case of a thin plate subjected to an arbitrary loading - one dependent, for instance on both the axial and spanwise coordinates. His result, adapted for the problem under consideration, is

$$\bar{A}_{mn} = \frac{4}{\left\{ 4 \left(\frac{\ell}{L} \right)^2 m^2 + n^2 \right\}^2 \Pi^4} \left\{ 12 (1 - \sigma^2) \left(\frac{\ell}{m} \right) \left(\frac{h}{\eta_0} \right) \left(\frac{\ell}{h} \right) \left(\frac{P_0}{E} \right) \right\} \\ \times \int_{-0.5}^{0.5} \int_0^1 \bar{P} \sin m \Pi \bar{x} \sin n \Pi (\bar{y} + 0.5) d\bar{x} d\bar{y} \quad 6.16$$

If now, the expression for the dimensionless pressure (equation 6.12 plus unity) is substituted into the above equation and the integration carried out, the coefficients \bar{A}_{mn} become

$$\bar{A}_{mn} = \frac{4(1 - \cos n \Pi)}{mn \left\{ 4 \left(\frac{\ell}{L} \right)^2 m^2 + n^2 \right\}^2 \Pi^6} \left\{ 12(1 - \sigma^2) \left(\frac{\ell}{m} \right)^3 \left(\frac{h}{\eta_0} \right) \right. \\ \times \left(\frac{\ell}{h} \right) \left(\frac{P_0}{E} \right) \left. \left[\left\{ 1 - \left(\frac{\Delta P_m}{P_0} \right) \right\} (1 - \cos m \Pi) \right. \right. \right. \\ \left. \left. \left. + \left\{ \left(\frac{-\beta L}{P_0} \right) + \left(\frac{\Delta P_D}{P_0} \right) \right\} \left\{ \frac{\sinh \sqrt{\gamma}}{\sqrt{\gamma}} \right\} \cos m \Pi \right] \right\}$$

$$+ \left(\frac{\Delta P_m}{P_o} \right) \left\{ \frac{1 - \cosh \sqrt{\gamma} \cos m \Pi}{\frac{\sqrt{\gamma}}{m \Pi}^2 + 1} \right\} - \left(\frac{\Delta P_D}{P_o} \right) \cos m \Pi \quad 6.17$$

The normal wall displacement, then, is given by the Fourier series 6.15, with coefficients determined by equation 6.17.

In an artificial kidney, however, the actual wall boundary conditions may very well be more nearly those of a clamped plate (zero displacement and zero first derivative along the normal to the edges at the edges) than those of a simply-supported one. (The actual conditions, as is the case in most physical situations, are ones somewhat between these two "extremes.") But a solution of the normal wall displacement equation for clamped plate conditions is extremely difficult to obtain at the present state of our knowledge (34,41). One particular difficulty is that no eigenfunctions exist which satisfy both the governing wall equation and the clamped plate conditions (41). The fact that the wall loading is not uniform adds further complications. Hence, such a solution has not been sought here.

On the other hand, the wall displacements obtained for simply-supported conditions, larger than the more constrained ones which would be obtained using clamped conditions, can be considered to be upper bounds on the actual deflections.

6.3 Limiting Cases of the General Solutions.

Two limiting cases of the flow and wall solutions obtained in this chapter are of particular interest.

CASE A

First, when the pressure difference across the membranes is large compared to pressure variations in the flow field, the velocity of flow through the walls assumes a nearly constant value. Mathematically this is stated as:

$$\left(\frac{\Delta P_m}{P_o}\right) \gg \left\{ \left(\frac{-\beta L}{P_o}\right) + \left(\frac{\Delta P_D}{P_o}\right) \right\} = 0 \quad (1), \quad 6.18$$

where $\left(\frac{\Delta P_m}{P_o}\right)$ is the ratio of the characteristic pressure difference across the membranes to the inlet blood pressure, $\left(\frac{-\beta L}{P_o}\right)$ is the ratio of the inlet axial pressure gradient to a characteristic non-porous channel axial pressure gradient, and $\left(\frac{\Delta P_D}{P_o}\right)$ is the ratio of the dialysate pressure drop to the inlet blood pressure.

Now, for values of the Reynolds number ratio α of order zero in the parameter $\left(\frac{\Delta P_m}{P_o}\right)$, the order of the modified Reynolds number ratio γ is given by

$$\begin{aligned} \gamma &= \frac{3}{R} \left(\frac{\rho_f U^2}{P_o} \right) \left(\frac{\alpha P_o}{\Delta P_m} \right) \\ &= 0.399 \left(\frac{P_o}{\Delta P_m} \right) \alpha = 0 \left(\frac{P_o}{\Delta P_m} \right) \end{aligned} \quad 6.19$$

Condition 6.18 together with the above ordering, then, leads to the following limiting case of the general solutions:

$$\begin{aligned}\frac{P-P_o}{P_o} &= - \left(\frac{-\beta L}{P_o} \right) + \frac{1}{2} \left(\frac{\Delta P_m}{P_o} \right) \gamma \bar{x}^2 \\ \frac{u}{U} &= \frac{R}{2} \left(\frac{P_o}{\rho_f U^2} \right) \left[\left(\frac{-\beta L}{P_o} \right) - \left(\frac{\Delta P_m}{P_o} \right) \gamma \bar{x} \right] (1 - \bar{z}^2) \\ \frac{w}{W_p} &= \frac{3}{2} \left(\bar{z} - \frac{1}{3} \bar{z}^3 \right)\end{aligned}\tag{6.20}$$

$$\begin{aligned}\frac{\eta}{\eta_o} &= \sum_{m=1}^{\infty} \sum_{n=1}^{\infty} \frac{4(1-\cos n\pi)}{mn \left\{ 4 \left(\frac{\ell}{L} \right)^2 m^2 + n^2 \right\}^2 \pi^6} \\ &\times \left\{ 12(1 - \sigma^2) \left(\frac{\ell}{m} \right)^3 \left(\frac{\ell}{h} \right) \left(\frac{h}{\eta_o} \right) \left(\frac{P_o}{E} \right) \right\} \left[(1 - \cos m \pi) \right. \\ &\quad \left. + \left\{ \left(\frac{-\beta L}{P_o} \right) - \frac{1}{2} \left(\frac{\Delta P_m}{P_o} \right) \gamma \right\} \cos m \pi \right]\end{aligned}\tag{6.21}$$

The flow solutions 6.20 are equivalent to Berman's zeroth-order solutions for a constant velocity of flow through the porous walls. Thus it is clear that Berman's solutions are a special case of the results derived herein.

The wall displacement 6.21 is that of a simply-supported plate under a loading quadratic in the axial coordinate.

CASE B

A second interesting special case arises when the ratio of the

total outflow through the porous walls to the inflow is small compared to unity. Mathematically this can be stated as

$$\gamma \ll 1, \quad 6.22$$

where γ is the modified Reynolds number ratio. Condition 6.22 results in :

$$\begin{aligned} \frac{P-P_o}{P_o} &= - \left(\frac{-\beta L}{P_o} \right) \bar{x} \\ \frac{u}{U} &= \frac{R}{2} \left(\frac{P_o}{\rho_f U^2} \right) \left(\frac{-\beta L}{P_o} \right) (1 - \bar{z}^2) \\ \frac{w}{W_p} &= \frac{3}{2} \left[1 - \left\{ \left(\frac{-\beta L}{P_o} \right) + \left(\frac{\Delta P_D}{P_o} \right) \right\} \bar{x} \right] \left(\bar{z} - \frac{1}{3} \bar{z}^3 \right) \end{aligned} \quad 6.23$$

$$\begin{aligned} \frac{\eta}{\eta_o} &= \sum_{m=1}^{\infty} \sum_{n=1}^{\infty} \frac{4(1-\cos n\pi)}{mn \left\{ 4 \left(\frac{\ell}{L} \right)^2 m^2 + n^2 \right\}^2 \pi^6} \\ &\times \left\{ 12(1 - \sigma^2) \left(\frac{\ell}{m} \right)^3 \left(\frac{\ell}{h} \right) \left(\frac{h}{\eta} \right) \left(\frac{P_o}{E} \right) \right\} \left[(1-\cos m\pi) \right. \\ &\quad \left. + \left(\frac{-\beta L}{P_o} \right) \cos(m\pi) \right] \end{aligned} \quad 6.24$$

Equations 6.23 describe the well-known Poiseuille channel flow, but with finite, though negligible, wall porosity. Hence, Poiseuille channel flow is the limiting case of the general flow solutions of

Section 6.1 as the modified Reynolds number ratio γ tends to zero. Equation 6.24, further, describes the deflection of a simply-supported plate under a hydrostatic loading.

According to the values ascribed to the various parameters in Section 5-3, γ has in the problem of this study the value

$$\gamma = 2.2 \times 10^{-2} < 1.$$

Consequently, this limiting case describes well the flow situation in present Kiil kidneys.

CHAPTER VII

Discussion of Results.

In the previous chapter dimensionless mathematical expressions have been found for the fluid pressure, velocity components, and the normal wall displacement. These solutions, in general form, are functions of six dimensionless parameters: $\frac{x}{L}$, the dimensionless axial coordinate; $\frac{z}{h}$, the dimensionless normal coordinate; γ , the modified Reynolds number ratio; $\left(\frac{-\beta L}{P_o}\right)$, the ratio of the inlet axial pressure gradient to a characteristic non-porous channel axial pressure gradient; $\left(\frac{\Delta P_m}{P_o}\right)$, the ratio of the characteristic pressure difference across the membranes to the inlet blood pressure; and $\left(\frac{\Delta P_D}{P_o}\right)$, the ratio of the dialysate pressure drop to the inlet blood pressure. The behavior of the solutions will now be examined as each of these parameters is allowed to vary while the others are held constant.

The fixed values of the various parameters used are, with one exception, in agreement with the values of these parameters determined in Section 5.3. The one exception is the modified Reynolds number ratio γ , for which a value of 0.2 has been employed. Such a value has been chosen in lieu of the much smaller actual value of this parameter for Kill kidneys in order to indicate the effects of wall porosity in future kidney designs for which γ is not necessarily small compared to unity (but still somewhat less than unity).

First, Figures 9 through 13 portray the dimensionless axial velocity component $\frac{2}{R} \left(\frac{\rho_f U^2}{P_o} \right) \left(\frac{P_o}{-\beta L} \right) \frac{u}{U}$ as a function of the above six parameters. This velocity component can be seen to be locally para-

bolic in the normal coordinate. However, its mid-plane value decays exponentially with the axial coordinate, reflecting the fact that the axial flow slows as fluid mass is lost through the porous walls. The profiles of Figure 9, therefore, are non-similar ones, in agreement with the fact that the velocity of flow through the porous walls has been allowed to depend on the pressure field.

The extent of the decay of the dimensionless axial velocity component, moreover, increases as the parameters γ , $\left(\frac{\Delta P_m}{P_o}\right)$ and $\left(\frac{\Delta P_D}{P_o}\right)$ are increased since increasing these parameters has the effect of augmenting the effects of wall porosity and decreasing the axial mass flow. On the other hand, the extent of decay decreases as the parameter $\left(\frac{-\beta L}{P_o}\right)$ is increased. This is because enlarging the latter parameter increases the axial flow rate and hence exposes the fluid for shorter times to the effects of wall porosity.

From the flow solutions, it can be seen that in the limit as the ratio of the total flow through the porous walls to the inlet flow tends toward zero ($\gamma \rightarrow 0$), the uniform Poiseuille velocity profile results. (See Section 6.3).

Secondly, Figures 14 through 18 illustrate the effects of these same six dimensionless parameters on the dimensionless normal velocity component, $\frac{w}{W_p}$. This velocity component is locally cubic in the normal component. Further, since its value at the porous walls can be observed to decay exponentially with the axial coordinate, the profiles of Figure 14, like those of Figure 9, are non-similar. However, unlike the situation in the case of the axial velocity

component, the extent of this decay decreases as the parameters γ , $\left(\frac{\Delta P_m}{P_o}\right)$ and $\left(\frac{\Delta P_D}{P_o}\right)$ are increased and increases as the parameter $\left(\frac{-\beta L}{P_o}\right)$ is made larger. The explanation for this lies in the fact that as the total amount of fluid passing through the porous channel increases (γ , $\left(\frac{\Delta P_m}{P_o}\right)$, or $\left(\frac{\Delta P_D}{P_o}\right)$ increasing) relative to the amount of fluid entering the channel, less and less of the entering fluid need be driven the entire channel length. Energy losses - and hence the axial pressure drop - diminish. As a result, the local pressure and hence the normal velocity component, which depends on the local pressure, decreases to a lesser extent. The opposite, however, occurs as the parameter $\left(\frac{-\beta L}{P_o}\right)$ is increased.

Next, Figures 19 through 22 indicate the effects of varying the various parameters on the dimensionless pressure drop, $\frac{P-P_o}{P_o}$. Like the velocity components, the pressure drop, too, decays exponentially, but in such a way that the total pressure drop is lessened. (The dotted curve of Figure 20, for example, corresponds to that for a non-porous channel flow and is the lower bound for the other curves.) The dependence of the extent of decay on the various parameters, however, is of course, similar to that for the normal velocity component.

It should be particularly noted from Figures 21 and 22 that, for the range of the parameters examined, varying the parameters $\left(\frac{\Delta P_m}{P_o}\right)$ and $\left(\frac{\Delta P_D}{P_o}\right)$ has little effect on the dimensionless pressure drop. Hence, this pressure drop is largely independent of these dimensionless quantities.

The dimensionless normal wall displacement, $\frac{1}{12(1-\sigma^2)} \left(\frac{m}{l}\right)^2 \chi\left(\frac{\eta_o}{h}\right) \left(\frac{h}{l}\right) \left(\frac{E}{P_o}\right) \frac{\eta}{\eta_o}$, evaluated at $y/l = 0$, is illustrated in Figures 23 and 24. This wall displacement is primarily pressure driven, a fact reflected in the dependence of this displacement on the local pressure; that is, while the normal wall displacement satisfies the boundary conditions for a simply-supported plate, away from boundaries it closely parallels the pressure field. In particular, the effect of increasing the modified Reynolds number ratio γ is to increase wall displacements somewhat downstream (where the pressure is most affected by the cumulative effects of wall porosity). (For comparative purposes, the dotted curve of Figure 23 illustrates the limiting case as γ tends to zero). On the other hand, larger values of the ratio of the absolute value of the inlet axial pressure gradient to the characteristic non-porous channel axial pressure gradient, $\left(\frac{-\beta L}{P_o}\right)$, leads to diminished displacements somewhat downstream.

Although the dimensionless normal wall displacement also depends on the parameters $\left(\frac{\Delta P_m}{P_o}\right)$ and $\left(\frac{\Delta P_D}{P_o}\right)$, the variation of this displacement with these parameters is negligible and has, therefore, not been depicted. This is because, inasmuch as the parameter γ must be restricted to values small compared to one (0.2 in these figures), the degree of blood pressure - dialysate pressure coupling is small. (See, for instance, Figures 21 and 22). Hence, the dependence of the normal wall displacement on the parameters $\left(\frac{\Delta P_m}{P_o}\right)$ and $\left(\frac{\Delta P_D}{P_o}\right)$ can be expected to be small.

Finally, the curves of Figures 9 through 24 are, strictly speaking, valid only for a homogeneous fluid. They are meaningful for the non-homogeneous blood flow under consideration only to the extent to which the total flow through the porous walls is small compared to the inlet flow; that is, they are meaningful to the extent to which the Reynolds number ratio α , and hence the modified Reynolds number ratio γ , is small compared to unity.

Small values of the parameter α , moreover, lead to the second limiting flow case described in Section 6.3. In this case, the effects of wall porosity on the flow are negligible and the axial velocity component and the pressure field become those for Poiseuille channel flow. The normal velocity component, however, remains coupled to the local pressure and takes on a linear variation in the axial coordinate.

Large osmotic pressure differences, on the other hand, can lead to the first limiting case of Section 6.3. In this situation the velocity of flow through the porous walls approaches a constant value all along the channel and flow solutions equivalent to Berman's result.

CHAPTER VIII

CONCLUSIONS AND SUMMARY

The general nature of flows in porous elastic channels for which the ratio of unstressed channel half-thickness to channel width and length is small has been delineated. A mathematical model has been chosen which assumes an incompressible, homogeneous, Newtonian fluid in laminar flow. The channel walls are uniformly porous, Hookean elastic thin plates. Further, the flexural rigidity of the walls is such that normal wall displacements are small compared to the unstressed channel half-thickness.

In particular, conditions are given for which the analysis applies to the thin-film blood flows encountered in parallel plate artificial kidneys. Such flows are generally bounded by flexible, somewhat porous membranes. However, it is assumed here that the membranes are supported by material of relatively high rigidity in such a manner that the membranes and this material together comprise porous, elastic channel walls. In the light of recent research trends, such an assumption can be expected to be a reasonable one for future kidney designs.

The most general, time-depedent equations and boundary conditions describing the flow and channel wall motions have been formulated. (The flow is time-dependent inasmuch as it is driven by the pulsatile arterial-venous pressure gradient.) These equations and boundary conditions have then been simplified by means of a formal nodimensionalization and ordering of the terms appearing in

the equations followed by a perturbation solution in the modified axial Reynolds number. The result has been a system of linear zeroth-order (in the above Reynolds number) equations in which inertia terms are absent.

More important, the simplification procedure has made it clear that inertia effects are unimportant for a wide class of flows in porous channels. The importance of such effects in these flows is governed by the modified inlet axial Reynolds number, $\left(\frac{UL}{\nu}\right) \times \left(\frac{h}{L}\right)^2$. And when this Reynolds number is small compared to unity, as is the case in the problem which has been considered, inertia effects can be neglected. This conclusion cannot be deduced from present work in the field of porous channel flows.

The relative importance of the total flow through the porous walls compared to the axial flow has been shown to depend on a second parameter, α , the ratio of a Reynolds number for the flow through the porous walls based on unstressed channel half-thickness (a Reynolds number used in other work) to the modified inlet axial Reynolds number. When the parameter α is of unit order, wall porosity significantly affects the axial flow. However, when α is small compared to unity, small deviations from Poiseuille channel flow result. (A modified version of the parameter α , a dimensionless group denoted by γ , has actually been used herein).

For values of α larger than unit order, inertia effects cannot be neglected no matter how small the modified inlet axial Reynolds number may be. Equations found in existing work in porous channel

flows must then be used to obtain correct solutions for the flow.

In pulsatile, porous elastic channel flows, further, the relative importance of wall unsteadiness in the normal direction to wall porosity in determining the boundary condition on the normal velocity component at the channel walls has been shown to be described by the parameter $\left\{ \frac{1}{\alpha} \left(\frac{\eta_o}{h} \right) \left(\frac{L}{UT} \right) \right\}$, where α is the Reynolds number ratio, $\left(\frac{\eta_o}{h} \right)$ is the ratio of the characteristic normal wall displacement to the unstressed channel half-thickness, and $\left(\frac{L}{UT} \right)$, is the well-known Strouhal number.

Although valid for time-dependent flows, the simplified governing equations and boundary conditions have been solved for the sub-case of steady flow. This flow situation is a meaningful one for artificial kidneys which make use of several feet of pulse-dampening elastic interconnecting tubing.

General solutions have been obtained for the dimensionless axial and normal fluid velocity components, the dimensionless fluid pressure, and the dimensionless normal wall displacement. These solutions indicate that all but the last of these quantities decay exponentially with the dimensionless axial coordinate. The extent of the decay depends upon the magnitudes of the various flow parameters. It was found, however, that the parameters $\left(\frac{\Delta P_m}{P_o} \right)$, the ratio of the characteristic pressure difference across the artificial kidney membranes to the inlet blood pressure, and $\left(\frac{\Delta P_D}{P_o} \right)$, the ratio of the dialysate pressure drop to the inlet blood pressure, have a negligible influence on the dimensionless pressure field and the

dimensionless normal wall displacement.

As for the dimensionless normal wall displacement itself, the magnitude of this displacement is somewhat increased downstream as the Reynolds number ratio α is increased. The magnitude of this displacement, however, decreases markedly as the parameter $\left(\frac{-\beta L}{P_0}\right)$, the ratio of the absolute value of the inlet axial pressure gradient to a characteristic non-porous channel flow axial pressure gradient, is enlarged.

Two limiting cases of the general solutions have been discussed. The first of these describes what happens as pressure variations in the flow field become small compared to the reference pressure: the velocity of flow through the porous walls approaches a constant value and flow solutions equivalent to those found in the literature for this case result. In an artificial kidney this flow situation corresponds to the use of large osmotic pressure differences across the porous membranes.

The second points out that Poiseuille channel flow results as the ratio of the total flow through the porous walls to the inlet flow tends to zero ($\alpha \rightarrow 0$). This case is of interest in present artificial kidneys, in which the parameter α is finite but small compared to unity. In this application, the axial flow is independent of the wall porosity. However, the dimensionless normal velocity component is still coupled to the axial flow.

The integration of this velocity component over the wall area, moreover, yields the ultrafiltration rate. (Ultrafiltration is the

desirable loss of excess blood fluid through the porous membranes). This rate is then known as a function of various flow parameters.

The general solutions obtained, it must be kept in mind, while valid for all values of α for a homogeneous fluid, are valid for artificial kidney blood flows only to the extent to which α is small compared to unity. For large values of α (α greater than about 0.1 to 0.2) blood can no longer be assumed to be homogeneous.

The present work has described the nature and effects of wall porosity in flows in porous, elastic channels for which the unstressed half-thickness is small compared to the other channel dimensions. It has determined and discussed the significant dimensionless parameters governing the flow field and the normal wall displacement. In particular, the analysis has been applied to the blood flow in parallel plate artificial kidneys. A better understanding of this flow has resulted in the light of new knowledge obtained concerning the axial and normal velocity components, the pressure field, and, for kidneys of the type discussed in Section 2.1, the normal wall displacement. Such a better understanding can provide guidelines for optimizing ultrafiltration, minimizing the effects on the flow of wall displacement, and, therefore, designing improved artificial kidneys.

REFERENCES

1. A.L. Babb and L. Grimsrud, "A New Concept in Hemodialyzer Membrane Support," Trans. Amer. Soc. Artif. Int. Organs, Vol. X, p. 31, 1964.
2. A.S. Berman, "Laminar Flow in Channels with Porous Walls," Journal of Applied Physics, Vol. 24, p. 1232, December 1953.
3. F.W. Billmeyer, Jr., Textbook of Polymer Science, Interscience Publishers, New York and London, p. 502, 1962.
4. R.B. Bird, W.E. Stewart, and E.N. Lightfoot, Transport Phenomena, Wiley New York, 1960.
5. L.W. Bleumle, Trans. Amer. Soc. Artif. Int. Organs, Vol. IX, p. 71, 1963.
6. S.E. Charm, W. Mc Comis, and G. Kurland, "Rheology and Structure of Blood Suspensions," Journal of Applied Physiology, Vol 19, p. 127, 1964.
7. J.J. Cole, J.L. Pollard, and J.S. Murray, "Studies on the Modified Polypropylene Kill Dialyzer," Trans. Amer. Soc. Artif. Int. Organs, Vol. IX, p. 67, 1963.
8. R. Courant and D. Hilbert, Methods of Mathematical Physics, Interscience Publishers, New York, 1962.
9. W.G. Esmond and H. Clark, "Mathematical Analysis and Mass Transfer Optimization of a Compact, Low Cost, Pumpless System for Hemodialysis (Dialung)," Biomedical Fluid Mechanics Symposium (proceedings), ASME, New York, p. 161, 1966.
10. R Fahraeus and J. Lindquist, Am. Journal of Physiology, Vol. 95, -. 562, March, 1931.
11. L. Grimsrud and A.L. Babb, "Optimization of Dialyzer Design for the Hemodialysis System," Trans. Amer. Soc. Artif. Int. Organs, Vol. X, p. 101, 1964.
12. G. Kareman, "Some Contributions to the Mathematical Biology of Blood Circulation. Reflections of Pressure Waves in the Arterial System," Bulletin of Math. Biophysics, Vol. 14, p. 327, 1952.

13. W.J. Kolff, "Outline of Internal Organs," Trans. Amer. Soc. Artif. Int. Organs, Vol. IX, p. 380, 1963.
14. N.R. Kuchar and S. Ostrach, "Flows in the Entrance Regions of Circular Elastic Tubes," Master's Thesis, Case Institute of Technology, Cleveland, June 1965.
15. E.F. Leonard, "Large-Scale Hemodialysis: Engineering and Economic Considerations," Trans. Amer. Soc. Artif. Int. Organs, Vol. XI, p. 26.
16. E.F. Leonard and L.W. Bluemle, "Engineering in Medicine: Design of an Artificial Kidney," Trans. N - Y Acad. Sciences, Ser. 11, Vol. 21, No. 7, p. 585, May 1959.
17. J. Ludwigson, "Portable Artificial Kidney is Research Goal," The Plain Dealer, p. 6, Wednesday, April 6, 1966.
18. E.W. Merrill and R.E. Wells, Jr., "Flow Properties of Biological Fluids," Applied Mechanics Reviews, Vol. 14, No. 9, p. 663, 1961.
19. G.W. Morgan, "On the Steady Laminar Flow of a Viscous Incompressible Fluid in an Elastic Tube," Bulletin of Mathematical Biophysics, Vol. 14, p. 19, 1952.
20. G.W. Morgan and W.R. Ferrante, "Wave Propagation in Elastic Tubes Filled with Streaming Liquid," Journal of Acoustical Society of America, Vol. 27, p. 715, 1955.
21. G.W. Morgan and J.P. Kiely, "Wave Propagation in a Viscous Liquid Contained in a Flexible Tube," Journal of the Acoustical Society of America, Vol. 26, p. 323, 1954.
22. E. Reissner, "On Some Aspects of the Theory of Thin Elastic Shells," J. Bos. Soc. of Civil Eng's, Vol. 42, p. 100, 1955.
23. G. Rudinger, "Review of Current Mathematical Models for the Analysis of Blood Flow," Biomedical Fluid Mechanics Symposium, 1966.
24. A.H. Sachs and D.E. Abbot, "An Analytical Study of the Relationship between Blood Pressure and Arterial Wall Displacements," Vidya Report, No. 40, Vidya, Inc., Palo Alto, California, 1961.
25. A.H. Sachs and D.E. Abbot, "Determination of the Physical Constants Relating Blood Pressure and Arterial Wall Displacements," Vidya Report No. 65, Vidya, Inc.,

Palo Alto, California, 1962.

26. C.E. Sachs and J.L. Funck-Bretano, "Stretching of the Dialysis Membrane: A New Device for the Treatment of Chronic Nephritis (Preliminary Report)," Trans. Amer. Soc. Artif. Int. Organs, Vol. IX, p. 79, 1963.
27. H. Schlichting, Boundary Layer Theory, Fourth Edition, McGraw-Hill, New York, 1960.
28. J.R. Sellars, "Laminar Flow in Channels with Porous Walls," Journal of Applied Physics, Vol. 26, p. 489, 1955.
29. R.E. Sparks, Proposal for, A Research Program Leading Toward a Wearable Artificial Kidney, Case Institute of Technology, Cleveland, 1966.
30. J.L. Synge and B.A. Griffith, Principles of Mechanics, McGraw-Hill, New York, 1959.
31. R.M. Terrill, "Laminar Flow in a Uniformly Porous Channel," The Aeronautical Quarterly, Vol. XV, p. 299, Aug., 1964.
32. R.M. Terrill, "Laminar Flow in a Uniformly Porous Channel with Large Injection," Aeronautical Quarterly, Vol. XVI, p. 323, November, 1965.
33. R.M. Terrill and G.M. Shrestha, "Laminar Flow through a Channel with Uniformly Porous Walls of Different Permeability," Applied Scientific Research, The Hague, Vol. 15, Section A, p. 440, 1966.
34. S. Timoshenko and S. Woinowsky - Krieger, Theory of Plates and Shells, Second Edition McGraw-Hill, New York, 1959.
35. S. Uchida, "The Pulsating Viscous Flow Superposed on the Steady Laminar Flow of Incompressible Fluid in a Circular Pipe," Zeitschrift fur angewandte, Mathematik und Physik, Vol. VII, p. 403, 1956.
36. M. Van Dyke, Perturbation Methods in Fluid Mechanics, Academic Press, New York, 1964.
37. C. Wang, Applied Elasticity, McGraw-Hill, New York 1953.

38. J.R. Womersley, "An Elastic Tube Theory of Pulse Transmission and Oscillating Flow in Mammalian Arteries," WADC Technical Report TR 56 - 614, Wright Air Development Center, 1957.
39. S.W. Yuan, "Further Investigations of Laminar Flow in Channels with Porous Walls," Journal of Applied Physics, Vol. 27, p. 267, March 1956.
40. C. Wilcox, R.B. Freeman, J.F. Maher, and G.E. Schreiner, "Comparison of Physical Properties and Permeability of Six Cellulose Membranes," Trans. Amer. Soc. Artif. Int. Organs, Vol. XII, p. 44, 1966.
41. D. Young, "Bending of Clamped Plates," J. of Applied Mech., p. A - 254, Sept., 1947.
42. D.A. McDonald, Blood Flow in Arteries, Edward Arnold Publishers, LTD., London, 1960.
43. E.R.G. Eckert, P.L. Donoughe, and B.J. Moore, "Velocity and Friction Characteristics of Laminar Viscous Boundary Layer and Channel Flow Over Surfaces with Ejection or Suction," NACA TN 4102, 1957.
44. W.E. Wageman and F.A. Guevara, "Fluid Flow Through a Porous Channel," Physics of Fluids, Vol. 3, No.6, Nov.- Dec., 1960.
45. B.W. Knight and B.B. McInteer, "Laminar Incompressible Flows in Channels with Porous Walls," LA - DC - 5309, Los Alamos Sci. Lab., 1965.

APPENDIX A

DETERMINATION OF CHARACTERISTIC DATA FOR THE FLOW VARIABLES AND CHANNEL HALF-THICKNESS NOT GIVEN EXPLICITLY IN THE LITERATURE.

The selection of characteristic data for the fluid velocity components, pressure drops, and channel half-thickness in the blood-handling circuit of a modified Kiil artificial kidney is by no means straightforward. One difficulty, for example, is that no accurate measurement of the actual mean blood film thickness (hence, mean channel thickness) has yet been made. (Because the membranes are subject to sag and relaxation, "mean" thicknesses will be spoken of.) Thicknesses given in the literature are nominal ones based on the spacing between the ribs of one of the ribbed parallel plates and those of the other. These thicknesses do not take into account membrane sag in the between-rib spaces and hence are on the small side.

Another difficulty is that certain of the characteristic flow quantities do not appear explicitly in the literature and must be estimated from other data. These quantities include U , the characteristic axial velocity component; W_p , the characteristic velocity of flow through the porous walls; $-\beta$, the absolute value of the inlet axial pressure gradient for steady flow; ΔP_D , the dialysate pressure drop; and ΔP_m , the inlet across-membrane pressure difference.

To begin with, a better estimate for the mean channel half-thickness can be made. Cole, Pollard and Murray⁽⁷⁾ give the

nominal membrane half-spacing as 0.0057 cm. Babb and Grimsrud ⁽¹⁾ on the other hand, have determined that the ratio of the actual to theoretical volume of a modified Kill blood flow channel is about 5.3. Hence, one would expect that a more reasonable mean channel half-thickness h is given by

$$\begin{aligned} h &= 5.3 \times 0.0057 \text{ cm.} \\ &= 0.030 \text{ cm.} \end{aligned}$$

In this analysis, however, a slightly conservative value of 0.020 cm is actually used.

Next, estimates for certain of the characteristic flow quantities can be made. First, the characteristic axial velocity component is given by the following Poiseuille flow relation:

$$U = \frac{3}{2} \frac{Q_o}{(2\ell)(2h)} \quad \text{A.1}$$

where Q_o is the inlet flow rate, ℓ is the channel half-width, and h is the unstressed channel half-thickness. (In our idealized model of the channel, the mean half-thickness will be the actual half-thickness.) Now, according to Sparks ⁽²⁹⁾,

$$\begin{aligned} Q_o &= \text{inlet flow rate per flow channel} \\ &\quad \text{(four channels)} \\ &= 50 \text{ cm}^3/\text{min} \end{aligned}$$

Using this value for the quantity Q_o and the values for the characteristic dimensions ℓ and h given in Section 5.3, it is found from equation A.1 that

$$U = 1.56 \text{ cm/sec.}$$

Secondly, another Poiseuille relation (equation 4.9 can be used to obtain $-\beta$, the absolute value of the inlet axial pressure gradient, in terms of known quantities:

$$-\beta = \frac{3}{2} \frac{\mu Q_0}{(2L) h^3} \quad 4.9$$

It is found that

$$-\beta = 3.28 \times 10^2$$

(Since for values of the porosity parameter α small compared to unity the blood flow pressure drop is given approximately by

$$-\beta L = 3.6 \times 10^4 \text{ dynes/cm}^2,$$

where L is the channel length, and since Cole, Pollard and Murray observe the actual blood flow pressure drop to be 3.0×10^4 dynes/cm², in good agreement, the choice of half-thickness h used in determining the quantity $(-\beta)$ can now be seen to be a good one.)

Thirdly, the dialysate pressure drop ΔP_D is not really known for a dialysate flow channel composed of porous material. However, it has been assumed that dialysate flow viscous shear forces acting on the channel walls are of the same magnitude as or less than viscous shear forces acting on these walls caused by the blood flow. Hence, for values of the porosity parameter α small compared to unity, it is reasonable to expect that

$$\begin{aligned} \Delta P_D &= \sigma'(-L) \\ &= \sigma'(10^4) \text{ dynes/cm}^2, \end{aligned}$$

where L is the channel length, given in Section 5.3, as 111 cm.
In this study a value of 5×10^4 dynes/cm² is actually used for the quantity ΔP_D .

Fourthly, the characteristic across-membrane pressure difference, ΔP_m , can be calculated neglecting normal viscous stresses from equation 5.19.

$$\Delta P_m = P_o - P_{Di} + \Delta P_D + \Delta P_{os}, \quad 5.19$$

where P_o is the inlet blood pressure, P_{Di} is the dialysate pressure at the dialysate inlet, ΔP_D is the dialysate pressure drop, and ΔP_{os} is the osmotic pressure difference across the membranes. Using the value for the pressure drop ΔP_D just given and the values for the quantities P_o , P_{Di} and ΔP_{os} presented in Section 5.3 it is found that

$$\Delta P_m = 1.0 \times 10^6 \text{ dynes/cm}^2.$$

Further, in the absence of an osmotic pressure difference, a much smaller value results:

$$\Delta P_m = 1.0 \times 10^5 \text{ dynes/cm}^2$$

Finally, the characteristic velocity of flow through the porous walls, W_p , can be determined from equation 5.19

$$W_p = \frac{\phi}{m'} (\Delta P_m), \quad 5.19$$

where ϕ is the membrane permeability, m' is membrane thickness, and ΔP_m is the characteristic across-membrane pressure difference.

Sparks (29) gives the membrane permeability ϕ as

$$\phi = 5.5 \times 10^{-14} \text{ cm}^4 / \text{sec} - \text{dynes}$$

And Wilcox, Freeman, Maher and Schreiner give the membrane thickness m' as

$$m' = 9.9 \times 10^{-3} \text{ cm.}$$

Thus,

$$w_p = 5.5 \times 10^{-6} \text{ cm/sec.}$$

in the presence of a maximum osmotic pressure difference, while

$$w_p = 5.5 \times 10^{-7} \text{ cm/sec}$$

in the absence of such a pressure difference.

The former value agrees well with that obtained by dividing the maximum ultrafiltration rate in a Kolff kidney, $20 \text{ cm}^3 / \text{min.}$ (29), by the total membrane area, $20,000 \text{ cm}^2$ (29):

$$\frac{20 \text{ cm}^3 / \text{min}}{20,000} \times \frac{1 \text{ min}}{60 \text{ sec.}} = 17 \times 10^{-6} \text{ cm/sec.}$$

APPENDIX B

CHARACTERISTIC VALUES FOR THE NORMAL WALL DISPLACEMENT AND THE WALL THICKNESS

Assuming the deflections of the channel walls can be treated by a linear thin-plate theory, the maximum normal deflection of the walls, η_o , if the walls are subjected to a uniform loading q_o , is given by (37)

$$\eta_o = \frac{K q_o (2\ell)^4}{E m^3} \quad \text{B.1}$$

where ℓ is the channel half-width, E is Young's modulus for the walls, m is wall thickness, and K is a constant which depends on both the wall boundary conditions and the ratio of channel (or wall) length L to width 2ℓ . In particular, for simply-supported boundary conditions and the length-to-width ratio of this problem, Timoshenko and Woinowsky - Krieger⁽³⁴⁾ give the constant K as

$$K = 0.142$$

Now, if the ratio of the maximum normal wall displacement η_o to the unstressed channel half-thickness h (this ratio must be small) is taken to be 0.1 ($\eta_o = 2.0 \times 10^{-3}$ cm.) and if the loading q_o is conservatively taken to be the inlet blood pressure P_o , equation B.1 becomes an equation which can be solved for the wall thickness m ; that is, equation B.1 can be written

$$m = \sqrt[3]{\frac{10 K P_o (2\ell)^4}{E h}} \quad \text{B.2}$$

The value of wall thickness m given by equation B.2 is that required to keep normal wall displacements smaller than the specified fraction of the unstressed channel half-thickness h . This is the value of wall thickness to be used in this study. For the given value of the constant K and for the values of the quantities P_o , ℓ , E and h presented in Section 5.3, this wall thickness is found to be

$$m = 4.6 \text{ cm.}$$

Equation B.1, also, tacitly assumes that Poisson's ratio for the walls is 0.3.

APPENDIX C

A FURTHER NOTE ON THE RANGE OF VALIDITY OF THE SIMPLIFIED EQUATIONS OF THIS STUDY

Berman's solution for the axial velocity component $\bar{u}^{(2)}$ can be written in the form

$$\bar{u} = (1 - \alpha \bar{x}) \left\{ (1 - \bar{z}^2) + R_B f_1(\bar{z}) + R_B^2 f_2(\bar{z}) + \dots \right\}, \quad C.1$$

where the notation of this study has been adopted and where the functions f_1, f_2, \dots describe higher order corrections to the zeroth-order solution. However, since

$$R_B = R \alpha,$$

according to Section 5.4, equation C.1 can be expressed as

$$\bar{u} = (1 - \alpha \bar{x}) \left\{ (1 - \bar{z}^2) + (R \alpha) f_1(\bar{z}) + (R \alpha)^2 f_2(\bar{z}) + \dots \right\}. \quad C.2$$

Note that inertia effects are absent in the zeroth-order terms of both equations C.1 and C.2, but appear in the first - and higher - order corrections. Equation C.2, then, suggests a more general condition for which axial inertia effects can be neglected and for which the simplified equations of this study are valid:

$$R |\alpha| \ll 1. \quad C.3$$

Condition C.3 includes the situation for which axial inertia forces can be neglected described in Section 5.4 as a special case.

This condition, also, appears to be verified by the form of

the solutions of the simplified equations of this study to first order in the parameter R (for steady flow for which the velocity of flow through the porous walls, w_p , is a constant). For example, the axial velocity component \bar{u} is given by

$$\bar{u} = (1 - \alpha \bar{x}) \left\{ (1 - \bar{z}^2) + R g_1(\alpha, \bar{z}) + \dots \right\}, \quad \text{C.4}$$

where

$$g_1(\alpha, \bar{z}) = \alpha G_1(\bar{z}). \quad \text{C.5}$$

Hence, equation C.4 can be written

$$\bar{u} = (1 - \alpha \bar{x}) \left\{ (1 - \bar{z})^2 + (R \alpha) G_1(\bar{z}) + \dots \right\}. \quad \text{C.6.}$$

APPENDIX D: FIGURES

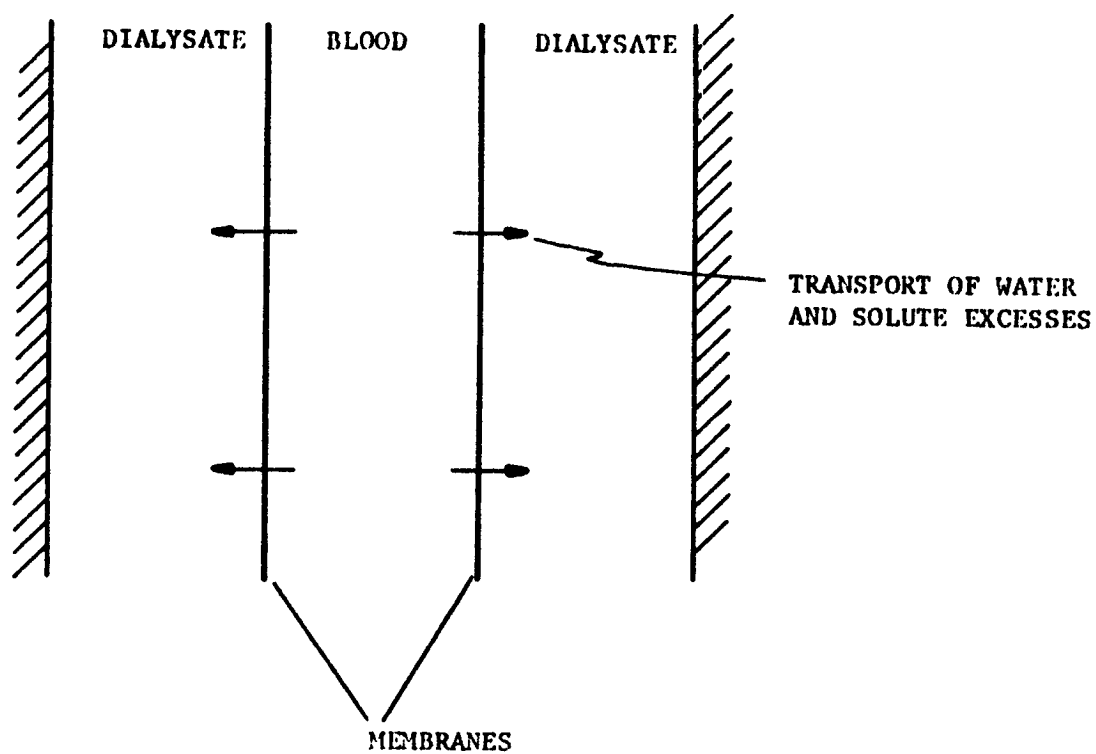


FIGURE 1. THE BLOOD AND DIALYSATE CHANNELS IN AN ARTIFICIAL KIDNEY

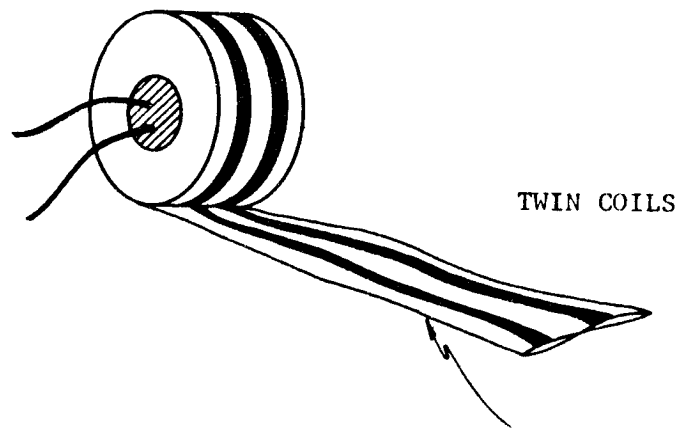


FIGURE 2. KOLFF KIDNEY (KULF)

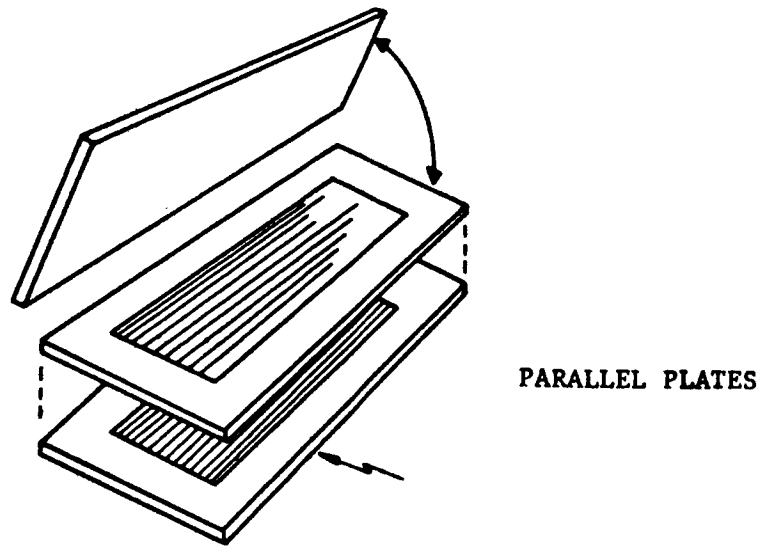


FIGURE 3. KIIL KIDNEY (KEEL)

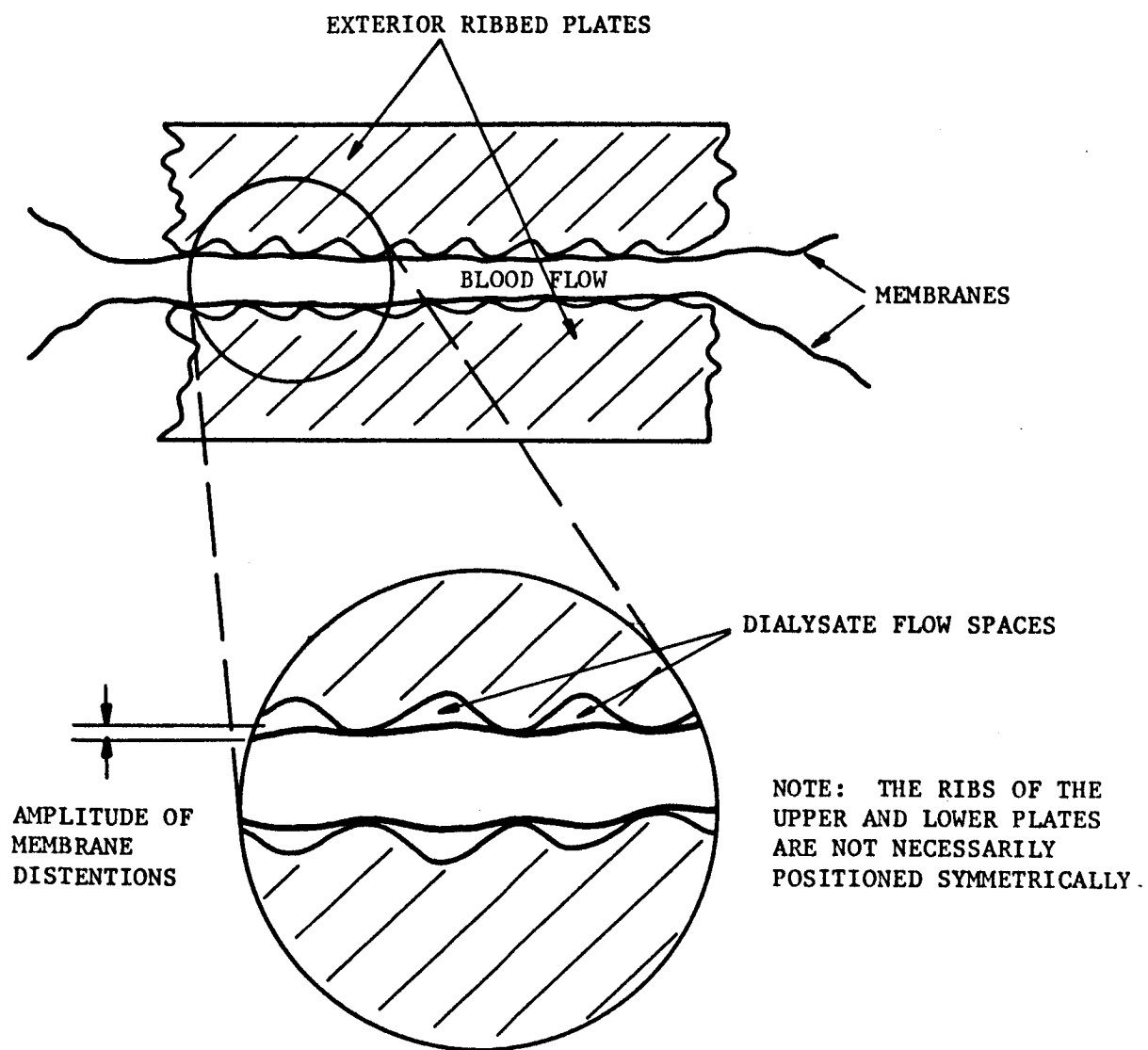


FIGURE 4. CROSS-SECTION OF BLOOD CHANNEL IN THE KIIL KIDNEY
(FLOW IS INTO THE PAPER)

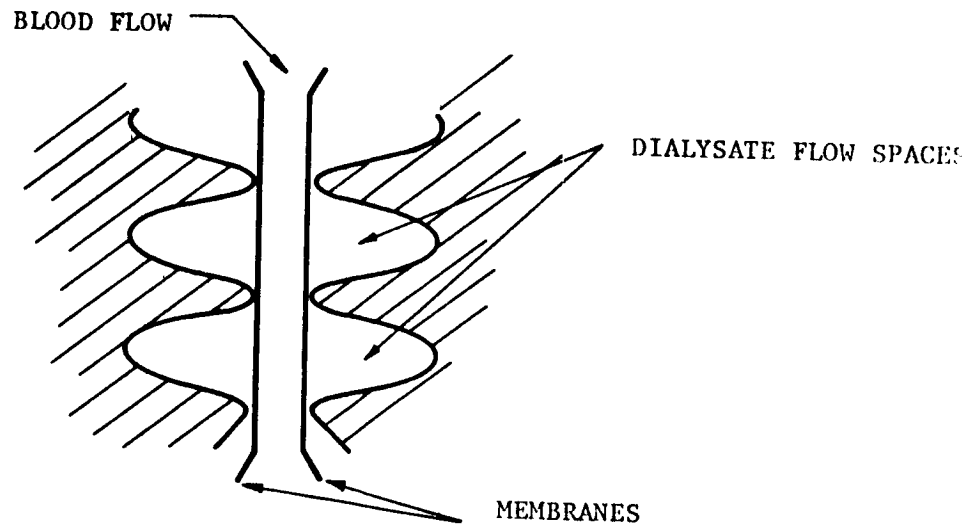


FIGURE 5. CONE SUPPORTS OF LEONARD AND BLUEMLE.

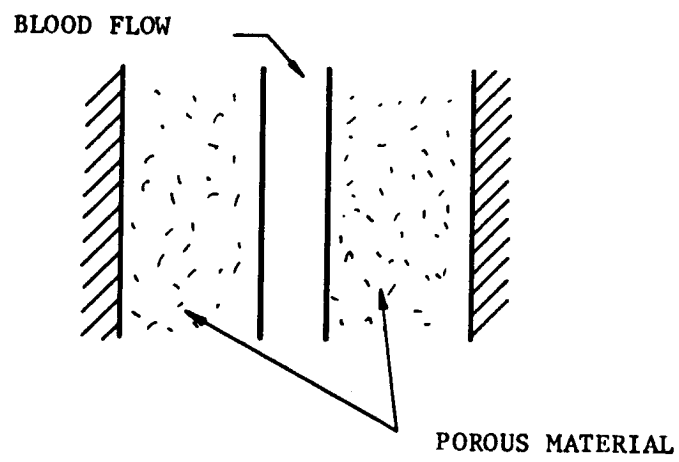


FIGURE 6. POROUS MATERIAL SUPPORTS OF BABB AND GRIMSRUD.

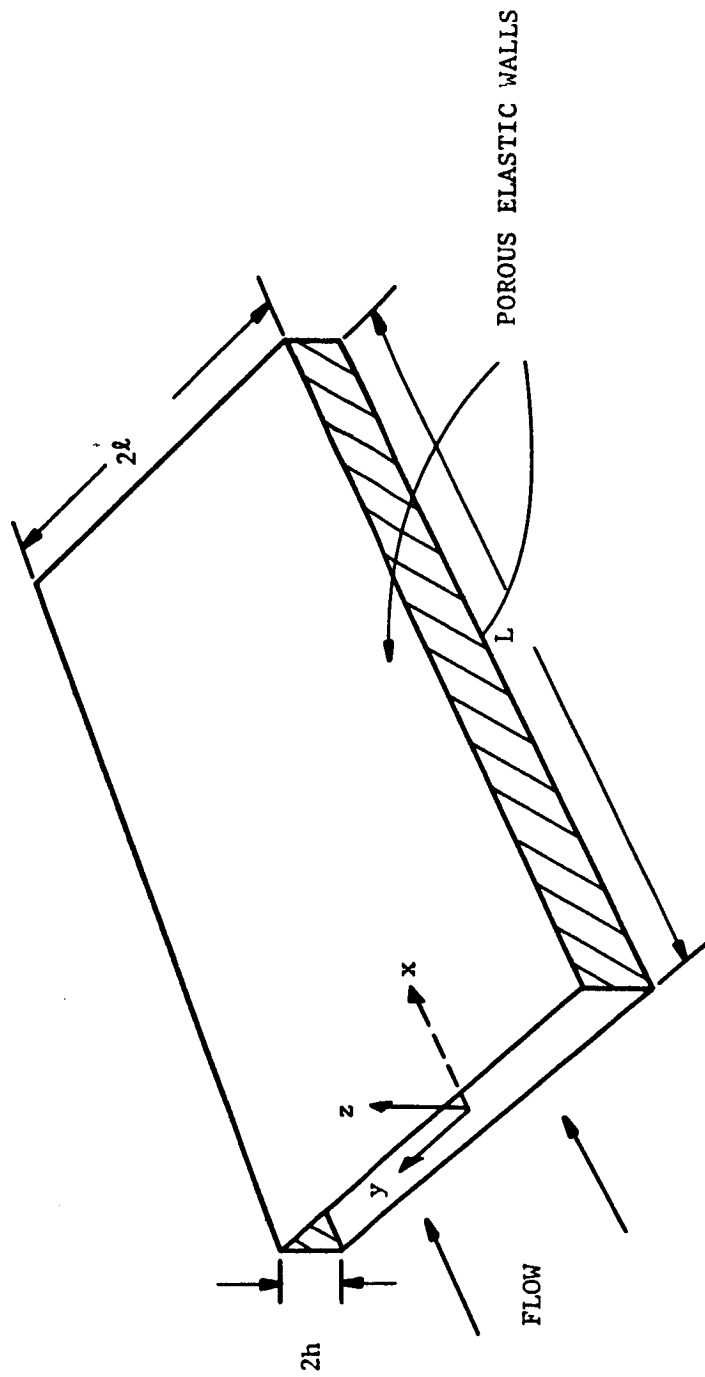


FIGURE 7. CHANNEL GEOMETRY

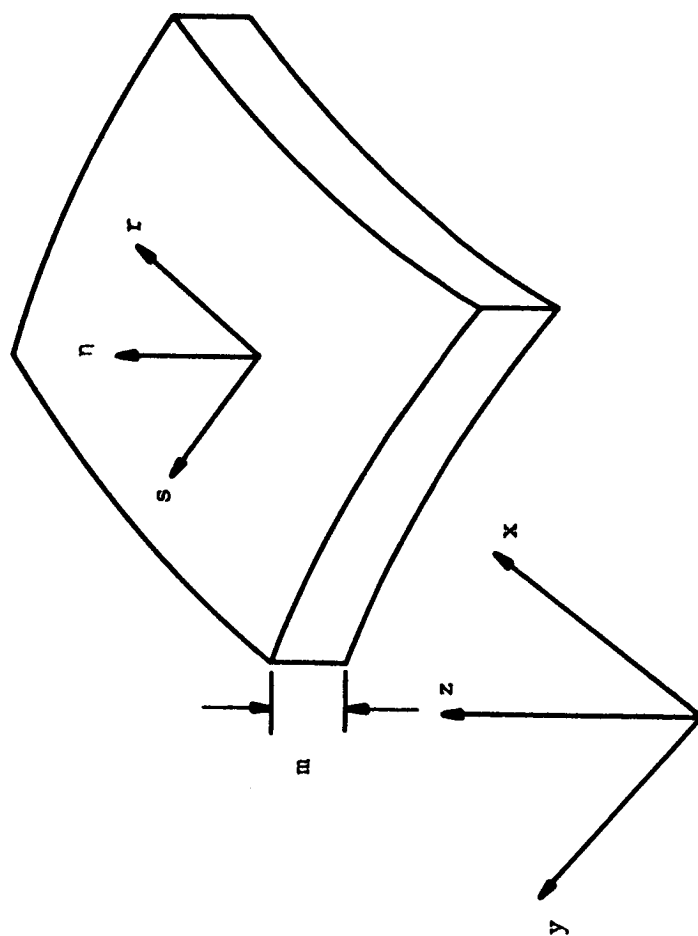


FIGURE 8. COMPONENTS OF DISPLACEMENT OF AN ELEMENT OF THE CHANNEL WALLS

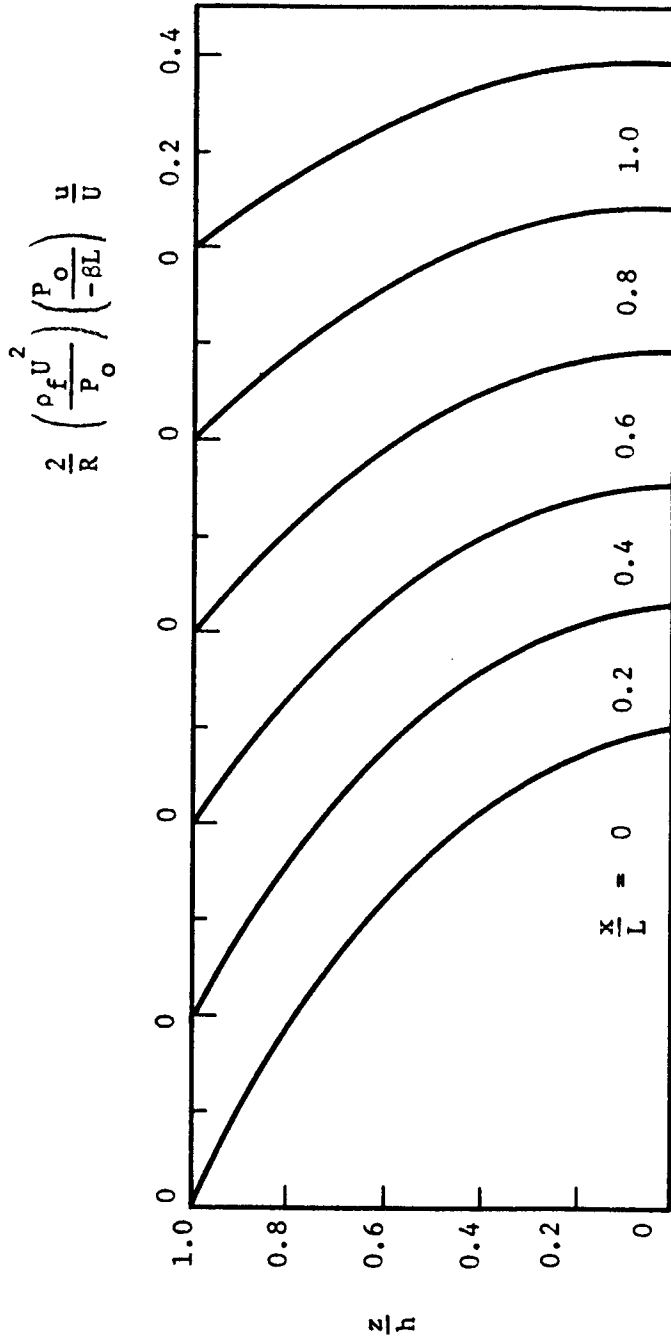


FIGURE 9. AXIAL FLUID VELOCITY PROFILES FOR VARIOUS VALUES OF $\frac{x}{L}$

$\left[\gamma = 0.2, \left(\frac{\Delta P_m}{P_0} \right) = 1.0, \left(\frac{\Delta P_D}{P_0} \right) = 0.25, \left(\frac{-BL}{P_0} \right) = 0.25 \right]$

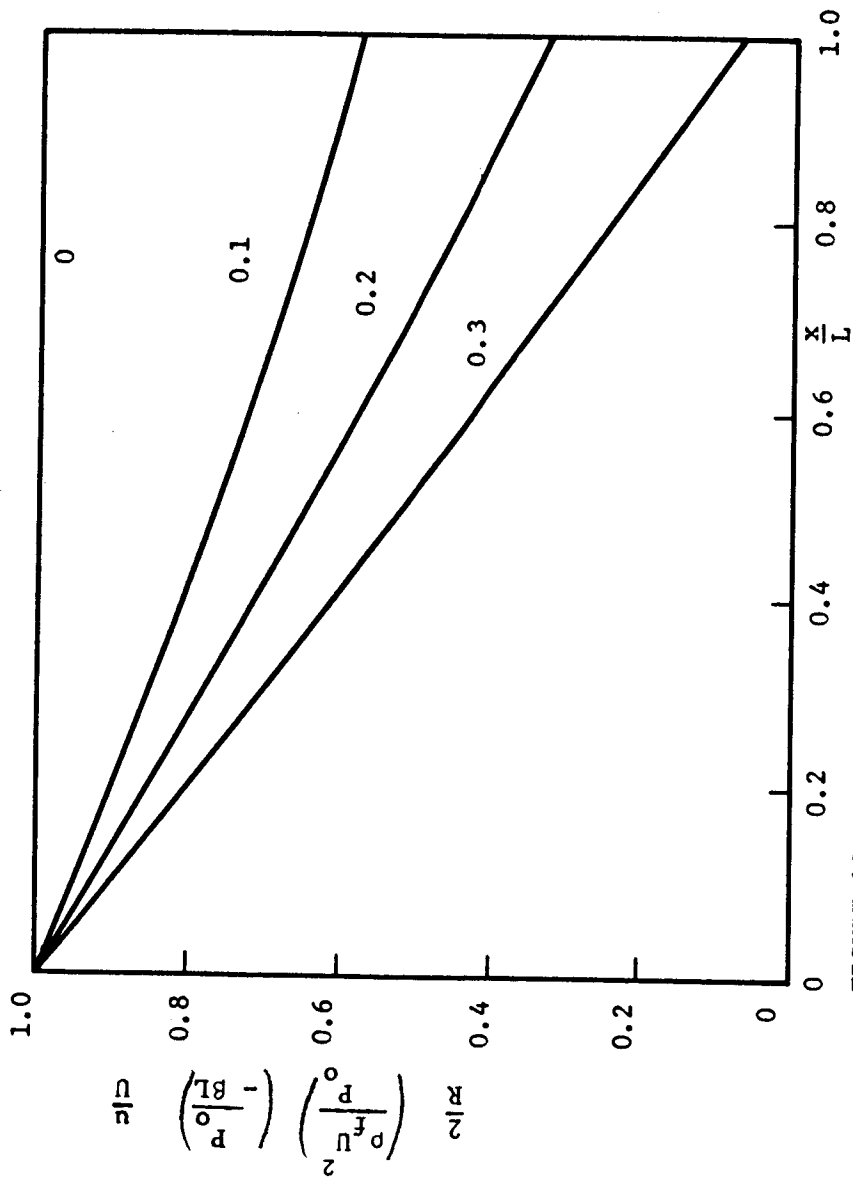


FIGURE 10. AXIAL FLUID VELOCITY COMPONENT AT MID-PLANE FOR VARIOUS VALUES OF γ

$$\left[\left(\frac{\Delta P}{P_o} \right) = 1.0, \left(\frac{\Delta P}{P_o} \right) = 0.25, \left(\frac{\Delta P}{P_o} \right) = 0.25 \right]$$

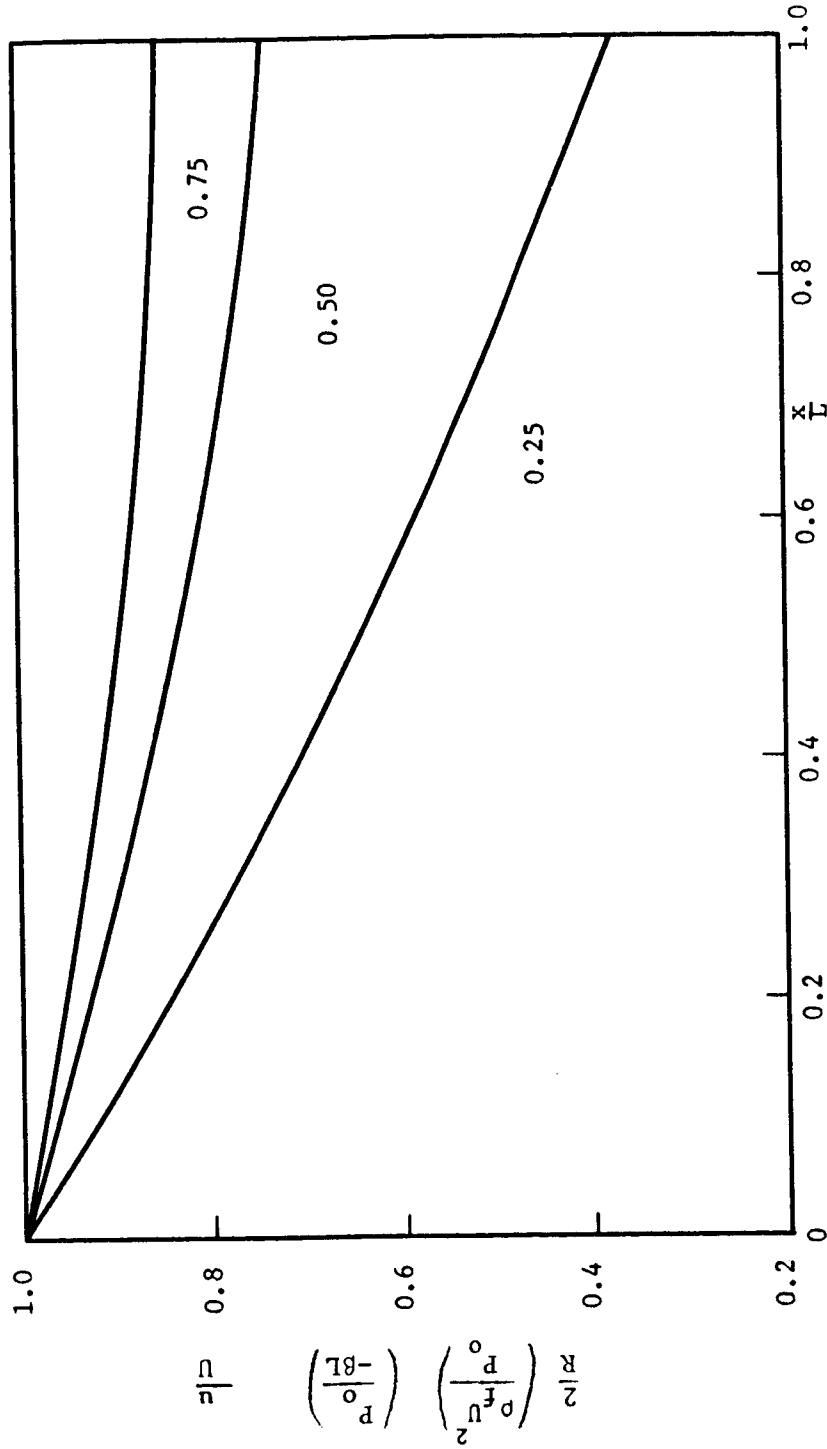
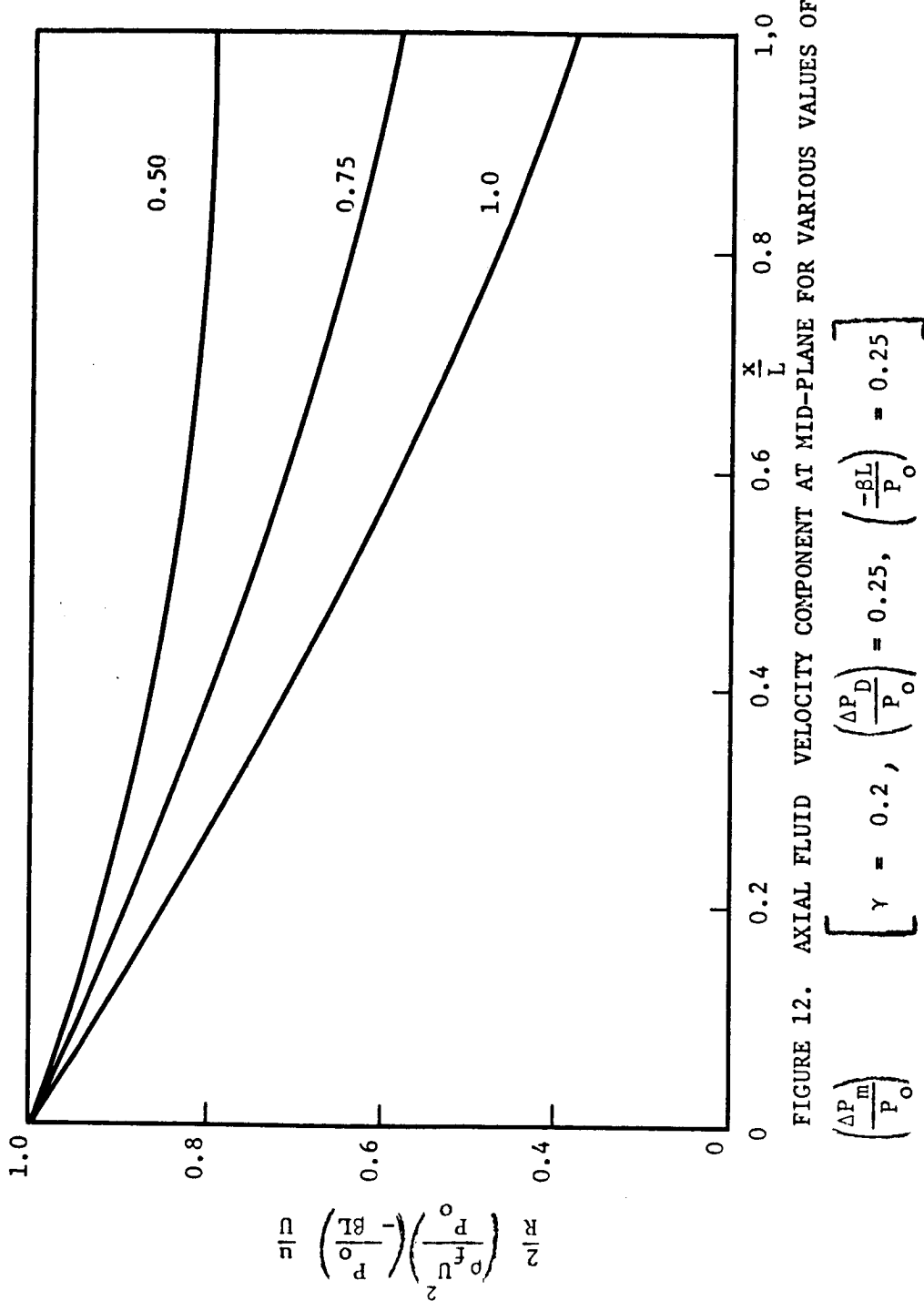


FIGURE 11. AXIAL FLUID VELOCITY COMPONENT AT MID-PLANE FOR VARIOUS VALUES OF

$$\left[\left(\frac{-\delta L}{p_0} \right) \quad \gamma = 0.2, \quad \left(\frac{\Delta p}{p_0} \right) = 1.0, \quad \left(\frac{\Delta p}{p_0} \right) = 0.25 \right]$$



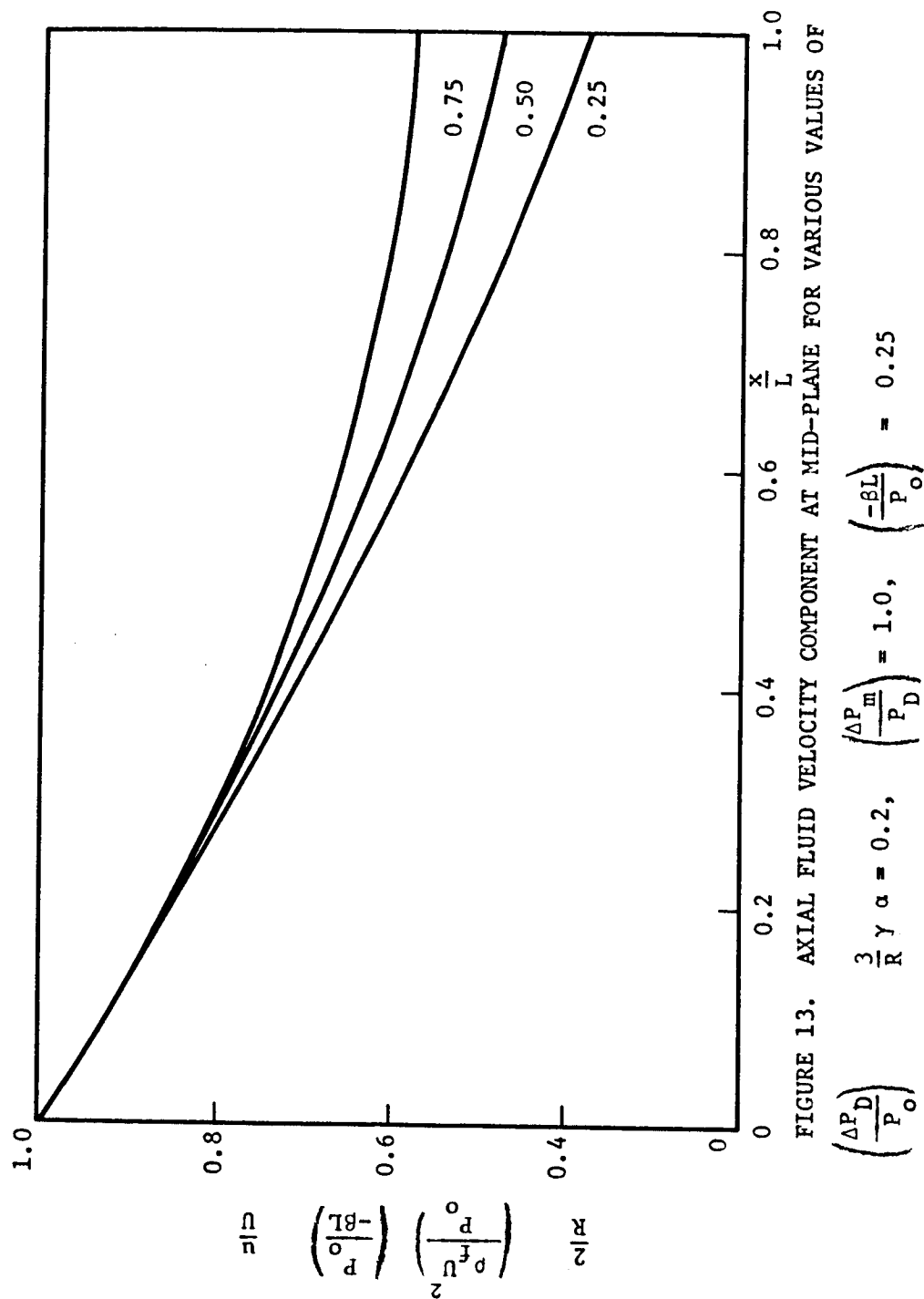


FIGURE 13. AXIAL FLUID VELOCITY COMPONENT AT MID-PLANE FOR VARIOUS VALUES OF

$$\left(\frac{\Delta P_D}{P_O}\right) \quad \frac{3}{R} \gamma \alpha = 0.2, \quad \left(\frac{\Delta P_m}{P_D}\right) = 1.0, \quad \left(\frac{-\beta L}{P_O}\right) = 0.25$$

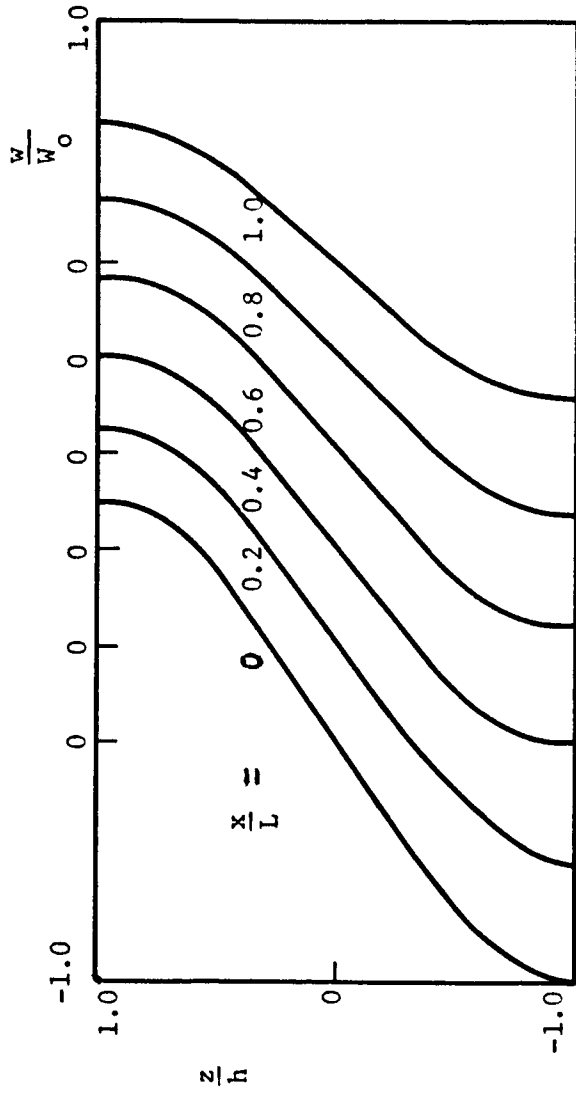


FIGURE 14. NORMAL FLUID VELOCITY PROFILES FOR VARIOUS VALUES OF

$$\left[\gamma = 0.2 \quad \left(\frac{\Delta P}{P_0} \right)^m = 1.0, \quad \left(\frac{\Delta P}{P_0} \right)^D = 0.25, \quad \left(\frac{-\partial L}{P_0} \right) = 0.25 \right]$$

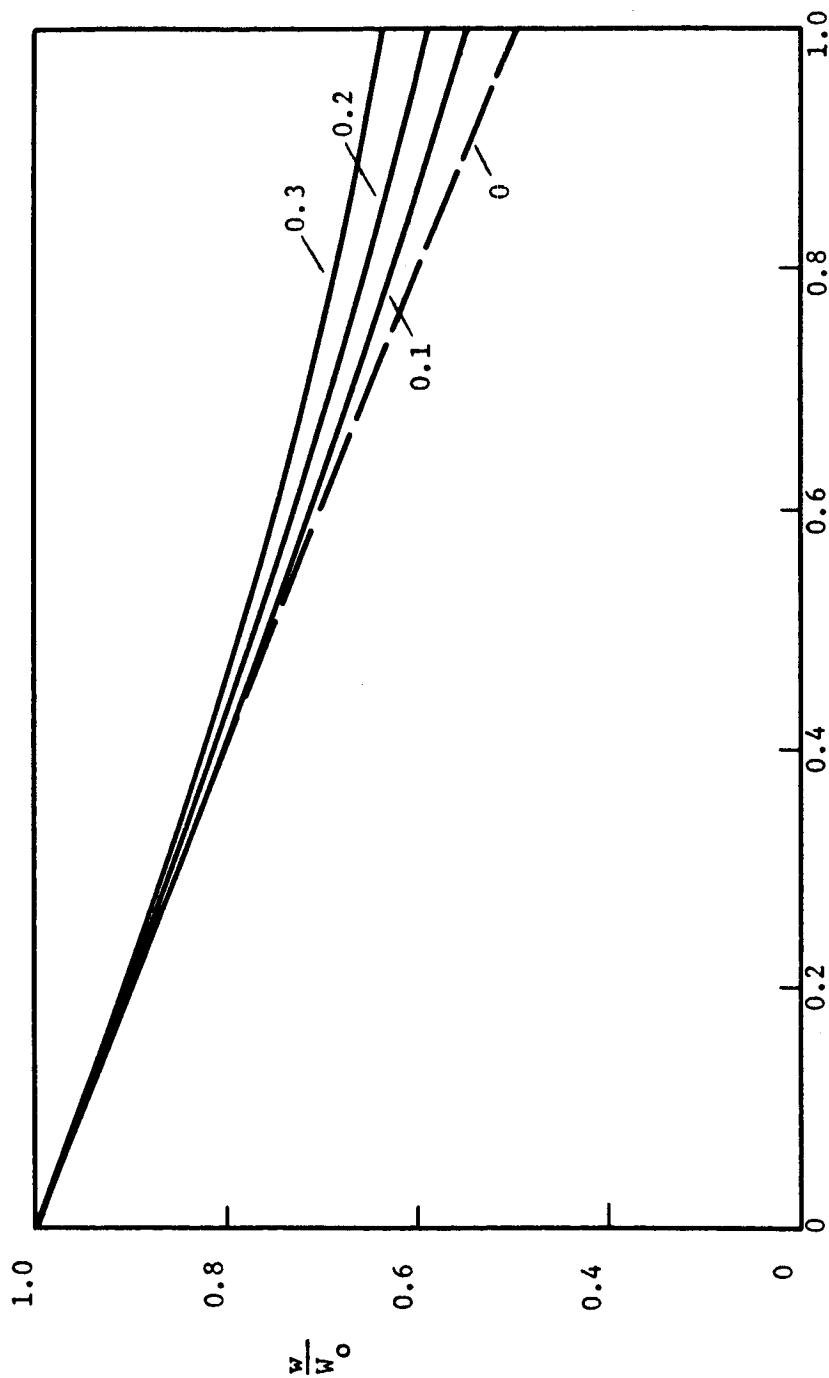


FIGURE 15. NORMAL FLUID VELOCITY COMPONENT AT WALL FOR VARIOUS VALUES OF γ

$$\left[\left(\frac{\Delta P}{P_o} \right) = 1.0, \left(\frac{\Delta P_D}{P_o} \right) = 0.25, \left(\frac{-BL}{P_o} \right) = 0.25 \right]$$

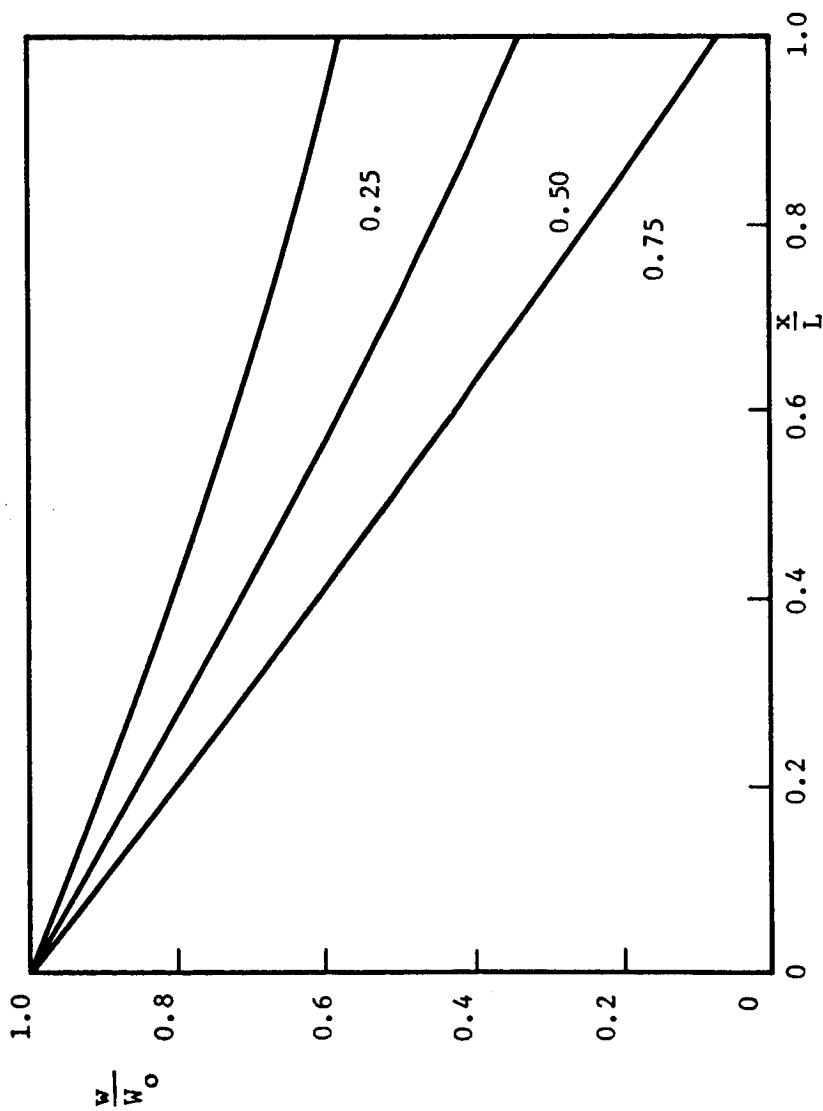


FIGURE 16. NORMAL FLUID VELOCITY COMPONENT AT WALL FOR VARIOUS VALUES OF

$$\left[\left(\frac{-\beta L}{P_0} \right) \left[\gamma = 0.2, \left(\frac{\Delta P^m}{P_0} \right) = 1.0, \left(\frac{\Delta P^D}{P_0} \right) = 0.25 \right] \right]$$

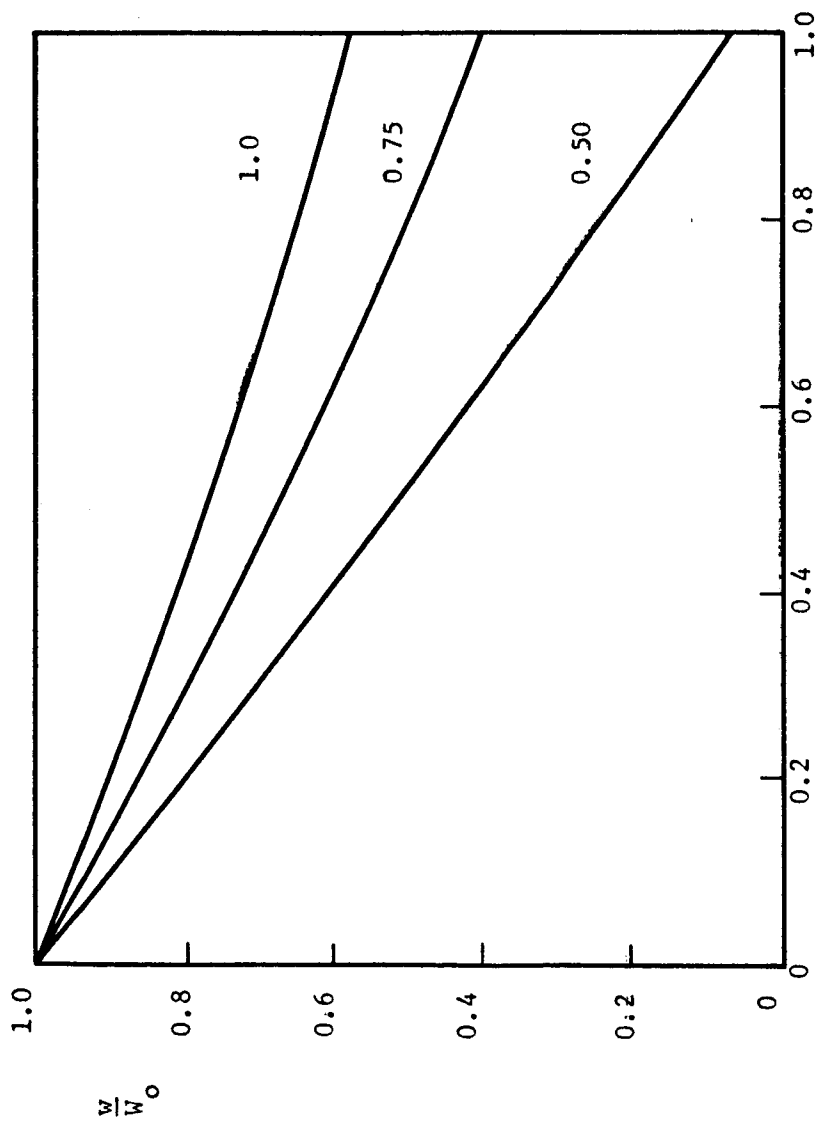


FIGURE 17. NORMAL FLUID VELOCITY COMPONENT AT WALL FOR VARIOUS VALUES OF

$$\left[\frac{\Delta P}{P_0} \right] \left[\gamma = 0.2, \frac{\Delta P}{P_0} = 0.25, \frac{-8L}{P_0} = 0.25 \right]$$

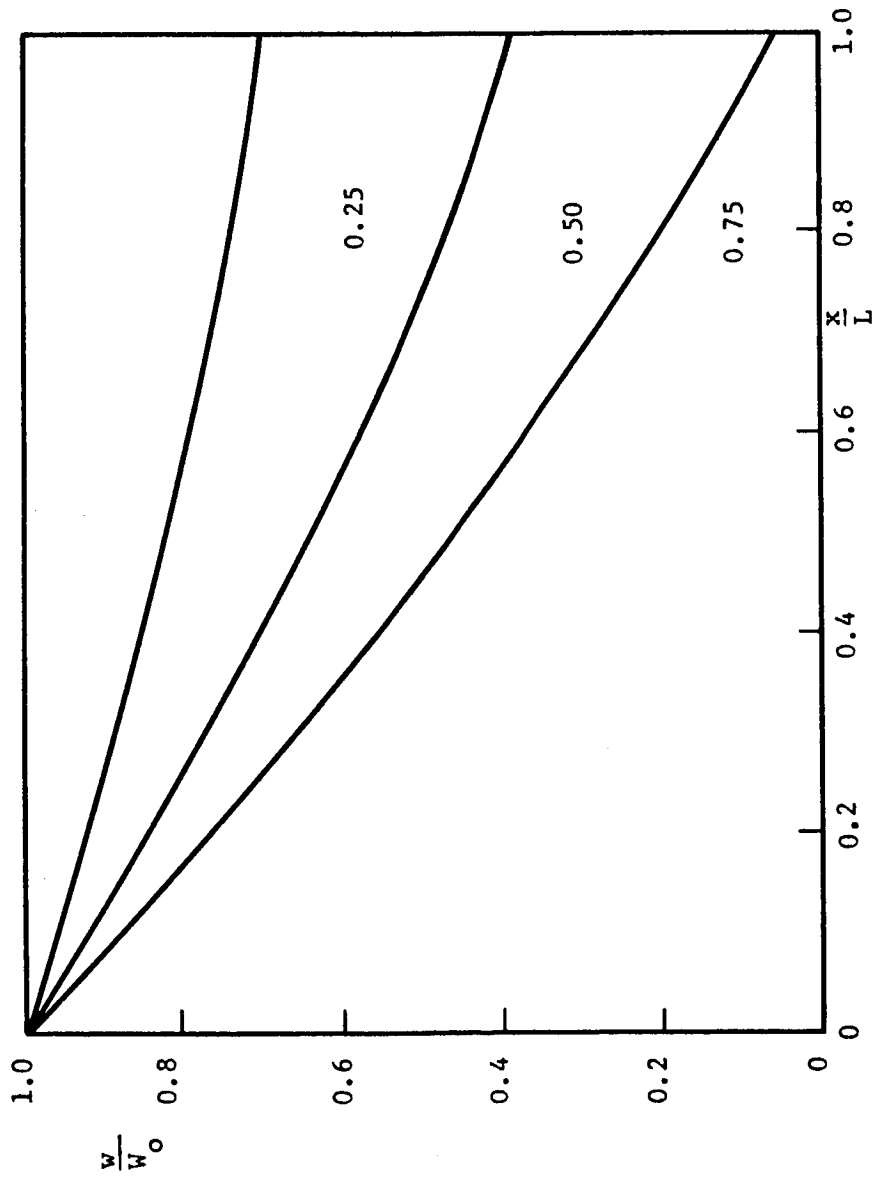


FIGURE 18. NORMAL FLUID VELOCITY COMPONENT AT WALL FOR VARIOUS VALUES OF

$$\left[\gamma = 0.2, \left(\frac{\Delta P_m}{P_0} \right) = 1.0, \left(\frac{-8L}{P_0} \right) = 0.25 \right]$$

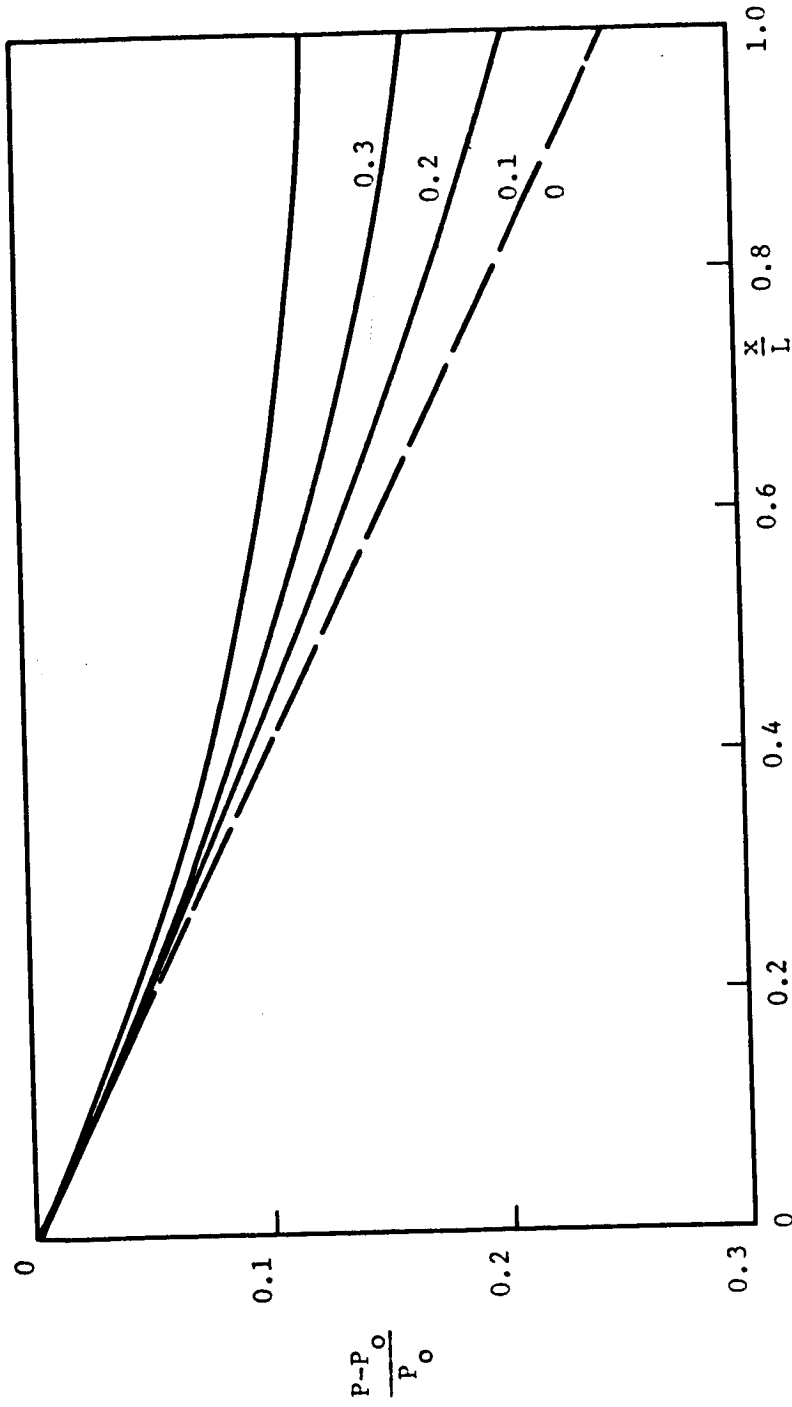


FIGURE 19. PRESSURE DISTRIBUTION FOR VARIOUS VALUES OF γ

$$\left[\left(\frac{\Delta P}{P_0} \right) = 1.0, \left(\frac{\Delta P_D}{P_0} \right) = 0.25, \left(\frac{-\beta L}{P_0} \right) = 0.25 \right]$$

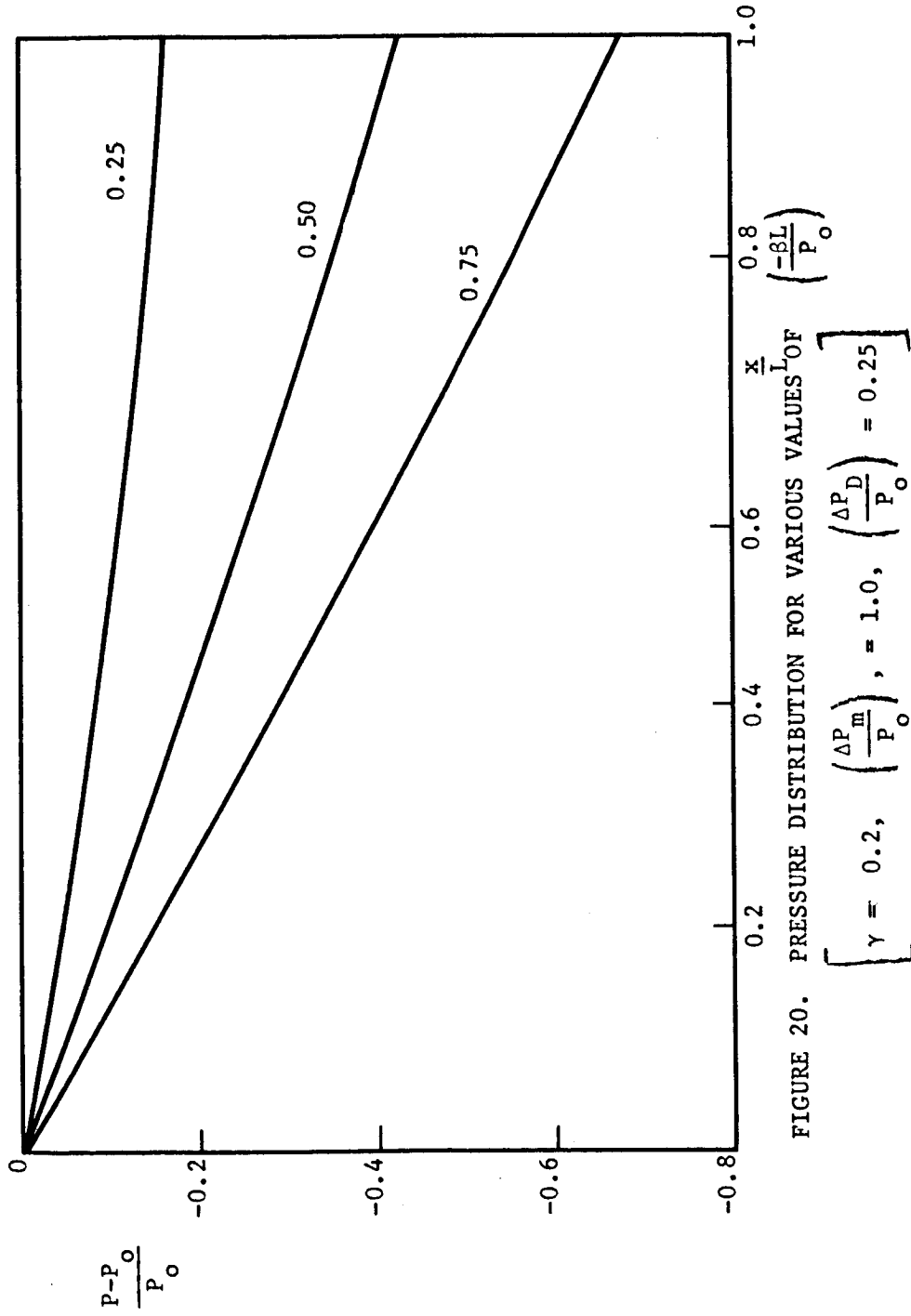


FIGURE 20. PRESSURE DISTRIBUTION FOR VARIOUS VALUES OF x/L

$$\left[\gamma = 0.2, \left(\frac{\Delta P_m}{P_0} \right) = 1.0, \left(\frac{\Delta P_D}{P_0} \right) = 0.25 \right]$$

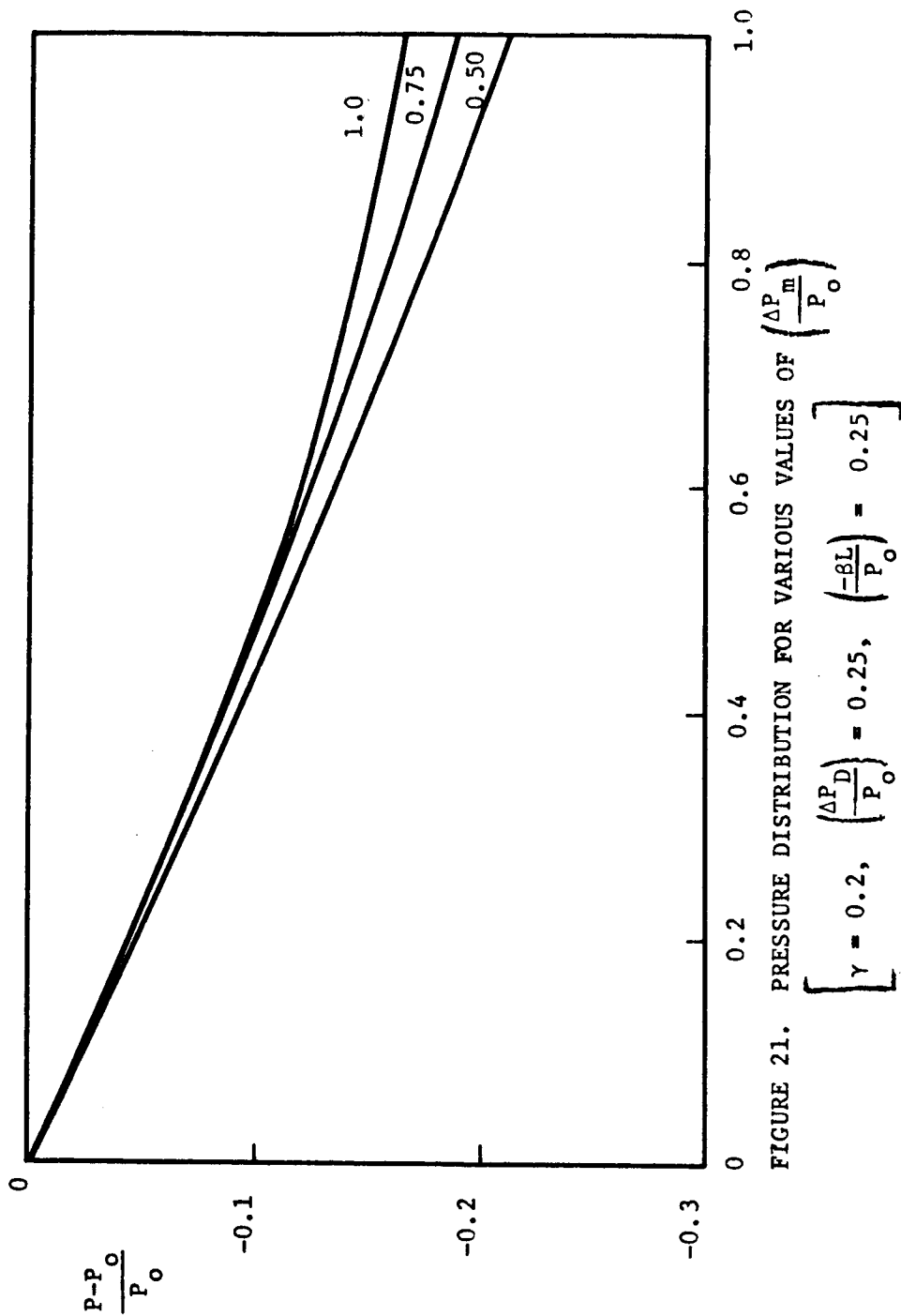


FIGURE 21. PRESSURE DISTRIBUTION FOR VARIOUS VALUES OF $\left(\frac{\Delta P}{P_0}\right)$
 $\left[\gamma = 0.2, \left(\frac{\Delta P}{D}\right) = 0.25, \left(\frac{-BL}{P_0}\right) = 0.25 \right]$

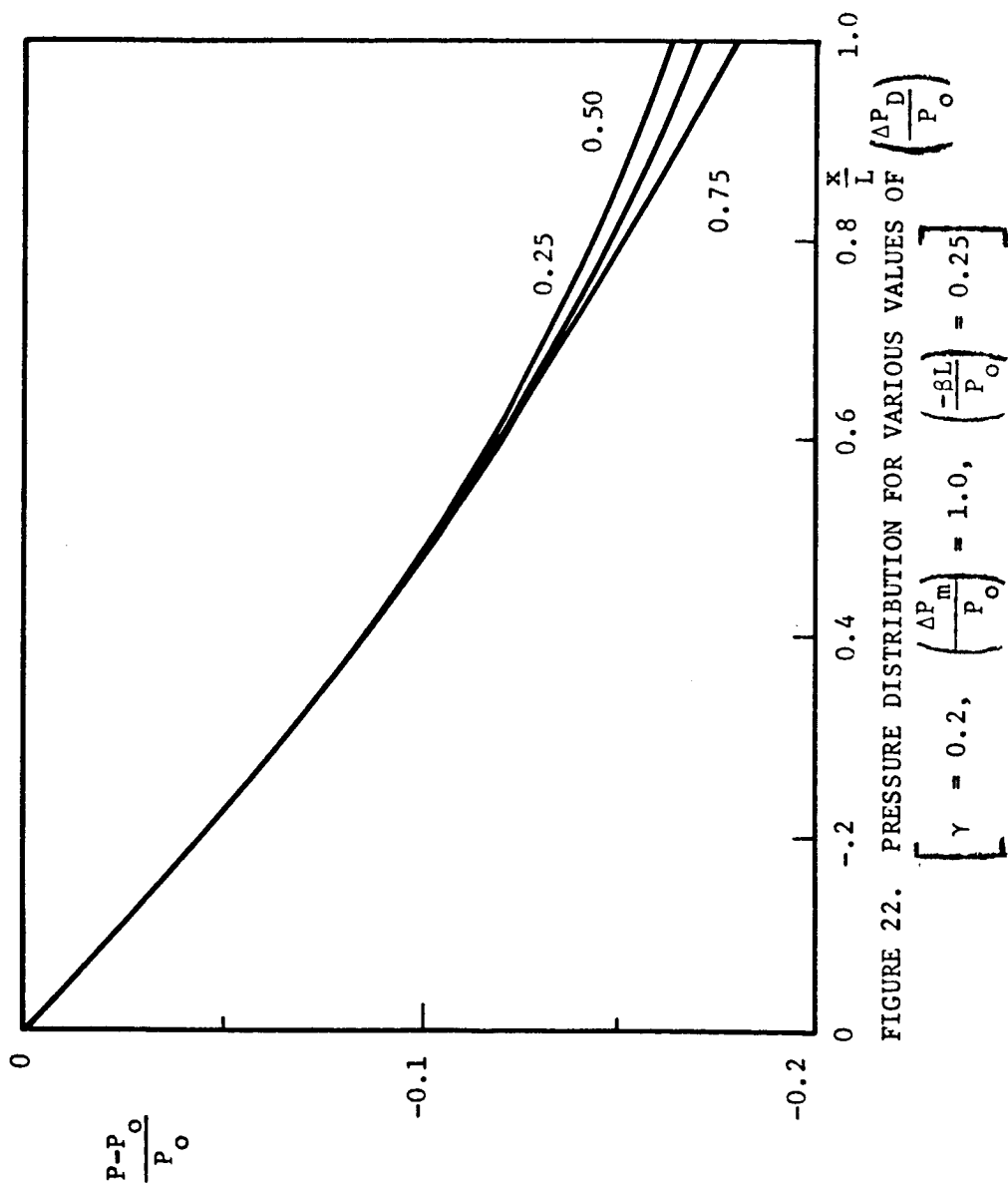


FIGURE 22. PRESSURE DISTRIBUTION FOR VARIOUS VALUES OF $\left(\frac{\Delta P_D}{P_o}\right)$
 $\left[\gamma = 0.2, \left(\frac{\Delta P_m}{P_o}\right) = 1.0, \left(\frac{-\beta L}{P_o}\right) = 0.25 \right]$

